

Electronic Thesis and Dissertation Repository

10-19-2018 1:00 PM

The 2 β Insert Perturbs Folding, Stability and Hydrophobic Exposure of Stromal Interaction Molecules


Steve Chung, *The University of Western Ontario*

Supervisor: Stathopoulos, Peter, *The University of Western Ontario*

A thesis submitted in partial fulfillment of the requirements for the Master of Science degree in Physiology and Pharmacology

© Steve Chung 2018

Follow this and additional works at: <https://ir.lib.uwo.ca/etd>

 Part of the [Biochemistry Commons](#), [Molecular Biology Commons](#), and the [Structural Biology Commons](#)

Recommended Citation

Chung, Steve, "The 2 β Insert Perturbs Folding, Stability and Hydrophobic Exposure of Stromal Interaction Molecules" (2018). *Electronic Thesis and Dissertation Repository*. 5978.
<https://ir.lib.uwo.ca/etd/5978>

This Dissertation/Thesis is brought to you for free and open access by Scholarship@Western. It has been accepted for inclusion in Electronic Thesis and Dissertation Repository by an authorized administrator of Scholarship@Western. For more information, please contact wlsadmin@uwo.ca.

Abstract

Stromal interaction molecule (STIM)1 and 2 regulate agonist-induced and basal cytosolic calcium (Ca^{2+}) levels through oligomerization and translocation to endoplasmic reticulum (ER)-plasma membrane (PM) junctions. At these junctions, the STIM cytosolic coiled-coil domains couple to PM Orai1 protein subunits to form Ca^{2+} released activated Ca^{2+} (CRAC) channels that facilitate store-operated Ca^{2+} entry (SOCE). One splice variant of STIM2, STIM2 β , contains an extra 8-residue (2β insert) located within the coiled-coils and inhibits SOCE through an unresolved mechanism, adding another layer of complexity to Ca^{2+} regulation in mammals. I hypothesize that the 2β insert perturbs the coiled-coil conformation and dynamics commensurate with an ability to activate SOCE. My data show the 2β insertion induced an overall reduction in α -helicity, thermal stability, and promoted a conformation of greater exposed hydrophobicity which affected oligomerization. Previous studies show STIM2 couples weakly to Orai1 compared to STIM1, and STIM2 β is completely incapable of binding to Orai1. My functional studies show the 2β insertion in the STIM1 context also significantly inhibits SOCE. Therefore, my data suggests that the 2β insert inhibits STIM function and SOCE through a mechanism which perturbs α -helical levels and destabilizes the cytosolic domain coiled-coil structure, independent of the requirement for weaker STIM2 coupling to Orai1.

Keywords

Stromal interaction molecule-1 (STIM1), stromal interaction molecule-2 (STIM2), store-operated calcium entry (SOCE), calcium, alternative splicing, coiled-coil domains, stability oligomerization, Orai1, structure

Co-Authorship Statement

Dr. Peter B. Stathopoulos supervised and contributed to the design of all experiments. Dr. Gregory A. Wasney (Structural & Biophysical Core Facility, The Hospital for Sick Children, Toronto, ON) collected the SAXS data.

Acknowledgments

I wish to extend my sincerest gratitude towards my supervisor Dr. Peter B. Stathopoulos for his continuous support, patience and guidance. I am thankful for his assistance with not just the experimental design, but with the publication of my work and completion of my Master's thesis. His extensive knowledge in the field of biochemistry and structural biology coupled with his commendable mentoring in molecular techniques have allowed me to expand and improve my laboratory skills and critical thinking skills. Furthermore, he also given me various opportunities to learn how to produce academic literature which has drastically improved my written communication skills. I would also like to thank my advisory members Dr. Qingping Feng, Dr. Wei-Yang Lu and Dr. Donald Welsh for their valuable feedback, support and assistance in my project.

I would like to thank past and present lab members in Dr. Stathopoulos' Lab: Jinhui Zhu, Naveed Siddiqui, Matthew Novello, Vicky Hung, Rachel Lee, and Allen Feng. Their support and encouragement made my road to obtaining a Master's in Science an enjoyable experience. I would also like to thank our lab volunteer Ryan Park and Shipla Jyothikumar as well as our summer NSERC student Mengqi Zhang, for their assistance with numerous experimental preparations that would otherwise limit the rate of my project completion which allowed me to devote more of my time and resource in other areas of my research ensuring efficiency and productivity.

A special thanks to my friends and family for their continual support and patience they have given to me throughout academia and in life. My special bonds with them, gave me the strength to continue to persevere through the most daunting of experiences so that I can achieve my goals.

Finally, I would like to extend further thanks to Rurika Okuda, her drive and passion for cell research inspired me to pursue my M.Sc in physiology and pharmacology.

Table of Contents

Abstract.....	ii
Co-Authorship Statement.....	iii
Acknowledgments.....	iv
Table of Contents.....	v
List of Tables.....	viii
List of Figures.....	ix
List of Abbreviations.....	xi
Chapter 1 : Introduction.....	1
1.1 Ionized calcium (Ca ²⁺).....	1
1.1.1 A general overview of Ca ²⁺ in physiological functions.....	1
1.1.2 The compartmentalization of Ca ²⁺	3
1.2 Store operated Ca ²⁺ entry (SOCE) and Ca ²⁺ release-activated Ca ²⁺ (CRAC) channels.....	4
1.3 Stromal Interaction Molecule (STIM) and Orai.....	5
1.3.1 STIM domain organization.....	6
1.3.2 Orai organization.....	14
1.3.3 Modifications to STIM.....	15
1.4 STIM2 is a basal modular of SOCE.....	17
1.5 Mutating the CC regions alter SOCE functionality.....	18
1.6 Alterative splicing of STIM2.....	19
1.7 STIM splice variants.....	20
1.8 Rationale.....	21
1.9 Hypothesis and Research Aims.....	22
Chapter 2: Methods.....	24
2.1 Generation of the STIM2 OASF pET-28a recombinant vector.....	24

2.1.1	PCR mutagenesis for incorporation of the 2 β insert into the STIM1 and STIM2 OASF pET-28a recombinant vectors	26
2.1.2	PCR mutagenesis for incorporation of the 2 β insert into the full-length monomeric cherry fluorescence protein (mCh)-STIM1 and mCh-STIM2 pCMV6 vectors.....	27
2.2	Recombinant protein expression and purification	31
2.2.1	pET-28a STIM1-OASF and STIM2-OASF wildtype and 2 β insert mutants	31
2.3	Far-UV circular dichroism (CD) spectroscopy.....	39
2.4	8- Anilidonaphthalene-1-sulfonic acid (ANS) binding assay.....	39
2.5	Size-exclusion chromatography with in line multi-angle light scattering (SEC-MALS).....	40
2.6	Dynamic Light Scattering (DLS).....	40
2.7	Solution Small Angle X-ray Scattering (SAXS)	41
2.8	Human embryonic kidney (HEK) 293 cell culture.....	42
2.9	Transfection of HEK293 with pCMV6-mCh-STIM vectors	43
2.10	Fura-2 ratiometric fluorescence spectroscopy to assess SOCE	43
Chapter 3: Results		45
3.1	The 2 β insertion decreases the α -helicity of OASF	45
3.2	The 2 β insertion reduces the thermal stability of STIM1-OASF.....	47
3.3	Calcium (Ca ²⁺) induces an increase in hydrophobic exposure which is exacerbated by 2 β	50
3.4	Ca ²⁺ minimally affects the α -helicity of the OASF domains with or without 2 β	55
3.5	Ca ²⁺ thermally destabilizes STIM1-OASF and STIM1-2 β OASF	58
3.6	STIM1-OASF, STIM1-2 β -OASF and STIM2 β -OASF undergo a Ca ²⁺ -dependent increase in aggregation propensity.....	62
3.7	The 2 β insertion does not alter OASF quaternary structure	66
3.8	The 2 β insertion does not alter gross OASF structure	69

3.9 The 2 β insertion inhibits OASF function in SOCE independent of the STIM2 context.....	76
Chapter 4: Discussion	80
4.1 Summary	80
4.2 OASF structure, variations and function	81
4.3 Ca ²⁺ and OASF function.....	83
4.4 The 2 β insert inhibits SOCE in the context of the OASF structure.....	86
4.5 Conclusions.....	87
4.6 Future Directions and Limitations	88
Bibliography	92
Curriculum Vitae	104

List of Tables

Table 2.1: Oligonucleotide primers used in the research described in this study (Sigma-Aldrich St. Louis, MO)	29
Table 2.2: PCR amplification parameters used in LifeECO (Bioer) thermocycler	30
Table 3.1: Summary of the thermal stabilities for STIM1-OASF and STIM2-OASF with their respective 2 β insertions	48
Table 3.2: Summary of basal ANS fluorescence and saturated ANS fluorescence of STIM1-OASF and STIM2-OASF with their respective 2 β insertions	54
Table 3.3: Summary of the thermal stabilities for STIM1-OASF, STIM1-2 β -OASF, STIM2-OASF and STIM2 β -OASF in the presence and absence of high Ca ²⁺	61
Table 3.4: Summary of the SEC-MALS data of STIM1-OASF, STIM1-2 β -OASF, STIM2-OASF and STIM2 β -OASF proteins	68

List of Figures

Figure 1.1: Pictorial representation of store operated Ca^{2+} entry (SOCE).	9
Figure 1.2: STIM1 and STIM2 domain architecture depicting the conserved domains.....	10
Figure 1.3: Multiple amino acid sequence alignment of STIMs from lower to higher order organisms.....	13
Figure 2.1: Pairwise alignment of the sequenced DNA showing successful 2β insertion	34
Figure 2.2: Coomassie blue R-250 staining of STIM1-OASF and STIM1- 2β -OASF separated on 15% (w/v) SDS-PAGE gels.....	35
Figure 2.3: Superdex S200 HiLoad 10/60 size exclusion chromatography elution profile of STIM1-OASF and STIM1- 2β -OASF	36
Figure 2.4: Coomassie blue R-250 staining of STIM2-OASF and STIM1- 2β -OASF separated on 15% (w/v) SDS-PAGE gels.....	37
Figure 2.5: Superdex S200 HiLoad 10/60 size exclusion chromatography elution profile. STIM2-OASF and STIM2 β -OASF	38
Figure 3.1: The 2β insertion decreases α -helicity of the OASF regions of STIM1 and STIM2.	46
Figure 3.2: The 2β insertion reduces the thermal stability of STIM1-OASF	49
Figure 3.3: Ca^{2+} induces an increase in exposed hydrophobicity in the STIM OASF domains which is exacerbated by the 2β variation.....	52
Figure 3.4: The 2β insert promotes apparently saturable Ca^{2+} binding within STIM2-OASF which enhances solvent exposed hydrophobicity.....	53
Figure 3.5: Ca^{2+} causes only minor changes in the secondary structure levels of the human OASF domains.....	57

Figure 3.6: Far-UV CD thermal melts of STIM1-OASF, STIM1-2 β -OASF), STIM2-OASF and STIM2 β -OASF in the presence and absence of 25 mM CaCl ₂	60
Figure 3.7: DLS analysis of STIM1-OASF STIM1-2 β -OASF, STIM2-OASF, and STIM2 β -OASF	64
Figure 3.8: The 2 β insertion promotes similar STIM1-2 β -OASF and STIM2 β -OASF conformations with low aggregation propensity.....	65
Figure 3.9: SEC-MALS analysis of STIM1-OASF, STIM1-2 β -OASF, STIM2-OASF , and STIM2 β -OASF.	67
Figure 3.10: The 2 β insertion causes only minor changes to the STIM1-OASF R _g and D _{max}	72
Figure 3.11: The 2 β insertion causes only minor changes to the STIM2-OASF R _g and D _{max}	74
Figure 3.12: <i>Ab initio</i> reconstructed DAMMIF structures based on the respective scattering profiles	75
Figure 3.13: The 2 β insertion perturbs the SOCE-inducing function of STIM1 in the full-length molecular context.....	79
Figure 4.1: Proposed model of the STIM2 β mechanism of SOCE inhibition based on the data presented in this thesis.	91

List of Abbreviations

2 β	two beta
AEBSF	4-benzenesulfonyl fluoride hydrochloride
ANG II	angiotensin II
APC	antigen-presenting cell
ANS	8-anilinonaphthalene-1-sulfonic acid
ARC	arachidonic acid-activated channels
BP	basepairs
BME	β -mercaptoethanol
Ca ²⁺	calcium
CaCl ₂	calcium chloride
CAD	CRAC activating domain
CaM	calmodulin
CC	coiled-coil
CD	circular dichroism
cEF	canonical EF-hand
CD4 ⁺	cluster of differentiation 4
CD8 ⁺	cluster of differentiation 8
CMD	CRAC modulatory domain
CRAC	Ca ²⁺ released activated Ca ²⁺

DLS	dynamic light scattering
DMEM	dulbecco's modified eagle media
DNA	deoxyribonucleic acid
DTT	dithiothreitol
<i>E.coli</i>	escherichia coli
EB1	end-tracking protein-1
EGTA	ethylene glycol tetraacetic acid
ER	endoplasmic reticulum
ET-1	endothelin 1
EtBr	ethidium bromide
FBS	fetal bovine serum
FGLR	fibroblast growth factor receptor gene
FRET	fluorescence resonance energy transfer
Fura 2 AM	Fura-2 acetoxymethyl ester
GdnHCl	guanidine hydrochloride
GPCR	G-protein coupled receptor
H ⁺	hydrogen
HBSS	HEPES buffered saline solution
HEPES	4-(2-hydroxyethyl)-1-piperazineethanesulfonic acid
HEK	human embryonic kidney

HUVEC	human umbilical vein endothelial cell
ID	inhibitory domain
IH	inhibitory helix
IP ₃	inositol 1,4,5-trisphosphate
IP ₃ R	inositol 1,4,5-trisphosphate receptor
IPTG	isopropyl β-D-1-thiogalactopyranside
K _d	equilibrium dissociation constant
LB	Luria-Bertani broth
mCh	mcherry
mRNA	messenger ribonucleic acid
Na ²⁺	sodium
NaCl	sodium chloride
NADH	nicotinamide adenine dinucleotide
NADPH	nicotinamide adenine dinucleotide phosphate
Ni-NTA	nickel-nitrilotracetice acid
NMR	nuclear magnetic resonance
OASF	Orai-activating STIM fragment
OD600	optical density at 600 nm
PBS	phosphate-buffered saline
pCMV	porcine cytomegalovirus

PCR	polymerase chain reaction
PE	phenylephrine
PIP ₂	phosphatidyl inositol 4,5 – bisphosphate
PM	plasma membrane
PMT	photomultiplier tube
ROS	reactive oxygen species
SAM	sterile α -motif
SAXS	small-angle X-ray scattering
SCID	severe combined immunodeficiency
SDS-PAGE	sodium dodecyl sulfate–polyacrylamide gel electrophoresis
SEC-MALS scattering	size-exclusion chromatography with in line with multi-angle light
SERCA	sarco/endoplasmic reticulum Ca ²⁺ -ATPase
siRNA	small interfering ribonucleic acid
SOAR	STIM-Orai activating region
SOAP	STIM-Orai association pocket
SOCE	store-operated Ca ² entry
SR	sarcoplasmic reticulum
STIM	stromal interaction molecule
TCE	T-cell receptor
T _m	apparent midpoint of temperature unfolding

TIRF	total internal reflective fluorescence
TM	transmembrane
TRIS-HCl	trisaminomethane hydrochloride
TRPC	transient receptor potential canonical
TSH	thyroid stimulating hormone
TSHR	thyroid stimulating hormone receptor
UV	ultraviolet
WT	wildtype
YFP	yellow-fluorescent protein

Chapter 1 : Introduction

1.1 Ionized calcium (Ca^{2+})

1.1.1 A general overview of Ca^{2+} in physiological functions

Ca^{2+} ions are essential factors for a myriad of physiological processes. While a majority of Ca^{2+} is used for bone remodeling and dental enamel formation during development, a small fraction of total body Ca^{2+} is reserved for critical cell signaling and metabolic functions such as muscle contraction, intracellular signaling, and neural transmissions, to name a few. In synaptic transmissions Ca^{2+} ions play a role in transducing action potentials into a chemical signal through the rise of cytosolic Ca^{2+} concentrations from the extracellular medium through voltage-gated Ca^{2+} channels. The rise of localized Ca^{2+} within the cytosol of axons, permit neurotransmitter packaged vesicles to undergo exocytosis, allowing them to bind to postsynaptic receptors which further propagate the neural signal (Augustine, 2001). Interestingly, proteins that interact with Ca^{2+} often have a helix-loop-helix structural motif known as the “EF-hand” which functions as an intracellular Ca^{2+} receptor that elicits a downstream response; the downstream response is typically dependent on a conformational change within the EF-hand (Ikura, 1996). One such example occurs during muscle contraction in skeletal muscles, where depolarization of the t-tubule membranes results in Ca^{2+} release from the sarcoplasmic reticulum (SR). The released Ca^{2+} binds to troponin C, one of three troponin subunits which interact (Herzberg et al., 1986). Troponin T binds tropomyosin, interlocking them to form the troponin-tropomyosin complex while troponin C binds actin and holds the troponin-tropomyosin complex in place under resting conditions (Yamamoto et al., 1987). Ca^{2+} binding to troponin C results in a conformational change which causes the troponin-tropomyosin complex to shift and expose a binding site for myosin filaments to elicit actin-myosin cross-bridge formation (Zot et al., 1987). Subsequently, adenosine triphosphate (ATP) hydrolysis by myosin drives the relative movement of actin and myosin in process known as cross bridge cycling (Jewell, 1977; McDonald et al., 1994).

Ca^{2+} ions function as a secondary messenger which bind to and activate calmodulin (CaM), a Ca^{2+} binding messenger protein that is ubiquitously expressed in eukaryotic cells. CaM

activation drives downstream cell signaling through interactions with hundreds of protein binding partners such as kinases or phosphatases (Chin et al., 2000). Elevated cytosolic Ca^{2+} is also known to facilitate the metabolic activity required for fertilization once the sperm fuses with the ovum, thus, driving the formation of new life (Slusarski et al., 2007). Conversely, increasing cytosolic Ca^{2+} levels can signal apoptosis through interactions with various members of the Bcl-2 family in tandem with the release of cytochrome c and other pro-apoptotic factors from the mitochondria (Rong et al., 2008).

Indeed, the above examples highlight the importance and versatility of Ca^{2+} ions in physiological functions. Still, the role of Ca^{2+} ions also plays a critical role in maintaining the body's defensive capabilities against foreign invaders (i.e. the immune system). Ca^{2+} ions play an essential role as a secondary messenger in innate and adaptive immune responses. In innate immunity, the increase in cytosolic Ca^{2+} through gap junctions at the site of the wounded epidermis is necessary to attract and initiate an inflammatory response (Razzell et al., 2013). Conversely, in long term adaptive immunity, elevated Ca^{2+} concentrations are the result of interactions between a cell surface receptor [i.e. B-cell receptor (BCR) for B-cells and T-cell receptor (TCR) for T-cells] binding an antigen provided by antigen-presenting cell (APC), thus, stimulating the activation of the B-cell and T-cells. The cytosolic elevation of Ca^{2+} concentration is regulated by the phospholipase C (PLC) and inositol 1,4,5-trisphosphate (IP_3) signaling pathway that leads to release of Ca^{2+} from ER stores (Baba et al., 2014; Joseph et al., 2014). This release of Ca^{2+} from the ER stores signals additional Ca^{2+} entry into the cytosol from the extracellular space, in a crucial cellular process which is the focus of this thesis (see below). The activation of calpain, a Ca^{2+} dependent protease, mediates T-cell immobilization which allow T-cells to shape their membrane to better accommodate APCs (Selliah et al., 1996). Ultimately, given the vast physiological processes that require Ca^{2+} ions, it is evident that Ca^{2+} homeostasis is pivotal to maintaining daily bodily functions and avoiding pathologies.

1.1.2 The compartmentalization of Ca^{2+}

To closely regulate these physiological processes, Ca^{2+} ions are compartmentalized in non-continuous vesicular and continuous stores. Non-continuous vesicular stores such as lysosomes, and phagosomes are useful in local regulation such as membrane fusion and vesicular movements, while continuous stores include the intracellular organelles that can act as major Ca^{2+} storage sites such as the endo/sarcoplasmic reticulum (ER/SR) (Haller et al., 1996; Hilden et al., 1989; Z. Yang et al., 2015). Additionally, under basal conditions, the Ca^{2+} concentration within the mitochondria is ~ 0.1 nM like the cytosol. However, during cell stimulation, the mitochondrial Ca^{2+} concentration has been shown to rise to ~ 100 nM – 10 mM in certain cell types (Alonso et al., 2006). Post cell stimulation, mitochondrial Ca^{2+} ions are promptly dissipated by various transmembrane $\text{Na}^+/\text{Ca}^{2+}$ antiporters and $\text{Ca}^{2+}/\text{H}^+$ exchangers (Palty et al., 2010). Improper Ca^{2+} and Na^+ handling in mitochondria can result in heart failure which has been associated with reduced nicotinamide adenine dinucleotide (NADH) and nicotinamide adenine dinucleotide phosphate (NADPH) production, ultimately leading to energetic deficits and increased reactive oxygen species (ROS) (Bertero et al., 2018). The Golgi apparatus has been shown to accumulate relatively large amounts of Ca^{2+} (i.e. ~ 0.3 mM) in HeLa cells which can be released in association with histamine-induced IP_3 production (Pinton et al., 1998). Finally, the ER/SR are known to have largest intracellular Ca^{2+} store (i.e. ~ 0.4 – 0.7 mM) that can be released in to the cytosol, as required during specific electrical or chemical signals (H. E. Collins et al., 2013). The inability to regulate Ca^{2+} stores in the ER/SR can result in various diseases such as muscle disorders and immunodeficiency (Maus et al., 2015; Noury et al., 2017). Remarkably, the release of intracellular Ca^{2+} into the cytosol also induce extracellular Ca^{2+} to enter the cytosol which, in tandem, augment the cytosolic Ca^{2+} levels (see below), after receiving voltage dependent or independent signals, to promptly activate Ca^{2+} dependent pathways (Putney, 1986). Furthermore, extracellular Ca^{2+} movement into the cell allows for restoration of basal Ca^{2+} levels necessary for ER Ca^{2+} dependent processes such as protein folding and chaperone function (Braakman et al., 2013; Gidalevitz et al., 2013; Halperin et al., 2014).

1.2 Store operated Ca^{2+} entry (SOCE) and Ca^{2+} release-activated Ca^{2+} (CRAC) channels

In 1986, J.W Putney first proposed a cell signaling model for store operated Ca^{2+} entry (SOCE). Putney proposed that cell surface receptor stimulation leads to PLC-induced IP_3 production which binds to IP_3 receptors (IP_3R)s and leads to depletion of intracellular ER Ca^{2+} stores. Importantly, his model suggested that this ER Ca^{2+} depletion, activated PM Ca^{2+} channels, leading to extracellular Ca^{2+} entry into the cytosol (Putney, 1986). It was later discovered that the major players involved in SOCE were STIMs (Liou et al., 2005; Roos et al., 2005), which function as the ER/SR Ca^{2+} sensor, and the PM Ca^{2+} channel subunits known as Orai (Feske et al., 2006; Prakriya et al., 2006; Vig et al., 2006; Yeromin et al., 2006). The conservation of the SOCE signaling mechanism in lower order eukaryotes such as the common fruit fly to higher order vertebrates such as humans highlights its evolutionary significance in Ca^{2+} regulation and signaling (Cai et al. 2007).

To induce SOCE, cell surface G-protein coupled receptor (GPCR)s bind various agonists such as endothelin 1 (ET-1), phenylephrine (PE) and angiotensin II (ANG II), to name a few, which ultimately elicits the downstream conversion of phosphatidyl inositol 4,5 – biphosphate (PIP_2) into IP_3 mediated by PLC. IP_3 , acting as a secondary messenger, binds to IP_3R s anchored on the ER/SR membrane (Wang et al., 2005) which open and allow Ca^{2+} entry into the cytosol from the ER lumen down the steep concentration gradient. These initial events result in a decrease of Ca^{2+} concentration in the ER (Korzeniowski et al., 2010; Muik et al., 2011; Wu et al., 2006). This drop of ER-luminal Ca^{2+} results in Ca^{2+} unbinding from the sensory luminal N-terminal side of STIM1 and a conformational change which propagates throughout the molecule (Luik et al., 2006; Zheng et al., 2008; Zheng et al., 2011). First, dimerization and/or oligomerization of the N-terminal STIM1 domain occurs; second, this oligomerization promotes a compact to extended state conformational change on the C-terminal, cytosolic side of the protein (Muik et al., 2011); finally, the oligomerized/conformationally extended STIMs translocate to ER-plasma membrane (PM) junctions (Stefan et al., 2013). At ER-PM junctions, the polybasic domain of STIM1 interacts with phosphoinositides of the PM and specialized cytosolic domains of STIM1 interact with Orai1 subunits, recruiting Orai1 to the same ER-PM junctions and forming

Ca²⁺ release activated Ca²⁺ (CRAC) channels. STIM1 also gates CRAC channels which facilitate the entry of Ca²⁺ into the cytosol from the extracellular space. The interactions between STIM1 and Orai1 are necessary for forming and opening CRAC channels which selectively permit Ca²⁺ entry thereby also inducing an inward current (I_{CRAC}) due to Ca²⁺ traversing down its concentration gradient (Stathopoulos et al., 2008).

1.3 Stromal Interaction Molecule (STIM) and Orai

As a prominent player in myriad physiological processes, understanding the underlying molecular mechanisms of Ca²⁺ level regulation has far reaching implications. The existence of SOCE through CRAC channels is vital for Ca²⁺ signaling in both excitable as well as non-excitable cells. As discussed above, the ER is a major organelle involved in Ca²⁺ storage; remarkably, this organelle also has proteins which regulate Ca²⁺ entry in other parts of the cell. Embedded on the ER membrane is STIM1, a type I transmembrane protein which interacts with Orai, on the PM, to form CRAC channels (Cahalan, 2009). STIMs function as finely tuned ER/SR Ca²⁺ sensors and CRAC channel activators (Liou et al., 2005; Zhang et al., 2005), whilst Orai subunits make up the CRAC channels which facilitate Ca²⁺ entry from the extracellular space into the cytosol (Cahalan, 2009; Gudlur et al., 2013; Ji et al., 2008; Penna et al., 2008; Soboloff et al., 2006). Interestingly, STIM1 and Orai1 were shown to play an apoptotic role in pancreatic adenocarcinoma cell lines which was further exuberated with chemotherapeutic drugs such as 5-fluorouracil or gemcitabine shown to induce SOCE. However, siRNA-mediated knockdown of STIM1 or Orai1 resulted in a marked reduction in apoptosis when used with either chemotherapeutic agent. This suggests a novel form of chemotherapeutic treatment for pancreatic cancer cells through a calcium-dependent mechanism of action (Kondratska et al., 2014).

In knockout mice lacking Orai1, SOCE was impaired in naïve CD4⁺ and CD8⁺ T-cells whereas *in vitro* differentiated cells exhibited nearly complete abolishment of SOCE and CRAC functionality resulting in compromised immune function (Shaw et al., 2012). Similarly, lymphocytes extracted from patients with primary immunodeficiencies had exhibited defective I_{CRAC}, and thus, a loss of CRAC functionality (Le Deist et al., 1995; Partiseti et al., 1994). Furthermore, heritable mutations in Orai1 (e.g. R91W) have been identified in severe combined immunodeficiency (SCID) human patients where there was

loss of CRAC functionality coupled with the reduction in cytokine production (Feske et al., 2006). Taken together, these studies using cell lines, animal models and primary cells obtained from humans with genetic defects in SOCE have emphasized the importance of STIM and Orai proteins in regulating SOCE function and CRAC channel activity in health and disease (Penna et al., 2008).

1.3.1 STIM domain organization

STIMs are essential Ca^{2+} sensors and activators of SOCE that are expressed ubiquitously throughout most eukaryotic cells. These Ca^{2+} sensors are required to maintain normal human physiology and drive pathophysiological alterations (Bergmeier et al., 2013; Cui et al., 2017; Soboloff et al., 2012). There are two human homologues that share high similarity in amino acid sequence and domain architecture, STIM1 (685 residues; NCBI Accession: NP_003147.2) and STIM2 (746 residues; NCBI Accession: NP_065911.3) (Hooper et al., 2013). As human STIM1 is a type I TM protein, it consists of two distinct regions which are separated by a single TM and where region each plays a vital role in SOCE activation and Ca^{2+} regulation. In addition to a role in SOCE, STIM2 has a major role in mediating basal Ca^{2+} homeostasis (Brandman et al., 2007). Unlike STIM1, a fraction of STIM2 is active when the ER Ca^{2+} stores are full which is probably attributed to the weaker Ca^{2+} binding affinity of STIM2 further discussed below (Brandman et al., 2007; Stathopulos et al., 2013; Zhou et al., 2009).

In the luminal N-terminal region of STIM1 downstream of the ER signaling peptide (i.e. residues 1 – 22), there are two conserved cysteine residues (Cys49 and Cys56), the canonical EF-hand (i.e. residues 63 – 96), non-canonical EF-hand (i.e. residues 97 – 128) motifs, and sterile α motif (SAM) (Hooper et al.) (i.e. residues 132 – 200) which collectively mediate the Ca^{2+} sensing function of STIMs (i.e. EF-SAM). According to the three-dimensional structure of STIM1 EF-SAM, the non-canonical EF hand and SAM region are connected through a linker region. Furthermore, this non-canonical EF-hand also forms hydrogen (H)-bonds with the canonical EF-hand and together the EF-hands form a pocket for SAM domain interactions in the presence of Ca^{2+} . In the depleted state, the canonical EF-hand loses the Ca^{2+} , STIM1 undergoes destabilization followed by

dimerization/oligomerization which initiates the SOCE process (Stathopoulos et al., 2010; Stathopoulos et al., 2009; Stathopoulos et al., 2008).

Fluorescence resonance energy transfer (FRET) and total internal reflective fluorescence (TIRF) have demonstrated that the oligomerization and translocation of STIM1 in response to luminal Ca^{2+} depletion, causes distinct STIM1 punctate aggregates to form at ER-PM junctions (Liou et al., 2005; Stathopoulos et al., 2009). Furthermore, substitution of the STIM1 EF-SAM region with FK506-binding protein, a rapamycin-binding protein and the addition of rapamycin, induce oligomerization and translocation of the STIM1 chimera (Luik et al., 2008). Conversely, complete removal of SAM prevents puncta formation at ER-PM junctions (Baba et al., 2006). These findings highlight how essential oligomerization of the N-terminal domain is for translocation of STIM1 to ER-PM junctions and activation of CRAC channels.

After the single-pass TM, the cytosolic C-terminal region of STIM1 contains three coiled-coils (i.e. CC1-CC2-CC3) that each play different roles in mediating SOCE (Stathopoulos et al., 2013). CC1 (i.e. residues 238-337), the first and longest of the three conserved domains, has an α -helical structure spanning approximately 13 nm in length (Cui et al., 2013). CC1 does not contain any of the machinery required for physically coupling to and opening of CRAC channels; however, after the transition of the cytosolic C-terminal domains to the extended conformation, the CC1 length allow STIMs to bridge the distance between the ER and the PM and physically couple with Orai1 channel subunits on the opposite membrane (Calloway et al., 2011). CC2 (i.e. residues 363-389) together with CC3 (i.e. residues 399 – 423) make up the minimal boundaries within CC domains necessary for coupling to and opening CRAC channels. This region is known as the CRAC activating domain (CAD) (Park et al., 2009), STIM-Orai activating region (SOAR) (i.e. residues 344 – 442) (Yuan et al., 2009), or cc boundary 9 (Kawasaki et al., 2009) defined by the residues 342 – 448, 344 – 442 and 339 – 446, respectively, by three independent studies. Together, the three coiled-coil domains fall within the Orai-activating STIM fragment (OASF) (i.e. residues 234-491) which are critical for mediating the compact to extended conformation of the molecule as well as coupling to and activation of Orai channels, and thus, SOCE (Fahrner et al., 2009). Mutations that occur along these CC regions can lead to pathological

diseases in humans via either persistent activation or abolishment of SOCE (Maus et al., 2015; Miederer et al., 2015).

Further downstream of CC1-CC2-CC3 is an acidic inhibitory domain (ID) (i.e. residues 470 – 491) that is involved in the Ca^{2+} dependent inactivation of STIM1, after the activation SOCE (Derler et al., 2009a). A Pro/Ser-rich region (i.e. residues 600 – 629) has several Ser residues that undergo phosphorylation and a polybasic (i.e. Lys-rich) region (i.e. residues 671 – 685) that directly interacts with PM phosphoinositides, as deleting this region disrupts STIM's ability to interact with the PM (Stathopoulos et al., 2013). Ultimately, the EF-SAM, CC regions, Pro/Ser and polybasic regions collectively enable STIM1 to undergo the multi-step process required to couple with Orai1, activate SOCE and confer a complex molecular regulation which is not fully understood.

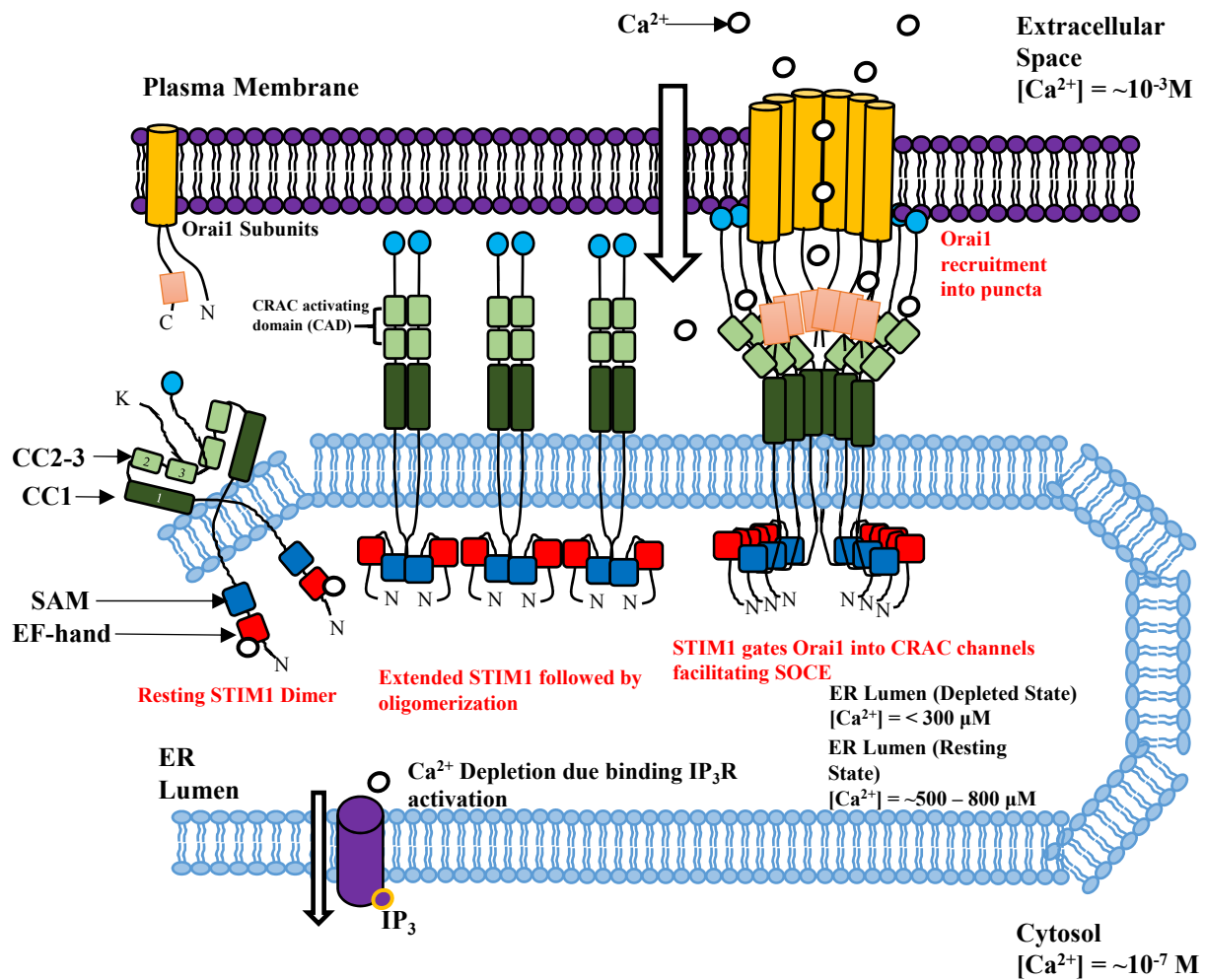


Figure 1.1. Pictorial representation of store operated Ca^{2+} entry (SOCE). When ER luminal Ca^{2+} levels are low, the N-terminal STIM1 domain dimerizes and oligomerizes. This N-terminal change results in the structural conversion of the cytosolic domains from a compact state into an extended state. What follows is coiled-coil domain oligomerization and translocation of STIM1 to the ER-PM junctions where the SOAR/CAD region of the STIM1 oligomer interacts with the N- and C-terminal domains of Orai1 to form the CRAC channel necessary for SOCE.

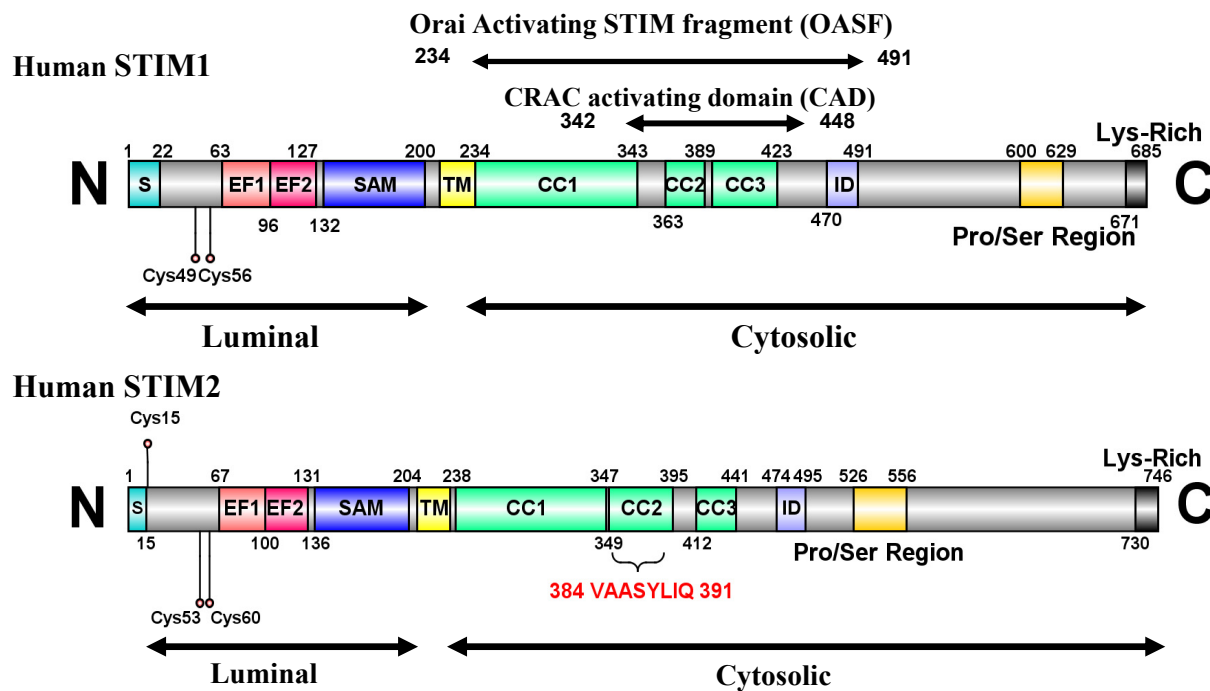


Figure 1.2. STIM1 and STIM2 domain architecture depicting the conserved domains. Human STIM1 domain architecture (upper diagram). The ER luminal side of STIM1 contains the EF-SAM region (residues ~63-200) that play a role in sensing the change in ER Ca^{2+} concentration levels. The cytosolic region consists of the OASF which contains the conserved coiled-coil domains and the CAD domain. N-terminus (N); signal peptide (S), canonical EF-hand (EF1); non-canonical (EF2); SAM (sterile α -motif domain); coiled-coil (CC1, CC1 and CC3); Pro/Ser-rich region; Lys-rich/polybasic region (Lys-Rich); carboxyl terminus (C). Human STIM2 domain architecture (lower diagram). Domain nomenclature is as per STIM1. The residue numbers bounding each domain are indicated.

Organism	Amino acid Number
H.SapiensSTIM1	-----MDVCVRLALW--LLWGPLLH-----Q 19
H.SapiensSTIM2	-----M--LVLGLLVAG-----AAD 13
H.SapiensSTIM2β	-----M--LVLGLLVAG-----AAD 13
M.MusculusSTIM1	-----M--LLFGLLVAG-----VAD 13
M.MusculusSTIM2	-----M--LLFGLLVAG-----VAD 13
M.MusculusSTIM2β	-----M--LLFGLLVAG-----VAD 13
G.GallusSTIM	----- 0
D.MelanogasterSTIM	MRKNTIWNYSLIFFCCVLKSI STL D H G P H T V S V D S N R H N T Q H Q Y K Q N P N V A S Q R H S S H E S 60
C.ElegansSTIM	----- 0
H.SapiensSTIM1	GQSLs-----HS-----HSEKATG-----TS-----SGANSE 41
H.SapiensSTIM2	GCELVPR-----HL-----RGRRTAG-----SA-ATAASSPAAAAGDS 45
H.SapiensSTIM2β	GCELVPR-----HL-----RGRRTAG-----SA-ATAASSPAAAAGDS 45
M.MusculusSTIM1	GCDLVPR-----HL-----RGRRASG-----SA-GAAASPAAAAGER 45
M.MusculusSTIM2	GCDLVPR-----HL-----RGRRASG-----SA-GAAASPAAAAGER 45
M.MusculusSTIM2β	GCDLVPR-----HL-----RGRRASG-----SA-GAAASPAAAAGER 45
G.GallusSTIM	----- 0
D.MelanogasterSTIM	GQSLHNSQS EHVTHIAASHAGSGGEHSTHLAQLNHRSSYNLLSEAMSQAVSNFESS--MG 118
C.ElegansSTIM	-----MGRVSWIIALYL-T--INVVIVV---- 20
H.SapiensSTIM1	ESTAAEFCDKIDKPLCHS--EDEKLSFEAVRN I H K L M D D D A N G D V D V E E S D E F L R E D L N Y H 99
H.SapiensSTIM2	PALMTDPCMSLSPPCFT--EEDRFSL E A L Q T I H K Q M D D D K D G G I E V E E S D E F I R E D M K Y K 103
H.SapiensSTIM2β	PALMTDPCMSLSPPCFT--EEDRFSL E A L Q T I H K Q M D D D K D G G I E V E E S D E F I R E D M K Y K 103
M.MusculusSTIM1	QALLTDP C M S L S P P C F T -- E E D R F S L E A L Q T I H K Q M D D D K D G G I E V D E S D E F I R E D M K Y K 103
M.MusculusSTIM2	QALLTDP C M S L S P P C F T -- E E D R F S L E A L Q T I H K Q M D D D K D G G I E V D E S D E F I R E D M K Y K 103
M.MusculusSTIM2β	QALLTDP C M S L S P P C F T -- E E D R F S L E A L Q T I H K Q M D D D K D G G I E V D E S D E F I R E D M K Y K 103
G.GallusSTIM	-----MDDDANGNV D V E E S D E F L R E D L N Y H 25
D.MelanogasterSTIM	SGSADGCA A D D F C Y S G S V Q D R F G M E A I A S L H R Q L D D D D N G N I D L S E S D D F L R E E L K Y D 178
C.ElegansSTIM	--NGDRVTRNV E T A E E E K I R D K L G Y E A I R D I H R M D D D H S G S I D R N E S T G F M K E D M Q M R 78
H.SapiensSTIM1	DPTVKHS--TFHGEDKLISVEDLWKAWKSSEVYNWTVDEVVQWLITYVELPQYEETFRLK 157
H.SapiensSTIM2	DATNKHS--HLHREDKKHITIEDLWKRWK TSEVHNW T L E D T L Q W L I E F V E L P Q Y E K N F R D N 161
H.SapiensSTIM2β	DATNKHS--HLHREDKKHITIEDLWKRWK TSEVHNW T L E D T L Q W L I E F V E L P Q Y E K N F R D N 161
M.MusculusSTIM1	DATNKHS--HLHREDKKHITVEDLWKQWK TSEVHNW T L E D T L Q W L I E F V E L P Q Y E K N F R D N 161
M.MusculusSTIM2	DATNKHS--HLHREDKKHITVEDLWKQWK TSEVHNW T L E D T L Q W L I E F V E L P Q Y E K N F R D N 161
M.MusculusSTIM2β	DATNKHS--HLHREDKKHITVEDLWKQWK TSEVHNW T L E D T L Q W L I E F V E L P Q Y E K N F R D N 161
G.GallusSTIM	DPTVKHS--TFHGEDKLISVEELWKAWKTSEVYNWTVDEVVQWLITYVELPQYEETFRLK 83
D.MelanogasterSTIM	SGYEKRQKAFHFNDMMHISVKELEWALRSEVHNW T I E Q T T D W L A Q S V Q L P Q Y V D L F K L H 238
C.ElegansSTIM	GSERTRRENKFKHGDDAITVDDLWEAWFES I E R T W T N E R L V E W L I N D V N L P S I V E A V K A K 138
H.SapiensSTIM1	QLSGHAMPRLAVNTTMTGTVLKMTDRSHRQK L Q L K A L D T V L F G P P L L T R H N H L K D F M L V 217
H.SapiensSTIM2	NVKGTTLPRIAVHETSPFMISQLKISDRSHRQK L Q L K A L D V V L F G P L T R P P H N W M K D F I L T 221
H.SapiensSTIM2β	NVKGTTLPRIAVHETSPFMISQLKISDRSHRQK L Q L K A L D V V L F G P L T R P P H N W M K D F I L T 221
M.MusculusSTIM1	NVKGTTLPRIAVHETSPFMISQLKISDRSHRQK L Q L K A L D V V L F G P L T R P P H N W M K D F I L T 221
M.MusculusSTIM2	NVKGTTLPRIAVHETSPFMISQLKISDRSHRQK L Q L K A L D V V L F G P L T R P P H N W M K D F I L T 221
M.MusculusSTIM2β	NVKGTTLPRIAVHETSPFMISQLKISDRSHRQK L Q L K A L D V V L F G P L T R P P H N W M K D F I L T 221
G.GallusSTIM	QLSGHAMPRLAVNNA T M M G T V L K M T D R S H R Q K L Q L K A L D T V L F G P P L L T R H N H L K D F M L V 143
D.MelanogasterSTIM	KVTGAALPRLAVNNLQYVGNVLGKDP I H K Q I S L K A M D V V L F G P P R E T G T R W - K D Y I L V 297
C.ElegansSTIM	KIDGKILPRFASPNDFLNKELGKISSVYRQKLR L N S L D V V L F G Y K D N N --NRTKDILLA 196
H.SapiensSTIM1	VSIVIGVGGCWFA Y I Q N R - Y S K E H M K K M M K D L E G L H R A E Q S L H D L Q E R L H K A Q E E H R T V E 276
H.SapiensSTIM2	VSIVIGVGGCWFA Y T Q N K - T S K E H V A K M M K D L E S L Q T A E Q S L M D L Q E R L E K A Q E E N R N V A 280
H.SapiensSTIM2β	VSIVIGVGGCWFA Y T Q N K - T S K E H V A K M M K D L E S L Q T A E Q S L M D L Q E R L E K A Q E E N R N V A 280
M.MusculusSTIM1	ISIVIGVGGCWFA Y T Q N K - T S K E H V A K M M K D L E S L Q T A E Q S L M D L Q E R L E K A Q E E N R T V A 280
M.MusculusSTIM2	ISIVIGVGGCWFA Y T Q N K - T S K E H V A K M M K D L E S L Q T A E Q S L M D L Q E R L E K A Q E E N R T V A 280
M.MusculusSTIM2β	ISIVIGVGGCWFA Y T Q N K - T S K E H V A K M M K D L E S L Q T A E Q S L M D L Q E R L E K A Q E E N R T V A 280
G.GallusSTIM	VSIVIGVGGCWFA Y I Q N R - Y S K E H M K K M M K D L E G L H R A E Q S L H D L Q E R L Q K A Q E E H R S V E 202
D.MelanogasterSTIM	TLLLSA I T G C W Y A Y Q Q N K - N A K R H L R R M A Q D M E G L Q R A E Q S L Q E M Q K E L E R A R M E Q E N V A 356
C.ElegansSTIM	FLAL--L L T S I L F L Y R Q K Q A Q Q K V N E L S N K L E L K C M E T E F E D V Q K M L N D E R S K ----- 250

	CC1	
H.SapiensSTIM1	VEKVHLEKKLRDEINLAKQEAQRLEKELREGTENERSRQKYAEELQVREALRKAKEKLE	336
H.SapiensSTIM2	VEKQNLERKMMDEINYAKEEACRLRELREGAECELSRRQYAEQLEQVRMALKKAKEKFE	340
H.SapiensSTIM2β	VEKQNLERKMMDEINYAKEEACRLRELREGAECELSRRQYAEQLEQVRMALKKAKEKFE	340
M.MusculusSTIM1	VEKQNLERKMMDEINYAKEEACRLRELREGAECELSRRQYAEQLEQVRMALKKAKEKFE	340
M.MusculusSTIM2	VEKQNLERKMMDEINYAKEEACRLRELREGAECELSRRQYAEQLEQVRMALKKAKEKFE	340
M.MusculusSTIM2β	VEKQNLERKMMDEINYAKEEACRLRELREGAECELSRRQYAEQLEQVRMALKKAKEKFE	340
G.GallusSTIM	VEKVHLEKKLQDEISIAKQEAHRLRELREGTENELSRQKYAEQLEQVRMALKNAEKELE	262
D.MelanogasterSTIM	TEKLDLERRLKEAPTLSSSNSD-----L-EVQQLKKEIEMLRNELSRAEFELV	403
C.ElegansSTIM	-----RS-----ISDGVVNHTEMENLRVQLEEAERRLE	278
	::*:*:*:*:*:*	
	CC2	
H.SapiensSTIM1	SHS-SWYAPEALQKWLQLTHEVEVQYNNIKKQNAEKQLLVAKEG-----AEKIKKKR	387
H.SapiensSTIM2	LRS-SWSVPDALQKWLQLTHEVEVQYNNIKRQNAEMQLAIAKDE-----AEKIKKKR	391
H.SapiensSTIM2β	LRS-SWSVPDALQKWLQLTHEVEVQYNNIKRQNAEMQLAIAKDEVAASLYLQAEKIKKKR	399
M.MusculusSTIM1	LRS-SWSVPDALQKWLQLTHEVEVQYNNIKRQNAEMQLAIAKDE-----AEKIKKKR	391
M.MusculusSTIM2	LRS-SWSVPDALQKWLQLTHEVEVQYNNIKRQNAEMQLAIAKDE-----AEKIKKKR	391
M.MusculusSTIM2β	LRS-SWSVPDALQKWLQLTHEVEVQYNNIKRQNAEMQLAIAKDEVAASYLLOAEKIKKKR	399
G.GallusSTIM	SHC-SWAAPPEALQKWLQLTHEVEVQYNNIKKQNAEKQLLVAKEG-----AEKIKKKR	313
D.MelanogasterSTIM	-DN-CWSPPPQLQSWLQYTYELSKNHQKKRTSAEKQLQSAREAE-----CEKLRKKR	453
C.ElegansSTIM	ANSGSQAPLALQPLLRRTCENEMAFLEKQRQDCFEMKEAIE-----VDRLQKKQ	330
	* ** * : * * * : : : : : : : * : : : : * :	
	CC3	
H.SapiensSTIM1	NTLFGTFHVAH--SSSLDDVDHKILTAKQALSEVTAALRERLHRWQQIEILCGFQIVNNP	445
H.SapiensSTIM2	STVFGTLHVAH--SSSLDEVDHKILEAKKALSELTTCLRERLFRWQQIEIKICGFQIAHNS	449
H.SapiensSTIM2β	STVFGTLHVAH--SSSLDEVDHKILEAKKALSELTTCLRERLFRWQQIEIKICGFQIAHNS	457
M.MusculusSTIM1	STVFGTLHVAH--SSSLDEVDHKILEAKKALSELTTCLRERLFRWQQIEIKICGFQIAHNS	449
M.MusculusSTIM2	STVFGTLHVAH--SSSLDEVDHKILEAKKALSELTTCLRERLFRWQQIEIKICGFQIAHNS	449
M.MusculusSTIM2β	STVFGTLHVAH--SSSLDEVDHKILEAKKALSELTTCLRERLFRWQQIEIKICGFQIAHNS	457
G.GallusSTIM	NTLFGTFHVAH--SSSLDDVDHKILTAKQALSEVTAALRERLHRWQQIEILCGFQIVNNP	371
D.MelanogasterSTIM	SSLVGFVSTH--GKSIDDVDRSIVERNALGDVTNELQERLHRWQQIEITCLGLNIVNNN	511
C.ElegansSTIM	GSLVSSLKLATGAASTSDQVDSKIFALKSRMEKIHTLRETQERWLQIESLQVPLLYLN	390
	: : : : : : : : * : * * * * : : : : : : * * * * * * : :	
H.SapiensSTIM1	GIHSLVAALNIDPSW---MGSTRPNPAHFIMTDDVDDMDEEIVSP-LSMQSPSLQSSVR	500
H.SapiensSTIM2	GLPSLTSSLYSDHSW---VVMPRVSIPPYIAGGVDDLDEDTPPI-VS-QFPG-----	497
H.SapiensSTIM2β	GLPSLTSSLYSDHSW---VVMPRVSIPPYIAGGVDDLDEDTPPI-VS-QFPG-----	505
M.MusculusSTIM1	GLPSLTSSLYSDHSW---VVMPRVSIPPYIAGGVDDLDEDTPPI-VP-QFPG-----	497
M.MusculusSTIM2	GLPSLTSSLYSDHSW---VVMPRVSIPPYIAGGVDDLDEDTPPI-VP-QFPG-----	497
M.MusculusSTIM2β	GLPSLTSSLYSDHSW---VVMPRVSIPPYIAGGVDDLDEDTPPI-VP-QFPG-----	505
G.GallusSTIM	GIHTLASALNIDPGW---MGTRPNPNSHFIMTDDVDDLEEIVSP-MSMQSPALPSTVR	426
D.MelanogasterSTIM	GLPYLENVLYGRNGGLQSSMGMSSTKGSRARITNSTEDLDEESIQKLNLENFSLATE-	570
C.ElegansSTIM	GKFRQ-----	395
	*	
H.SapiensSTIM1	QRLTEPQHGLGSQRDLTHSDSESSLH-MS-D--RQ-----RV	533
H.SapiensSTIM2	-TMAKPPGSLARSS--SLCRSRRSIVPSSPQRAQLAPHAPHSPHPRHPHPQHTPHSL	554
H.SapiensSTIM2β	-TMAKPPGSLARSS--SLCRSRRSIVPSSPQRAQLAPHAPHSPHPRHPHPQHTPHSL	562
M.MusculusSTIM1	-TVAKPAGSLARSS--SLCRSRRSIVPSSPQSQRAQLPAHAPLAAHPRHPHPQHPQHSL	554
M.MusculusSTIM2	-TVAKPAGSLARSS--SLCRSRRSIVPSSPQSQRAQLPAHAPLAAHPRHPHPQHPQHSL	554
M.MusculusSTIM2β	-TVAKPAGSLARSS--SLCRSRRSIVPSSPQSQRAQLPAHAPLAAHPRHPHPQHPQHSL	562
G.GallusSTIM	QRLVDPQHGHGSQRDLTRCDESSIPHLS-E--AQ-----RL	460
D.MelanogasterSTIM	-----	570
C.ElegansSTIM	-----	395
H.SapiensSTIM1	APKPP-----QMSRAADEALNAMTNSNGSHRLIEGVHPGSLVEK-----LPDSPA	577
H.SapiensSTIM2	PSPDDPILSVSSCPALYRNEEEEEAIYFS---AEKQWEVPDTASECDLNSSIGRKQSP	611
H.SapiensSTIM2β	PSPDDPILSVSSCPALYRNEEEEEAIYFS---AEKQWEVPDTASECDLNSSIGRKQSP	619
M.MusculusSTIM1	PSPDDPILSVSSCPALYRNEEEEEAIYFT---AEKQWEVPDTASECDLNSSSGRKQSP	611
M.MusculusSTIM2	PSPDDPILSVSSCPALYRNEEEEEAIYFT---AEKQWEVPDTASECDLNSSSGRKQSP	611
M.MusculusSTIM2β	PSPDDPILSVSSCPALYRNEEEEEAIYFT---AEKQWEVPDTASECDLNSSSGRKQSP	619
G.GallusSTIM	PSAAPKLAAR--PALLTRSIEDAVPGHTPNGGSRHAEPGPPE-----PSESPS	508
D.MelanogasterSTIM	-----	570
C.ElegansSTIM	-----	395

Figure 1.3. Multiple amino acid sequence alignment of STIMs from lower to higher order organisms. *Homo sapiens* STIM1 (Accession: AFZ76986.1), *H. sapiens* STIM2 (Accession:NP_065911.3), *H. sapiens* STIM2 β (Accession: NP_001162589.1), *Mus musculus* STIM1 (Accession: NP_033313.2), *M. musculus* STIM2 (Accession:NP_001074572.2), *M. musculus* STIM2 β (Uniprot:F6WBP9), *Drosophila melanogaster* STIM (Accession:NP_523357.2), *Gallus gallus* STIM (Accession:NP_001026009.1), *Caenorhabditis elegans* STIM (Accession:NP_001022916.1). Residues that are fully conserved, highly conserved, and partially conserved are indicated with (*), (:), and (.), respectively, under the alignment. Residues colour code in accordance to amino acid properties: acidic (blue), basic (pink), polar uncharged (green) and hydrophobic (red). Sequence alignment was performed using Clustal Omega. Each domain is shaded as per Figure 1.2.

1.3.2 Orai organization

Orai1 is the subunit component that, when recruited by STIM1, assembles into Ca²⁺-selective CRAC channels which mediate SOCE and cytosolic Ca²⁺ flux. The high-resolution structure of the human Orai homologue assembly has remained elusive. Fortunately, previous studies, through X-ray crystallography, have resolved an Orai homologue crystal structure of *D. melanogaster* sharing high sequence similarity (> 70%) with human Orai1 within the transmembrane (TM) region (Cai, 2007). The crystal structure has shown that a single Orai channel exhibits a hexameric quaternary structure (Hou et al., 2012; Ji et al., 2008; Maruyama et al., 2009; Penna et al., 2008). Sequence analysis and the structure has shown that Orai is composed of four major TM helices (i.e. M1-M4). These four TM helices are arranged in concentric rings whereby the innermost core consists of M1 from each of the six subunits (Hou et al., 2012). M2 and M3 immediately surround M1, with the M1 helix extending through the lipid bilayer into the cytosol. The M2 and M3 arrangement in surrounding M1 implies a role in promoting subunit structural integrity. Finally, the M4 helix, forming the outermost layer, extends into the cytosol and is kinked so that a C-terminal extension runs parallel to the plane of the inner PM leaflet. The extended C-terminal part of M4 interacts antiparallely with a neighboring extended M4 helix, which also adopts a kink which extends in the opposite direction. Ultimately, the gross structure of Orai shows the innermost pore exhibiting a six-fold symmetry, while the peripheral region exhibits a threefold symmetry due to pairwise M4 coiled-coil interactions (Enomoto et al., 2017).

Both the N- and C-termini of Orai face the cytosol and interact with the CAD domain of STIM1. The Orai N- and C-termini interactions with the CAD domain are involved in recruitment of the channel subunit and gating of the pore (Frischauf et al., 2009; Muik et al., 2009; Stathopoulos et al., 2013). There are three Orai human homologues: Orai1, Orai2, and Orai3. All Orai homologues contain highly conserved TM regions (i.e. M1-M4) and linker regions as well as acidic and basic residues required for Ca²⁺-selectivity and permeability. All three Orai homologues can be activated by STIM1 and exhibit varying biophysical properties depending on the STIM1:Orai combination in specific cell types (Frischauf et al., 2009). Interestingly, a missense mutation (i.e. R91W) in human Orai1

resulting in a loss of Ca^{2+} entry via CRAC channels causes a heritable form of SCID (Derler et al., 2009).

1.3.3 Modifications to STIM

SOCE activation is a methodical multi-step process culminating in STIM1:Orai1 coupling. As highlighted previously, STIM1 is the major Ca^{2+} sensor in the ER/SR which ultimately gates CRAC channels and facilitates Ca^{2+} entry into the cytosol. Through the EF-SAM domain, STIM1 senses changes in luminal Ca^{2+} concentration via Ca^{2+} binding or release while the OASF region with the three CC domains controls the conformational extension on the cytosolic side of the molecule and directly interacts with Orai subunits embedded in the PM (Stathopoulos et al., 2013).

When Ca^{2+} levels in the ER/SR lumen are high, Ca^{2+} is bound to the EF-SAM domain of STIM1 keeping it in a dormant, inactive state. The drop of Ca^{2+} concentration mediated by IP₃R channels, results in a loss of Ca^{2+} from EF-SAM leading to a conformational change which propagates throughout the molecule. First, dimerization and/or oligomerization of the N-terminal domain occurs; second, this oligomerization promotes a transition within the CC region of the cytosolic side of the molecule from a compact to extended state (Muik et al., 2011); finally, the oligomerized/conformationally extended molecule translocates to the ER-PM junctions. At ER-PM junctions, STIM1 recruits Orai1 subunits to form the CRAC channel complex (Stathopoulos et al., 2013). Active CRAC channels can also be deactivated by the previously mentioned ID region downstream of CC3 (i.e. 470 – 491) within STIM1 in a process known as Ca^{2+} dependent inactivation (CDI) (Derler et al., 2009; Mullins et al., 2009; Roos et al., 2005; Soboloff et al., 2006). Additionally, CaM has been found to inhibit SOCE via interaction with the polybasic domains of STIM1 and STIM2, preventing translocation to ER-PM junctions (Bauer et al., 2008; Calloway et al., 2011; Singh et al., 2002; Walsh et al., 2009; Yuan et al., 2009).

The luminal domain destabilization and subsequent conformational extension of STIM1 in response to ER/SR luminal Ca^{2+} depletion are integral steps in SOCE. Thus, in-depth studies have investigated the modifications that affect STIM1 stability revealing important mechanistic insights into STIM1 activation. Within the luminal domain of STIM1 are

modifiable residues that modulate the stability of EF-SAM, and thus, the activation of SOCE (Gui et al., 2018; Stathopoulos et al., 2009; Zhu et al., 2018). The *S*-nitrosylation of Cys49 and Cys56 in STIM1 increased thermodynamic stability of the luminal domain which resulted in suppressed hydrophobic exposure and a loss of Ca²⁺ depletion-dependent oligomerization (Zhu et al., 2018). Furthermore, *N*-glycosylation of Asn131 and Asn171 sites lead to the decreased Ca²⁺ binding affinity, reduced stability and enhanced oligomerization in response to ER Ca²⁺-depletion. In human embryonic kidney (HEK) 293 cells co-expressing Orai1 and STIM1, blocking Asn131 and Asn171 *N*-glycosylation sites diminishes SOCE, suggesting these sites enhance the EF-SAM destabilization-coupled oligomerization in response to ER Ca²⁺-depletion (Choi et al., 2017). These results show that these modifiable sites on the EF-SAM domain act as robust ON/OFF regulators of SOCE.

Modifications in the STIM CC regions can lead to a loss of Ca²⁺ homeostasis which give rise to various pathologies such as Stormorken Syndrome (i.e. R304W) which is the result of SOCE upregulation (Misceo et al., 2014; Morin et al., 2014; Noury et al., 2017) or SCID-like syndrome (i.e. R429C) due a reduction in SOCE activity (Maus et al., 2015). Still, modifications in the CC region can also act as a regulatory means for cells to control SOCE. One such example occurs through the phosphorylation of residue T389 that results in a selective inhibition of STIM and activation of store-independent arachidonic acid-activated (ARC) channels. ARC channels function differently from CRAC channel in that they activate independent of Ca²⁺ store depletion and are comprised of both Orai1 and Orai3 subunits (Thompson et al., 2015; Thompson et al., 2018). Recently, it was discovered that alternative splicing is a viable means of SOCE regulation; an 8-amino acid residue (i.e. referred to as the 2β insert in this thesis) spliced into exon 9 generates a STIM2 variant that can also inhibit SOCE (Miederer et al., 2015; Rana et al., 2015). Both phosphorylation and alternative splicing are fascinating features that enable cells to regulate SOCE. Alternative splicing and the R304W and R429C mutations are discussed in more detail below.

1.4 STIM2 is a basal modulator of SOCE

While STIM1 is a prominent activator of SOCE through dynamically changing its conformation and gating CRAC channels, STIM2 plays an important role in maintaining the basal luminal and cytosolic Ca^{2+} concentration, also by interacting with Orail-composed channels. The importance of tight control of basal Ca^{2+} concentration is emphasized by the various diseases that are associated to prolonged increased or decreased basal Ca^{2+} concentration (Brandman et al., 2007). Diseases associated with basal Ca^{2+} imbalance include endothelial dysfunction, kidney disease, cardiac dysfunction and neurodegenerative diseases such as Huntingtons and Alzheimers diseases (Schulman et al., 2005; Ter Keurs et al., 2007; Thebault et al., 2006). Indeed, a genetic inheritable mutation found in presenilin from Alzheimer patients is associated with defects in Ca^{2+} homeostasis due to changes in Ca^{2+} flux out of ER Ca^{2+} stores (Tu et al., 2006). Basal Ca^{2+} imbalance also associated with altered protein degradation and transcription that can affect intracellular signaling and thus the overall cell health (Berridge et al., 2003; Spira et al., 2001). In T-cells and fibroblasts, STIM2 is highly upregulated after stimulation of T-cells and allows for prolonged long-term Ca^{2+} signaling allowing ER Ca^{2+} levels to remain high which prevents an ER stress response whilst driving long term SOCE influx (Collins et al., 2011; Oh-Hora et al., 2008).

STIM2 can induce Ca^{2+} influx by interacting with Orail in a store-dependent or store-independent manner though its mechanism of activation which remains incompletely understood. One distinguishing factor between the STIM homologues is the EF-SAM Ca^{2+} sensitivity. Based on ER Ca^{2+} concentration estimates required for puncta formation, the STIM1 dissociation equilibrium constant (K_d) is $\sim 200 \mu\text{M}$ whereas STIM2 exhibits a relative functional K_d of $\sim 400 \mu\text{M}$ Ca^{2+} (Brandman et al., 2007). These data are in-line with previous K_d measurements of EF-SAM which suggest STIM2 has a relatively weaker Ca^{2+} affinity compared to STIM1 EF-SAM (Brandman et al., 2007; Stathopoulos et al., 2009; Zheng et al., 2008). Thus, STIM2 becomes Ca^{2+} depleted at higher ER luminal Ca^{2+} levels compared to STIM1. Interestingly, in cells where both proteins are present, the difference in STIM2 Ca^{2+} affinity implies that it is more suited as a feedback modulator to keep basal Ca^{2+} cytosolic and ER Ca^{2+} within a tight range. This idea is supported given that knocking

down STIM2 in HeLa, HUVEC and HEK293 cells selectively lowered overall basal cytosolic and ER Ca^{2+} concentrations whereas knocking down STIM1 in the same cell types had a less pronounced effect on basal Ca^{2+} levels (Brandman et al., 2007). Furthermore, STIM2 is present at lower levels relative to STIM1 in most human tissues, exhibits lower relative activity and responds to smaller changes in Ca^{2+} concentration when expressed and measured in HEK293 cells (Parvez et al., 2008).

While the majority of STIM2 is localized on the ER membrane, a secondary functional form of STIM2, pre-STIM2, may accumulate as a full-length pre-protein in the cytosol. Pre-STIM2 is found embedded in the inner leaflet of the PM and in the cytosol where it can interact with Orai1 to regulate basal Ca^{2+} concentrations and Ca^{2+} dependent gene transcription in an ER Ca^{2+} -independent manner (Graham et al., 2011).

1.5 Mutating the CC regions alter SOCE functionality

The cytosolic CC regions facilitate direct STIM interactions with PM Orai subunits. Modifications in the CC region can lead to a drastic change in Ca^{2+} homeostasis as the ability of STIM to interact with Orai can become constitutive or severely hindered. One major type of modification are missense point mutations. Missense mutations are point mutations where a single nucleotide is altered such that the codon is translated into a completely different amino acid. In STIM, changing specific amino acids due to missense mutations on the CC region have been shown to alter SOCE activity.

The Arg309Trp (R304W) mutation gives rise to an autosomal dominant disorder known as Stormorken Syndrome characterized by phenotype that includes profuse bleeding due to thrombocytopenia, aggregate tubular myopathy and miosis (Noury et al., 2017). Stormorken syndrome patients experience a gain-of-function where their STIM1 exhibits hyper-activation independent of luminal Ca^{2+} levels leading to upregulated SOCE. R304 of STIM1 is localized within the CC1 domain and is thought to form a salt bridge with E318 while simultaneously forming a hydrogen bond with the main oxygen atom of Q314 within this coiled-coil. By substituting in tryptophan, the salt bridge and hydrogen cannot be formed which effectively prevents the inhibitory helix from keeping the CAD domain

of STIM1 in its dormant state when ER Ca^{2+} levels are replete (Fahrner et al., 2018; Morin et al., 2014; Shen et al., 2012; Yang et al., 2012).

Conversely, Arg429Cys (R429C) has been associated with severe combined immunodeficiency (SCID)-like syndrome which is characterized by the inability to activate CD4^+ and CD8^+ in response to acute viral infections. This inability to activate immune cells is attributed to the severe abolishment of SOCE. R429 is localized on CC3 of the STIM1 cytosolic domains, and the substitution from Arg to Cys destabilizes the CC3. Interestingly, the mutation impairs cytoplasmic STIM1 oligomerization which abolishes STIM1-Orai1 interactions in fibroblast and T-cells despite being able to localize to the ER-PM junctions (Maus et al., 2015). Given that STIM1 cannot recruit Orai1 to form functional CRAC channels, SOCE is abolished which hinders the immune response.

1.6 Alternative splicing of STIM2

Alternative splicing is a regulated process that occurs in eukaryotes in which a single gene can code for multiple protein isoforms. Unlike mutations that occur at the nucleotide level resulting in gain or loss of functions, alternative splicing occurs during post transcriptional modifications, generating a new type of protein. During post transcriptional modification, exons from a gene can be spliced in or out of the processed messenger RNA (mRNA). Consequently, the proteins translated from the alternatively spliced mRNAs will have varying amino acid sequences and thus, also have varying biological functions. What makes alternative splicing so vital is that it has allowed the human genome to synthesize more proteins than would otherwise be possible from the ~20,000 genes, thereby expanding the human proteome (Graveley, 2001; Kim et al., 2014).

Alternative splicing can determine the intracellular localization, protein stability, and binding properties of many proteins. In intracellular localization, alternative splicing can influence localization of protein in various subcellular sites and organelles. Often, this mechanism is used for receptor molecules to regulate their retention in membrane-enclosed compartments. For example, a dopamine D2 receptor splice variant is retained more efficiently in the ER compared to other dopamine isoforms which reduces the overall dopamine D2 activity (Chan et al., 2001). By including alternative protein domains, the

overall half-life of protein can be regulated. An alternative form of human thyroperoxidase, an enzyme expressed in the thyroid which oxidizes iodine atoms, exhibits a reduced half-life and is very abundant in Grave's disease (Niccoli-Sire et al., 2001). Additionally, the effect of alternative splicing can alter the binding affinity of a protein (Kelemen et al., 2013). Generally, isoforms that exhibit a complete loss in ligand binding have a dominant-negative effect over isoforms still able to bind biological ligands (Kelemen et al., 2013). Alternative splicing of thyroid stimulating hormone (TSH) receptors (TSHR) generates a variant that is unable to bind TSH. These TSHR variants are often linked with TSH-secreting tumors and yield severe insensitivity to TSH (Ando et al., 2001). Alternative splicing can also affect the ligand specificity of a receptor such as in fibroblast growth factor receptor gene (FGLR)-2 that generates two isoforms differing by 49 amino acids on the extracellular domain. Whether or not the domain is present, dictates if the receptor binds both the fibroblast and keratinocyte growth factors or just the fibroblast growth factor (Miki et al., 1992).

1.7 STIM splice variants

STIM1 and STIM2 can be regulated at the transcriptional level through alternative splicing, generating novel isoforms from a single STIM1 or STIM2 gene. STIM1L is a longer splice variant generated by alternative splicing of the STIM1 gene and is expressed in human and mouse skeletal muscles (Horinouchi et al., 2012). STIM1L was initially thought to play a role in the quick activation of SOCE to induce sustained ER Ca^{2+} store refilling during intensive muscle stimulation since it was shown to be pre-clustered (Darbellay et al., 2011). Contrary to this view, it was found that STIM1L can recruit and activate PM Orai1 channels in a store-dependent manner without remodeling the ER cisternae as seen for STIM1. The ability to remodel the ER cisternae during SOCE activation is attributed to the polybasic C-terminal region (i.e. residues 671 – 685) involved in STIM1 binding to phosphoinositides. Despite STIM1L having the same lysine-rich region, the inability to expand the ER cisternae suggest that STIM1L does not mediate rapid SOCE like STIM1 but can trap and gate Orai1 subunits without remodeling the ER cisternae (Sauc et al., 2015). Previous studies have shown that STIM1L can also interact with transient receptor potential canonical (TRPC) channels, which are all activated downstream of the IP_3

pathway. TRPC channels are non-selective channels with some preference for mediating Ca^{2+} flux (Horinouchi et al., 2012). TRP channels are effectors of a variety of external sensations such as temperature, taste, pressure and vision (Brauchi et al., 2006; Levine et al., 2007; Vriens et al., 2014). STIM1L appears to be a specialized molecule which forms a pre-existing site of contact compared to the more versatile STIM1 capable of remodeling the ER during Ca^{2+} signaling.

Through the retaining of exon 9, STIM2 can be alternatively spliced into the STIM2 β isoform. STIM2 β has an extra 8-residue insertion (VAASYLIQ) near the end of CC2 called the 2 β insert that is absent in other isoforms of STIM and is the first STIM isoform shown to inhibit SOCE (Miederer et al., 2015; Rana et al., 2015). An amino acid sequence comparison across higher to lower order species (i.e. *C. elegans* to *H. Sapiens*) show that this 2 β insert is present only in vertebrates (Figure 1.2). Inducing mutations along the 2 β insert reduces the inhibitory activity of STIM2 β (Rana et al., 2015), implying the conservation of the 2 β insert sequence is critical for STIM2 β to exert its inhibitory effects. Inclusion of this insert prevents STIM2 β from recruiting Orai1 in response in Ca^{2+} depletion. Expression of STIM2 β in HEK293 cells shows that STIM2 β cannot activate Orai1 channels. Further, the mechanism by which STIM2 β can exert an inhibition on SOCE even in the presence of other co-expressed STIM isoforms without interacting with Orai1 remains unclear. When STIM2 β is heterodimerized with STIM1, it can be localized to ER-PM junctions and interact with Orai1 subunits (Rana et al., 2015). Thus, it is possible the STIM1:STIM2 β heteromeric interaction could play a role in the inhibitory activity of STIM2 β . Ultimately, alternative splicing is a form of largely unexplored SOCE regulation serving to balance and regulate activation and inhibition.

1.8 Rationale

The STIM-Orai system is central to Ca^{2+} signaling processes in health and disease. STIM1 is a major activator of SOCE and contains two distinctly functioning regions. The luminal domain region is responsible for Ca^{2+} sensing while the cytosolic domain region enables the oligomerization, translocation as well as interactions with Orai1. Thus, the cytosolic domains contain the machinery essential for CRAC channel activation. Although the

functions that the various STIM1 domains play in activating SOCE have been identified, the precise effects of the 2 β insert on the molecular mechanisms of SOCE regulation remains poorly understood. Given that mutations within the CC region of STIM1 profoundly change the biophysical properties of STIM1 which affect interactions with Orai1 activity (Maus et al., 2015; Morin et al., 2014; Thompson & Shuttleworth, 2015), I predict that the 2 β insert will also dramatically affect the CC region biophysical properties critical to the function of the molecule.

Some of these mutations directly hinder STIM1:Orai1 coupling after normal Ca²⁺-sensing, oligomerization, conformational extension and interactions with the PM (i.e. R429C). Similarly, the STIM2 β isoform does not appear to couple with Orai1. Thus, the 2 β insert in the CC region of STIM2 may alter the structural conformation of OASF which prevents STIM2 β localizing to the ER-PM junctions and gating of the Orai-composed Ca²⁺ channels. Remarkably, however, despite the inability to directly bind Orai, STIM2 β can still elicit an inhibitory action on SOCE, which is why I hypothesize that alternative splicing at the transcriptional level of STIM2 has an important regulatory role. This inhibition mechanism of STIM2 β remains poorly understood and represents a major knowledge gap in the field. Given that STIM2 is known to be basal modulator of luminal and cytosolic Ca²⁺, STIM2 β likely also plays a role in basal Ca²⁺ regulation.

1.9 Hypothesis and Research Aims

Hypothesis: I hypothesize that the 2 β insert (VAASYLIQ) within the OASF STIM1₂₃₄₋₄₉₁ and STIM2₃₂₅₋₅₈₃ (subscripted numbers represent the residue range) will perturb the CC conformation, structure, stability and dynamics commensurate with the ability to activate SOCE.

Aim 1: To introduce STIM1 and STIM2 2 β insert (VAASYLIQ) mutations into pET-28a recombinant STIM1₂₃₄₋₄₉₁ and STIM2₃₂₅₋₅₈₃ expression vectors and isolate high levels of homogeneous OASF proteins for subsequent structural and biophysical analyses.

Aim 2: To investigate the effects of the 2 β insertion on the *i*) structure, *ii*) association propensity and *iii*) Ca²⁺ sensitivity of STIM1 and STIM2 OASF, and to probe how structural and biophysical perturbations caused by the 2 β insert alter the mechanisms of full-length STIM-mediated SOCE. Since high-resolution structures of the STIM1 CC region, but not STIM2, are available, and given the high sequence conservation between the STIM1 and STIM2 CCs (i.e. >70% sequence similarity) (Zheng et al., 2008), we will use STIM1 as a helpful surrogate to study the structural, biophysical and biochemical effects of the 2 β insert. Considering the high sequence conservation of the CC region among all STIM homologues and isoforms (Figure 1.2), understanding the structural, biophysical, and biochemical consequences of 2 β insert incorporated into both STIM1 and STIM2 OASF will reveal insights into the molecular mechanisms of STIM function as well as the factors which contribute to dysfunctional SOCE and disease.

Chapter 2: Methods

2.1 Generation of the STIM2 OASF pET-28a recombinant vector

In order to assess the biophysical effects of the 2 β insert on STIM conformation, the OASF of STIM2 (residues 325-583; NCBI Accession: NP_065911.3) was first cloned into a pET-28a expression vector that was previously successful in the expression of the OASF region of human STIM1 (Muik et al., 2011). The generation of the STIM1-OASF (residues 234-491; NCBI Accession: NP_003147.2) pET-28a vector was completed in a previous study (Muik et al., 2011) and was used again in my study to assess the biophysical effects of 2 β insert on STIM1 OASF.

The *H. sapiens* STIM2 OASF region was subcloned from a pCMV6-STIM2 (residues 1-746) template into a pET-28a recombinant vector using NheI and XhoI restriction sites. A 100 μ L PCR solution mixture containing the NheI and XhoI restriction sites at the 5' and 3' ends, respectively, was prepared using 75 μ L dH₂O, 20 μ L 5 \times high fidelity (HF) buffer (Thermo Fisher Scientific), ~30 ng of pCMV6-STIM2 template, ~500 ng forward, ~500 ng reverse primer, 2.0 μ L of 10 mM dNTPs and 1.0 μ L Phusion DNA polymerase (Thermo Fisher Scientific). The PCR mixture was amplified in a thermal cycler (Eppendorf[®] Mastercycler) using the parameters detailed in Table 2.2.

The final PCR product was electrophoresed at 125 V for 50 min on a 1.5 % (w/v) agarose gel submerged in 0.5 \times TRIS, acetic acid and ethylene diamine tetra acetic acid (TAE) buffer. Moreover, to assess the band size of the PCR product, 2 μ L of DNA ladder (GeneRuler 1kb Plus, Thermo Fisher Scientific) was loaded into a separate lane. The agarose gel was submerged in 0.5 μ g mL⁻¹ ethidium bromide (EtBr) solution and allowed to shake at room temperature for 30 min. The gel was subsequently visualized under UV light (302 nm). The STIM2 OASF DNA insert encoding residues 325-583 and corresponding to ~774 basepairs (bp) was excised and transferred into a separate Eppendorf[®] tube. The DNA was extracted from the gel using GeneFlow Gel/PCR purification kit according to the manufacturer's protocol.

NheI and XhoI double digestions of the insert and target vector (i.e. pET-28a) were separately performed to generate compatible sticky end overhangs. The digestion mixtures were prepared in two individual Eppendorf® tubes. The first tube contained 35 µL of the STIM2 OASF insert (i.e. STIM2₃₂₅₋₅₈₃), 4.1 µL CutSmart buffer and 0.5 µL of each restriction enzyme (NheI and XhoI restriction enzymes). The second tube contained 7.5 µL pET-28a vector (~1 µg DNA), 2 µL CutSmart buffer, 1 µL of each restriction enzyme and 8.5 µL dH₂O. Both digestion mixtures were incubated overnight at 37 °C. The digested DNA samples were subsequently separated on an 1.5% (w/v) agarose gel, stained with 0.5 µg mL⁻¹ EtBr and visualized under UV light. The digested DNA bands containing the STIM2₃₂₅₋₅₈₃ insert and pET-28a vector with compatible sticky ends were extracted from excised gel fragments using the GeneFlow Gel/PCR kits.

The digested STIM2 OASF insert was ligated into the pET-28a recombinant vector by combining 4.5 µL dH₂O, 3.0 µL of the digested pET-28a vector, 10 µL of digested STIM2, OASF insert and 2 µL of 2× T4 DNA ligation buffer (New England Biolabs) into an Eppendorf tube. The mixture was heated at 42 °C for 2 min, subsequently chilled on ice for 1 min and supplemented with 1 µL of T4 DNA ligase (New England Biolabs). The ligation mixture was incubated in a water bath at 16 °C for ~16 h. Subsequently, the ligated DNA was transformed into DH5α *E. coli* by mixing 7.5 µL of the ligation product with 100 µL cells. The cells were incubated on ice for 60 min and subsequently heat shocked at 42 °C for 45 s. The heat shocked cells were subsequently transferred into 900 µL of Luria-Bertani (LB) broth contained within a 15 mL Falcon tube. The Falcon tube was incubated at 37 °C with constant shaking at 200 rpm. After 90 min, the LB broth was transferred into an Eppendorf tube and centrifuged at 10,000 ×g for 10 min. The resulting cell pellet was resuspended in ~100 µL LB and plated on an agar plate containing 60 µg mL⁻¹ kanamycin. The plate was incubated overnight in a 37 °C air incubator.

The resultant colonies were screened for the presence of the pET-28a vector containing the STIM2₃₂₅₋₅₈₃ insertion by PCR. Colonies were individually suspended in 20 µL of dH₂O. 5 µL of this “colony solution” was added to 10 µL of 2× Taq Frogga Master Mix (Froggabio), ~250 ng T7 forward primer, ~250 ng T78 reverse primer and 4 µL dH₂O. The mixture was subjected to 25 cycles of PCR as detailed in Table 2.2. The mixture was

subsequently separated by gel electrophoresis on a 1.5% (w/v) agarose gel at 125 V for 50 min and stained in 0.5 $\mu\text{g mL}^{-1}$ EtBr. Colonies that yielded the expected band size assessed using the PCR screening approach (i.e. ~ 900 bp) were subsequently grown in 5 mL of LB broth containing 60 $\mu\text{g mL}^{-1}$ of kanamycin overnight at 37 °C with constant shaking at 200 rpm. The following day, the pET-28a plasmids with the STIM2₃₂₅₋₅₈₃ insertion were isolated from the 5 mL liquid culture using the Presto Mini Plasmid Kit (Geneaid) in accordance to the manufacturer protocol. The isolated pET-28a-STIM2-OASF vectors were confirmed to contain the STIM2₃₂₅₋₅₈₃ OASF insertion in the correct reading frame by DNA sequencing (Robarts DNA Sequencing Facility, London, ON).

2.1.1 PCR mutagenesis for incorporation of the 2 β insert into the STIM1 and STIM2 OASF pET-28a recombinant vectors

To facilitate the 2 β insert into *H. sapiens* STIM1-OASF and *H. sapiens* STIM2-OASF, a global sequence alignment using Clustal Omega was performed comparing the position of 2 β insert on STIM2 β and its absence in the other STIM homologues. Two sets of complementary primers were designed after the correct residues positions were determined at the nucleotide level for both STIM1-OASF and STIM2-OASF. The primers were synthesized by Sigma-Aldrich using a 0.025 μmol scale and cartridge purification (see Table 2.1).

PCR-mediated mutagenesis was used to incorporate the 2 β insertions into the pET-28a STIM1- and STIM2-OASF vectors. A 20 μL PCR solution mixture was created using 13.8 μL dH₂O, 4 μL 5 \times HF buffer (Thermo Fisher Scientific), ~ 75 ng of the vector template, ~ 125 ng forward or reverse primer, 1.0 μL DMSO, 0.5 μL of 10 mM dNTPs and 0.5 μL Phusion DNA polymerase (Thermo Fisher Scientific). At this stage, each primer was kept in a separate PCR tube (i.e. one reaction with the forward and one reaction with the reverse primer). The two PCR mixtures for each of the STIM1 and STIM2 OASF vectors were placed into a LifeECO thermocycler (BioER) and subjected to an initial 10 cycles of PCR as detailed in Table 2.2. After the 10 cycles, the two mixtures were pooled together for a total volume of 50 μL and subjected to another 25 cycles with the parameters highlighted in Table 2.2.

As a first check of whether the mutagenesis was successful, a 1.5 % (w/v) agarose DNA gel was used to confirm the PCR amplification of the vectors. A 15 μ L aliquot was taken from the mixture and loaded onto a 1.5 % (w/v) agarose gel along with an equal amount of unamplified of vector template acting as a control and 2 μ L DNA ladder (GeneRuler 1kb Plus, ThermoFisher) to assess the PCR product size. Upon confirmation of vector amplification via increased band intensity over vector control amount, 0.3 μ L DpnI (New England BioLabs) was added to the remaining 25 μ L of PCR product and incubated for 2 h 30 min at 37 °C in an air incubator to digest the methylated template plasmid DNA.

The PCR-amplified, unmethylated mutant plasmid was subsequently transformed into DH5 α *E. coli* as described in Section 2.1.1. The following day, resultant colonies were selected and transferred into 5 mL of LB for overnight culture. The following day, a mini-prep using the Presto Mini Plasmid kit (Geneaid) was performed to isolate the mutated plasmid. The isolated plasmids were sequenced at the Robarts DNA Sequencing facility to confirm the correct insertion-mutation was incorporated at the nucleotide level. The sequencing results confirmed that the 2 β insertion was incorporated in the correct frame in both the pET-28a-STIM1-OASF and pET-28a-STIM2-OASF vectors (Figure 2.1).

2.1.2 PCR mutagenesis for incorporation of the 2 β insert into the full-length monomeric cherry fluorescence protein (mCh)-STIM1 and mCh-STIM2 pCMV6 vectors

The 2 β insertions were incorporated into pCMV6 vectors encoding full-length STIM1 and STIM2 proteins each fused to mCh (i.e. pCMV6-mCh-STIM1 and pCMV6-mCh-STIM2) essentially as described in Section 2.1.1 with modifications as described below. These mammalian expression vectors were from previously published work on STIM1 and STIM2 (Stathopoulos et al., 2008; Zheng et al., 2011). For these pCMV6-mCh-STIM vectors, 20 μ L PCR solution mixture was created using 14.65 μ L dH₂O, 4 μ L 5 \times HF buffer (Thermo Fisher Scientific), ~30 ng template pCMV6-mCh-STIM template, ~125 ng forward or reverse primer, 1.0 μ L DMSO, 0.5 μ L of 10 mM dNTPs and 0.25 μ L Phusion DNA polymerase (Thermo Fisher Scientific). Thermocycling was performed for an initial 10 cycles of PCR as detailed in Table 2.2. The two mixtures for each of pCMV6-mCh-

STIM1 and mCMV6-mCh-STIM2 were subsequently combined for a total volume of 50 μ L each and subjected to another 25 cycles of PCR as detailed in Table 2.2.

Methylated template DNA digestion, transformation into DH5 α *E. coli*, colony picking, plasmid propagation and purification was performed as described in Section 2.1.1 for the pET-28a-STIM-OASF vectors with the exception that ampicillin was used as the selection pressure in LB-agar plates (i.e. 100 μ g ml⁻¹). The final pCMV6-mCh-STIM1 and pCMV6-mCh-STIM2 vectors harboring the 2 β insertions were confirmed by sequencing at the Roberts DNA sequencing facility using the in-house designed primers targeting the OASF regions of the full-length STIM1 and STIM2 DNA sequences carried in the pCMV6 vectors (see Table 2.1).

Table 2.1: Oligonucleotide primers used in the research described in this study (Sigma-Aldrich St. Louis, MO)

Primer	Sequence
pET- 28a	5 – TTTGCTTATGCTAGCAATAAGACATCAAAAGAAC – 3 NHE I
STIM2	5- GGTTTAGCCTCGAGTCAGGGAAAATTGTGACACTATTGG – 3 XHOI
OASF^(a)	
pET- 28a	5 - CTGGTGGCCAAGGAGGGGGTTGCTGCTTCATATCTGATTGAGGCTGAGAAGATAAAAAAG – 3
STIM1 2β	3 - CTTTTTATCTTCTCAGCCTGAATCAGATATGAAGCAGCAACCCCTCCTTGGCCACCAG – 5
OASF^(b)	
pET- 28a	5 - CTGGTGGCCAAGGAGGGGGTTGCTGCTTCATATCTGATTGAGGCTGAGAAGATAAAAAAG – 3
STIM2	3 - CTTTTTATCTTCTCAGCCTGAATCAGATATGAAGCAGCAACCCCTCCTTGGCCACCAG – 5
OASF 2β	
Insert^(c)	
T7	5'-GCTAGTTATTGCTCAGCGG-3'
Terminator^(c)	
T7	5' TAATACGACTCACTATAG 3'
Promoter^(c)	

^(a)Subcloning primers for STIM1-OASF and STIM2-OASF

^(b)Mutagenesis primer for 2β insert into STIM1-OASF and STIM-OASF

^(c)Sequencing primer

2.2 Recombinant protein expression and purification

2.2.1 pET-28a STIM1-OASF and STIM2-OASF wildtype and 2 β insert mutants

The pET-28a-STIM1₂₃₄₋₄₉₁ wildtype (WT) OASF (simplified to “STIM1-OASF” for the rest of the thesis) plasmid was transformed using the heat shock method into BL21(DE3) *E. coli*. For this transformation, ~100 ng of vector DNA was mixed with ~50 μ L of cells in an Eppendorf tube on ice for ~20-30 min. Subsequently the tube was heat shocked at 42 °C for 45 s and placed back on ice for ~2 – 3 min. The cells were subsequently transferred into 900 μ L of LB contained in a 15 mL Falcon tube. The Falcon tube was incubated at 37 °C with constant shaking (i.e. 200 rpm) for 60 min. Subsequently, 100 μ L of the cell suspension was plated onto an agar plate containing 60 μ g mL⁻¹ kanamycin as the selection pressure. After ~16 h incubation in an air incubator set at 37 °C, one individual colony was selected and placed into 30 mL of LB contained in a sterile 250 mL Erlenmeyer flask supplemented with 60 μ L mg⁻¹ kanamycin. The following day, 5 mL of this liquid starter culture was transferred into three autoclaved 4 L flasks each containing 1 L LB and supplemented with 60 μ g mL⁻¹ of kanamycin.

The cultures were grown in a New Brunswick™ Excella® E25/E25R incubator shaker at 37 °C with 190 rpm of constant shaking until an optical density (OD₆₀₀) reached ~1.0. At this point protein expression was induced with the addition of isopropyl β -D-1thiogalactopyranoside (IPTG) to a final concentration of 400 μ M. IPTG is a lactose analog which promotes transcription of the insert by binding to the lac repressor and preventing its interaction with the lac operator in the pET-28a system. After the IPTG addition, the temperature was decreased from 37 °C to 20 °C to minimize protein degradation and incubated overnight with 190 rpm constant shaking. The following day, the BL21 *E. coli* cells were collected using a J2-21M Induction drive centrifuge equipped with a JA10 rotor (Beckman). The cells were harvested by centrifugation at 9,300 \times g, 4 °C for 30 min. The pelleted cells were collected and stored at -80 °C until protein purification.

WT STIM1-OASF protein was purified from the *E. coli* cells by homogenizing the ~5 mL wet bacterial pellet with 50 mL of 6M guanidine hydrochloride (GdnHCl), 20 mM TRIS-

HCl (pH 8.0) and 5 mM β – mercaptoethanol (BME) using a 10 mL transfer pipette. Sonication was required to completely homogenize small clumps of cells and to shear genomic DNA. The bacterial mixture was sonicated on ice at 30% power using the Fisher Sonic Dismembrator Model 150 for 5 min in 3 s on and 3 s off cycles. Subsequently, the homogenized mixture was attached to a hybridization oven and slowly rotated at ambient temperature for 90 min. Following this incubation, the mixture was centrifuged at 11,000 \times g and 8 °C for another 50 min using a JA20 rotor in a J2-21 Induction drive centrifuge (Beckman) to separate the insoluble cell debris from the supernatant. Next, ~45 mL of the resultant clarified lysate containing solubilized OASF protein was mixed with 300 μ L of 50% (v/v) nickel-nitrilotracetic acid (Ni-NTA) agarose beads (HisPur, ThermoFisher Scientific). The Ni-NTA was added to bind to the N-terminally fused hexahistidine (6 \times His)-tag of the OASF protein. The lysate:Ni-NTA mixture was slowly rotated end-over-end in a 50 mL conical tube overnight at 4 °C to promote maximal binding. The next day, the Ni-NTA beads were collected in a gravity flow protein purification column, washed three times with 10 mL of 6 M Urea, 20 mM TRIS-HCl (pH 8.0) and 5 mM BME to remove weakly bound protein and eluted seven times with 3 mL of 6 M Urea, 20 mM TRIS-HCl (pH 8.0), 5 mM BME and 300 mM imidazole. Each elution aliquot was incubated for 90 s to maximally displace the 6 \times His-OASF protein from the beads

The presence of the protein in the elution fractions was confirmed by separating aliquots of each fraction on a 15 % (w/v) SDS-PAGE gel, followed by Coomassie blue staining (Figure 2.2A). Elution fractions that contained the protein of interest (~15-20 mL) were pooled together into a 3,500 Da molecular weight cutoff dialysis membrane (BioDesign Inc.) and placed into 1 L protein refolding buffer containing 20 mM TRIS-HCl (pH 8), 300 mM NaCl, 1 mM dithiothreitol (DTT).

A magnetic stir bar was used to ensure homogeneous exchange between the unfolding buffer contained in the dialysis bag and the bulk folding buffer in the beaker. Refolding progressed overnight at 4°C. Following ~16 h, 1U of bovine thrombin (BioPharm Laboratories, Inc) per mg of protein was added to the dialysis bag and placed at 4°C for another ~24 h of dialysis. The cutting efficiency of thrombin was determined using a 15 % (w/v) SDS-PAGE gel by comparing the migration of OASF before and after the addition

of thrombin (Figure 2.2C). Upon verification of removal of the 6×His tag, 100 μ M of 4-(2-aminoethyl) benzenesulfonyl fluoride (AEBSF) was added to the sample to stop thrombin activity.

To achieve ~95% purity, a final size exclusion chromatography purification was performed to separate contaminants by size. This gel filtration was performed using a HiLoad Superdex S200 20/60 PG column connected to an ÄKTA Pure system (GE Healthcare). The running buffer used in this purification step was 20 mM TRIS, 1 mM DTT and 300 mM NaCl (pH 8.0) which was equilibrated into the 325 mL Hiload column prior to injecting the refolded OASF protein concentrated to ~8-10 mL. Furthermore, OASF was eluted in 1 mL fractions, collected in a 96× deep well plate. Elution was monitored by UV absorbance at 280 nm (Figure 2.3A). Fractions which showed UV 280 nm absorbance were then separated on a 15 % (w/v) SDS-PAGE gel to confirm the presence of STIM1-OASF and purity after Coomassie blue staining (Figure 2.3C). Fractions which showed a single band migrating near the theoretical molecular weight of the monomer were pooled and stored at 4 °C for experiments performed within 2 days or flash frozen with liquid nitrogen and housed at -80 °C for long term storage.

STIM1-2 β -OASF, STIM2-OASF and STIM2 β -OASF proteins were expressed and purified as exactly as detailed above for STIM1-OASF (Figure 2.2, Figure 2.3, Figure 2.4 and Figure 2.5). Protein concentration was determined using UV extinction coefficients of 0.9478, 0.9629, 0.9948 and 1.0088 mg mL⁻¹ cm⁻¹ at 280 nm for STIM1-OASF, STIM1-2 β -OASF, STIM2-OASF and STIM2 β -OASF, respectively.

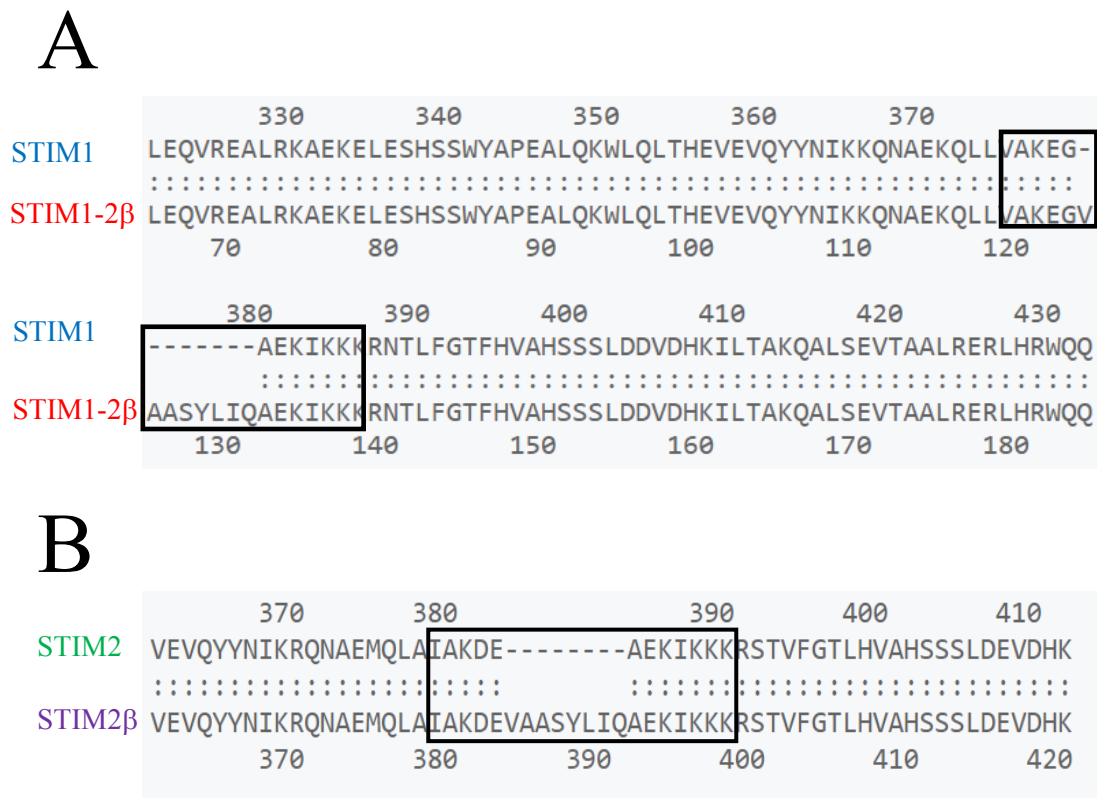


Figure 2.1. Pairwise alignment of the sequenced DNA showing successful 2 β insertion. **(A)** depicts STIM1-2 β insert in comparison to STIM1 (Accession: AFZ76986.1) and **(B)** shows STIM2 β in comparison to STIM2 (Accession: NP_065911.3).

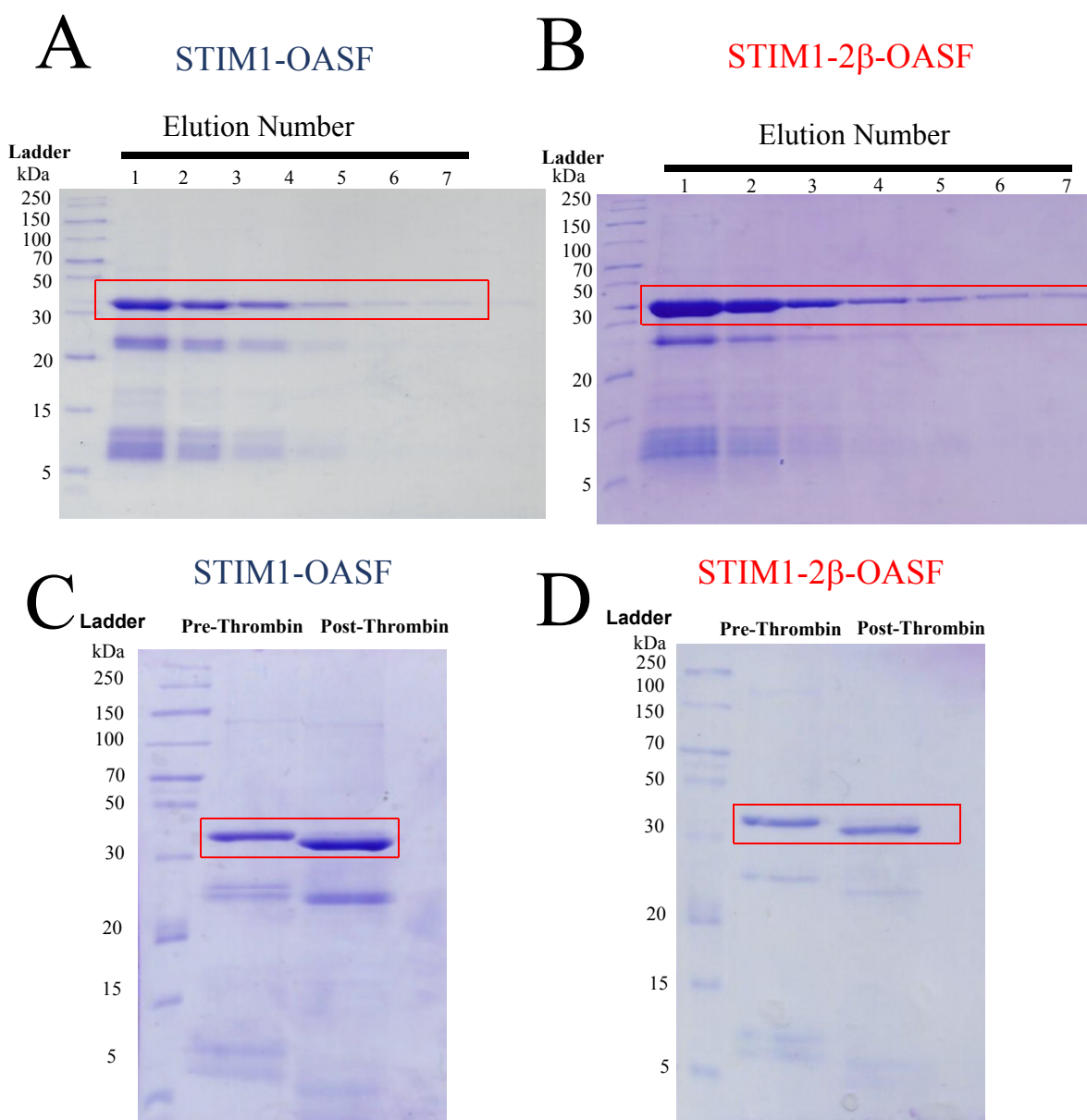


Figure 2.2. Coomassie blue R-250 staining of STIM1-OASF and STIM1-2 β -OASF separated on 15% (w/v) SDS-PAGE gels. (A) 6 \times His-STIM1-OASF (theoretical monomer weight of 33 kDa) Ni-NTA elution fractions. (B) 6 \times His-STIM1-2 β -OASF (theoretical monomer weight of 33kDa) Ni-NTA elution fractions. (C) Pre- and post-thrombin samples indicate the migration of the protein samples with presence and absence of the 6 \times His tag corresponding to 33 kDa and 31 kDa for STIM1-OASF; (D) 33 kDa and 32 kDa for STIM1-2 β -OASF, respectively. The reference proteins are from the PageRuler™ Broad Range Unstained Protein Ladder (ThermoFisherScientific).

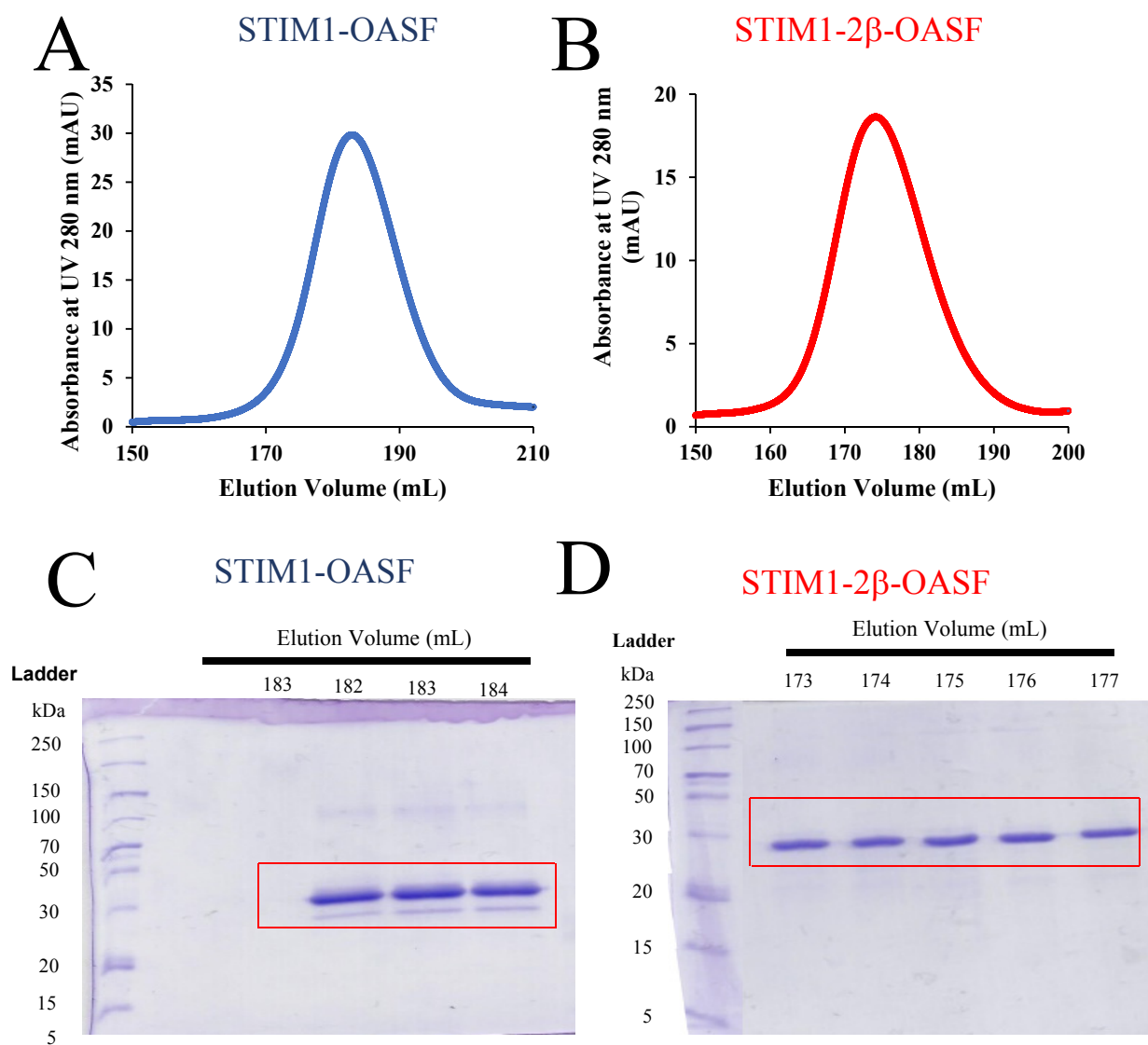


Figure 2.3. Superdex S200 HiLoad 10/60 size exclusion chromatography elution profile of (A) STIM1-OASF and (B) STIM1-2β-OASF. The elution profile was generated using absorbance at 280 nm as a function of elution volume. Coomassie blue R-250 staining of (C) STIM1-OASF (theoretical monomer weight of 31 kDa) and (D) STIM1-2β-OASF (theoretical monomer weight of 32 kDa) separated on a 15% (w/v) SDS-PAGE gel. The reference lane contains the PageRuler™ Broad Range Unstained Protein Ladder.

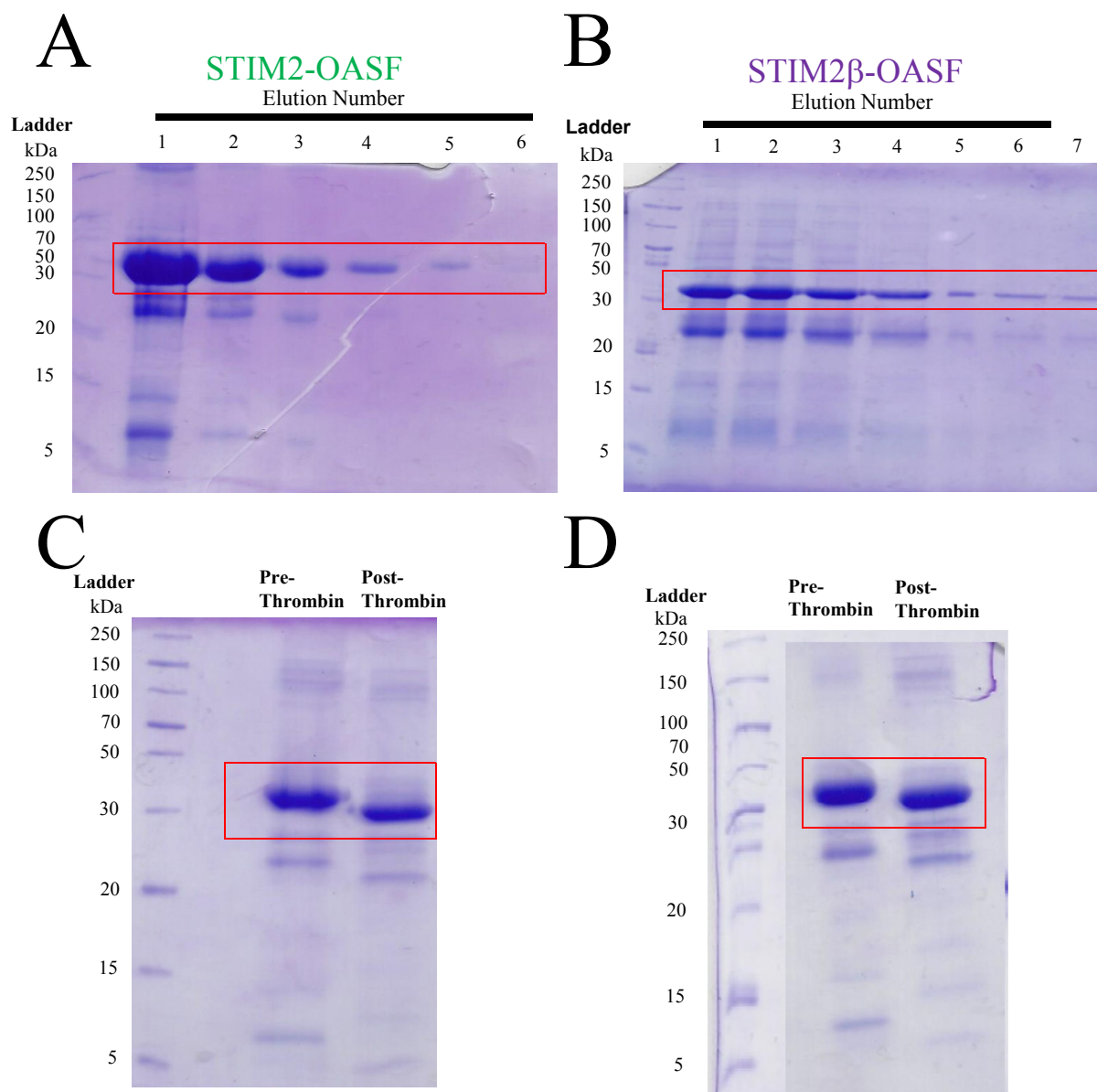


Figure 2.4. Coomassie blue R-250 staining of STIM2-OASF and STIM2 β insert-OASF separated on 15% (w/v) SDS-PAGE gels. (A) 6 \times His-STIM2-OASF (theoretical monomer weight of 33 kDa) Ni-NTA elution fractions. (B) 6 \times His-STIM2 β -OASF (theoretical monomer weight of 33kDa) Ni-NTA elution fractions. (C) Pre- and post-thrombin samples indicate the migration of the protein samples with presence and absence of the 6 \times His tag corresponding to 33 kDa and 31 kDa for STIM2-OASF; (D) 33 kDa and 32 kDa for STIM2 β -OASF, respectively. The reference proteins are from the PageRuler™ Broad Range Unstained Protein Ladder (ThermoFisherScientific).

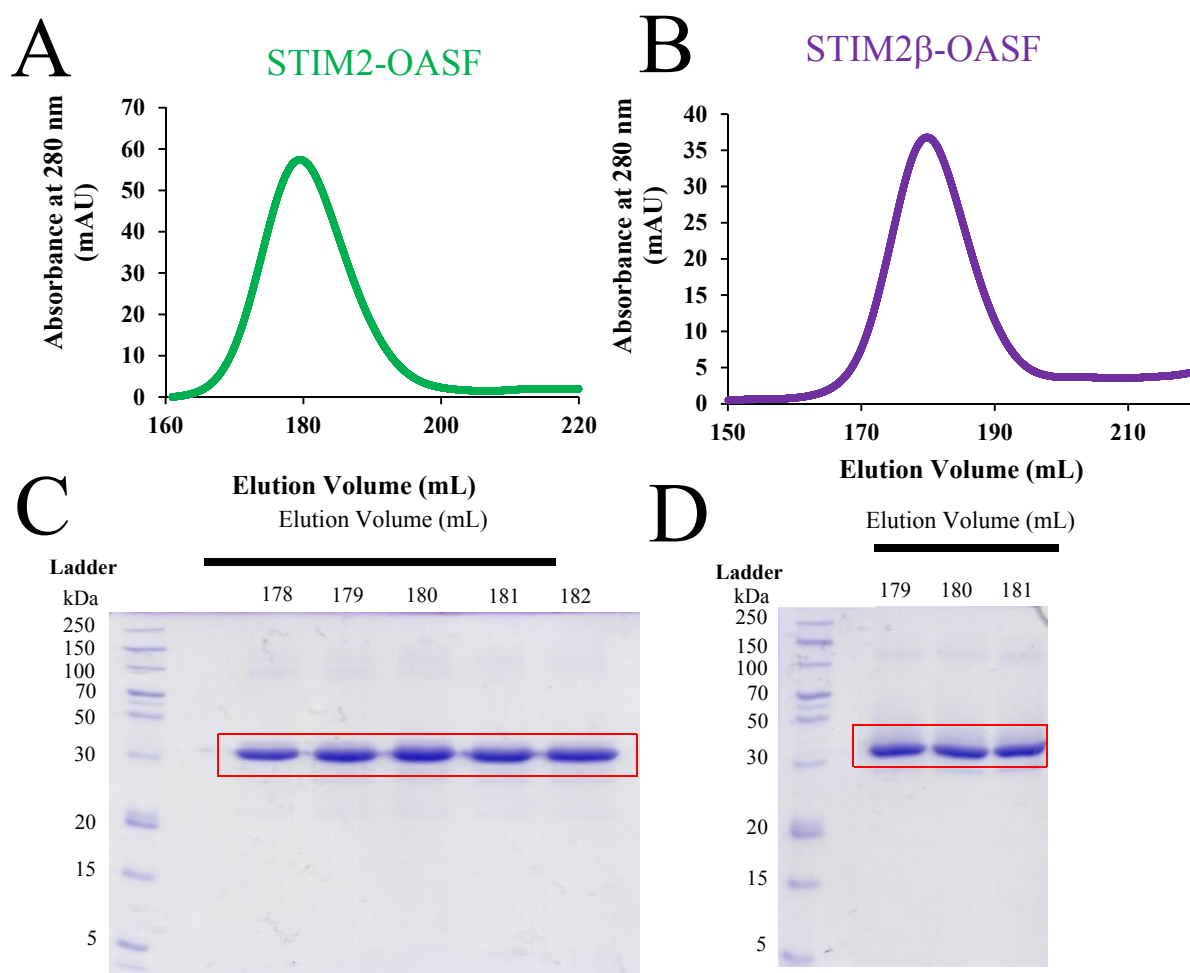


Figure 2.5. Superdex S200 HiLoad 10/60 size exclusion chromatography elution profile of (A) STIM2-OASF and (B) STIM2 β -OASF. The elution profile was generated using absorbance at 280 nm as a function of elution volume. Coomassie blue R-250 staining of (C) STIM2-OASF (theoretical monomer weight of 31 kDa) and (D) STIM2 β -OASF (theoretical monomer weight of 32 kDa) separated on a 15% (w/v) SDS-PAGE gel. The reference lane contains PageRuler™ Broad Range Unstained Protein Ladder.

2.3 Far-UV circular dichroism (CD) spectroscopy

To assess the effects of the 2 β insert on the secondary structure and thermal stability of the OASF proteins, far-UV CD spectroscopy was used. All far-UV CD experiments were performed using a Jasco J-815 CD spectrometer equipped with a Jasco PTC-423S temperature controller (Jasco Inc.). To prepare a far-UV CD sample, dilute protein solutions were first concentrated using an Amicon Ultra-15 centrifugal filter unit (10,000 MWCO) (Millipore) and UV absorbance at 280 nm was used to determine the protein concentration after centrifugation at 10,000 $\times g$ for 10 min to remove precipitate. Based on this stock concentration, a 275 μL sample of 0.2 mg mL⁻¹ protein was prepared by dilution in experimental buffer and transferred into a 0.1 cm pathlength quartz cuvette. Experimental buffer was 20 mM TRIS, 1 mM DTT and 300 mM NaCl, pH 8.0. Separate samples were also prepared in the presence of Ca²⁺ with the addition of 25 mM Ca²⁺ from a 1 M CaCl₂ stock

Far-UV CD spectra were acquired at 20 °C as an average of 3 accumulations between 240 nm to 200 nm in 1 nm increments using the 0.1 cm pathlength quartz cuvette, 8 s averaging time at each wavelength, 1 nm bandwidth. Moreover, thermal melt curves were acquired by monitoring the change CD signal at 222 nm as a function of temperature also using the 0.1 cm pathlength quartz cuvette, an averaging time of 8 s, 1 nm bandwidth and a 1 °C min⁻¹ scan rate. The thermal melt samples were prepared as described for the UV spectrum samples. The apparent midpoint of temperature denaturation (T_m) was used as an indicator of thermal stability. T_m was taken as the point of 50 % relative change in ellipticity at 222 nm.

2.4 8- Anilinonaphthalene-1-sulfonic acid (ANS) binding assay

The relative levels of hydrophobic exposure for the OASF proteins were assessed using ANS, a fluorescence probe which undergoes a change in fluorescence when bound to solvent-exposed hydrophobic protein regions. The extrinsic ANS fluorescence intensity was detected using a Cary Eclipse spectrofluorimeter (Varian/Agilent, Inc). The experimental buffer was 20 mM TRIS, 300 mM NaCl, 1 mM DTT, pH 8.0. The protein

samples were prepared at a final concentration of 0.143 mg mL^{-1} in $600 \text{ }\mu\text{L}$ total volume. Samples were supplemented with 0.5 mM EDTA to chelate residual Ca^{2+} and ANS was added to a final concentration of $10 \text{ }\mu\text{M}$. The extrinsic ANS fluorescence emission spectrum was acquired at $35 \text{ }^\circ\text{C}$ from 400 nm to 600 nm using an excitation wavelength of 372 nm . The excitation and emission slit widths were set to 10 nm and 20 nm , respectively, while the photomultiplier tube (PMT) was set to 680 V . Control spectra were acquired in the absence of protein using similar settings and buffer conditions. Ca^{2+} was titrated into the protein-containing and protein-free control samples with successive additions of 5 mM CaCl_2 from a 1 M CaCl_2 stock. 15 min incubation between CaCl_2 aliquots was determined to be sufficient for binding equilibration.

2.5 Size-exclusion chromatography with in line multi-angle light scattering (SEC-MALS)

The quaternary structure of the OASF proteins was assessed using SEC-MALS. $125 \text{ }\mu\text{L}$ of the OASF proteins at 1 mg mL^{-1} protein were injected onto a Superdex 200 increase 10/300 GL gel filtration column (GE Healthcare) using the AKTA Pure system (GE Healthcare). The column was connected in line to a Dawn HELEOS II MALS detector equipped with a 662 nm laser source and Optilab Trex differential refractometer equipped with 658 nm LED source (Wyatt Technology). The SEC-MALS system was housed in a cold-cabinet maintaining a temperature of $10 \text{ }^\circ\text{C}$.

The SEC-MALS experimental buffer was 20 mM TRIS, 1 mM DTT and 150 mM , pH 8.0 supplemented with or without 25 mM CaCl_2 , as specified. Protein concentrations through the eluted peaks were determined by the differential refractometer using a refractive index increment of $\text{dn}\cdot\text{dc}^{-1} = 0.185 \text{ mL}\cdot\text{g}^{-1}$. Samples were eluted at a flow rate of 0.5 mL min^{-1} and molecular weights were calculated by Zimm plot analysis using the ASTRA software (v6.1.5.22; Wyatt Technologies).

2.6 Dynamic Light Scattering (DLS)

The distribution of hydrodynamic radii of OASF protein solutions were determined by DLS. The DLS experiments were performed on a DynaPro Nanostar (Wyatt Technology)

equipped with a 658 nm laser. The experimental buffer was 20 mM TRIS, 1 mM DTT and 300 mM NaCl, pH 8.0. DLS samples were prepared by centrifuging 0.5 mg mL⁻¹ protein solutions at 12,000 ×g for 3 min, to remove any large particulates which can dominate DLS signal, before a 5 µL aliquot was loaded into a dust-free quartz MicroCuvette (JC501). All DLS acquisitions were performed at 37 °C, where the protein sample was allotted 5 min of equilibrium time prior to acquiring 10 consecutive readings averaged over 5 s. Furthermore, distributions of hydrodynamic radii were extracted from the autocorrelation function using the regularization algorithm for polydisperse solutions built into the accompanying instrumental software (Dynamics v7; Wyatt Technologies). The low and high cut-off for hydrodynamic size was set to 1.5 nm and 150 nm, respectively.

2.7 Solution Small Angle X-ray Scattering (SAXS)

To assess the effects of the 2β insert on the overall structure of STIM1-OASF and STIM2-OASF in solution, SAXS data was acquired. Protein solutions for of each OASF constructs were prepared at the highest possible concentration which did not readily precipitate. These concentrations were 1.041 mg mL⁻¹, 0.855 mg mL⁻¹, 1.045mg mL⁻¹ and 1.109 mg mL⁻¹ for STIM1-OASF, STIM1-2β-OASF, STIM2-OASF and STIM2β-OASF, respectively. Flow through samples collected during the ultrafiltration concentration procedure for each protein were used as the buffer controls. SAXS profiles for the protein and matching buffer controls were acquired by Dr. Gregory A. Wasney (Structural & Biophysical Core Facility, The Hospital for Sick Children, Toronto, ON). Measurements were performed in a 1 mm quartz cuvette (50 µL) at 4 °C using a 3 h X-ray exposure time (180 × 1 min frame). An aligned SAXSpace instrument (Anton PaarGmbH) working in line collimation mode was used to carry out the assessment. The SAXSpace X-ray generator contained a long-fine focus glass sealed copper tube (40 kV/50 mA, wavelength = 0.1542 nm), and the detector used was a Mythen2 R 1K 1D detector (DECTRIS Ltd). Sample cuvette temperature was regulated using a Peltier-controlled TCStage150.

The buffer-subtraced SAXS profiles were used to calculate the experimental radius of gyration (R_g), distance-distribution function $p(r)$ and reconstruct a low-resolution structure. Experimental R_g was calculated as $\sqrt{(3 \times \text{slope})}$ of the Guinier plot constructed as the natural

log of the intensity [$\ln(I)$] versus the square of scattering vector (s^2) (Boldon et al., 2015; Putnam, 2016). The maximum particle diameter (D_{\max}) was determined from the pair distance-distribution function [$p(r)$], initially estimated using DATGNOM, and then manually adjusted until a gradual decay to zero was observed in the $p(r)$ function. The D_{\max} was used in *ab initio* shape reconstruction using DAMMIF. Thirty DAMMIF *ab initio* structures were determined for each OASF protein. These thirty structures were clustered and averaged using DAMCLUST (Franke et al., 2009; Petoukhov et al., 2012; Maxim V. Petoukhov et al., 2007). The resultant bead models were visualized using PYMOL. (Cui et al., 2013; Stathopulos et al., 2013)

2.8 Human embryonic kidney (HEK) 293 cell culture

HEK293 cells stably expressing yellow fluorescent protein (YFP)-Orai1 were a generous gift from the laboratory of Dr. Monica Vig (Washington University in St. Louis). These adherent cells were cultured in Dulbecco's modified eagle media (DMEM) containing high glucose (Wisent) and supplemented with 10 % (v/v) fetal bovine serum (Wisent), 100 $\mu\text{g} - 100 \text{ U ml}^{-1}$ penicillin-streptomycin (Wisent) and 0.4 mg ml^{-1} G418 disulfate (Thermo Fisher Scientific). Cells were grown on 10 cm dishes and maintained at 37 °C in a 5 % (v/v) CO_2 / 95 % (v/v) air mixture within a humidified incubator. At ~ 85% - 90 % cell confluency, the culture medium was removed and 10 mL of 1× PBS was promptly added to the dish. The PBS was subsequently removed and 1 mL of 0.25 % trypsin with 2.21 mM EDTA (Wisent) was immediately distributed over the entire surface of the dish. The cells were incubated in the presence of the trypsin for ~2 - 3 min at 37 °C. Subsequently, 9 mL of DMEM medium containing FBS and antibiotic was added to the dish and thoroughly mixed using a transfer pipette to ensure complete detachment of cells from the dish surface. To conduct a 25 % cell passage, 2.5 mL of the trypsinized cell mixture was aliquoted into a sterile 10 cm cell culture dish containing 7.5 mL DMEM high glucose medium supplemented with FBS and antibiotic as detailed above.

2.9 Transfection of HEK293 with pCMV6-mCh-STIM vectors

After 20 – 24 h, at ~70 – 80 % confluency, HEK293 cells were transiently transfected with the pCMV6-mCh-STIM1, STIM2, STIM1-2 β or STIM2 β vectors using PolyJet™ transfection reagent (Froggabio) according to the manufacturers protocol. Briefly, 5 μ g of DNA was diluted in 250 μ L of high glucose DMEM which was free of antibiotics and FBS. Similarly, 15 μ L of PolyJet™ reagent was also diluted in 250 μ L of high glucose DMEM medium free of antibiotic and FBS. The diluted PolyJet™ reagent was immediately transferred into the diluted DNA solution and mixed ~3 – 4 times by pipetting. The PolyJet:DNA mixture was subsequently incubated at room temperature for 15 min. Finally, the 500 μ L transfection mixture was added in a drop-wise manner evenly over the cell culture dish containing the adherent HEK293 cells in the complete culture medium (i.e. with antibiotic and FBS). The cells were incubated at 37 °C for 24 h prior to use in the SOCE experiments (see below).

2.10 Fura-2 ratiometric fluorescence spectroscopy to assess SOCE

Transfected HEK293 cells were lifted off the cell culture dish by gentle pipetting and transferred into a 15 mL conical tube. Fura-2 acetoxymethyl ester (AM) was added to a final concentration of 2 μ M, and the cell suspension was mixed by gentle inversion. The cells were placed at 37 °C for a total of 45 min with mixing by inversion every 15 min. The cells were subsequently pelleted through centrifugation at 300 \times g for 3 min, the medium was aspirated out of the tube and the cells resuspended in 14 mL of Ca²⁺-free HEPES buffered saline solution (HBSS) composed of 140 mM NaCl, 5 mM KCl, 10 mM D-glucose, 1 mM MgCl₂ and 10 mM HEPES, pH 7.4. The suspended cells were then centrifuged at 300 \times g for another 3 min and this wash solution was removed by aspiration. The resultant cell pellet was homogeneously resuspended in a final 1.2 mL of Ca²⁺ free HBSS and transferred into a quartz cuvette. The 1.2 mL cell suspension was supplemented with a final concentration of 0.5 mM ethylene glycol tetraacetic acid (EGTA) to chelate any residual Ca²⁺. The resuspended HEK293 cells were incubated for 3 min at 25 °C in the

Cary Eclipse spectrofluorimeter (Varian/Agilent, Inc.) before measuring the Fura-2 fluorescence.

SOCE was assessed using Fura-2 ratiometric fluorescence measurements. Fura-2 fluorescence was measured using alternating excitation wavelengths of 340 and 380 nm and an emission wavelength of 510 nm. After a 100 s baseline acquisition, 2 μM of thapsigargin (TG) was added to passively deplete ER Ca^{2+} by blockade of the SERCA pumps. At 600 s, 2.5 mM of CaCl_2 was added to the cell suspension to induce Ca^{2+} entry into the cytosol from the extracellular space. The excitation and emission slit widths used in these Fura-2 experiments were 5 nm and 10 nm, respectively, and the PMT was set to 650 V.

To assess the relative transfection efficiencies and cell densities, mCh and YFP fluorescence of the cell suspensions were measured. For transfection efficiency assessment, mCh fluorescence emission spectra were acquired between 580 – 680 nm using an excitation wavelength of 565 nm at 25 °C. YFP-Orai fluorescence was taken as an indicator of cell density. YFP fluorescence emission spectra were acquired from 510 nm to 620 nm using an excitation wavelength of 490 nm. Excitation and emission slit widths were set to 10 nm and 20 nm, respectively, while the PMT was set to 650 V.

Chapter 3: Results

3.1 The 2 β insertion decreases the α -helicity of OASF

Secondary structure prediction using PSIPRED (McGuffin et al., 2000), suggests that the 2 β insert is unstructured within STIM2 β , and this lack of regular secondary structure could very well affect the overall structural integrity of the OASF domains. However, the precise effects of the 8-amino acid insert (i.e. 2 β insert) on the folding and stability of the conserved CC domains remains poorly understood. To assess the effects of the 2 β insert on protein structure and stability, I used far-UV CD spectroscopy to monitor the secondary structure and unfolding as a function of temperature. CC domains typically adopt extended α -helical structures, so I expected two intensity minima at 208 nm and 222 nm indicative of α -helicity in the far-UV CD spectra of the OASF proteins (Correcirc et al., 2009). Indeed, my far-UV CD data showed that all STIM-OASF homologues and the corresponding 2 β variants exhibited minima at 208 nm and 222 nm indicating they retain a high fraction of α -helicity even in the presence of the 2 β insertion. Nevertheless, after normalizing the CD signal on a per residue basis, it was clear that inclusion of the 2 β insert reduced the overall α -helicity, indicated by less negative ellipticity compared to the WT homologues (Figure 3.1). Thus, the 2 β insert significantly reduces the overall α -helicity of the STIM1-OASF and STIM2-OASF regions.

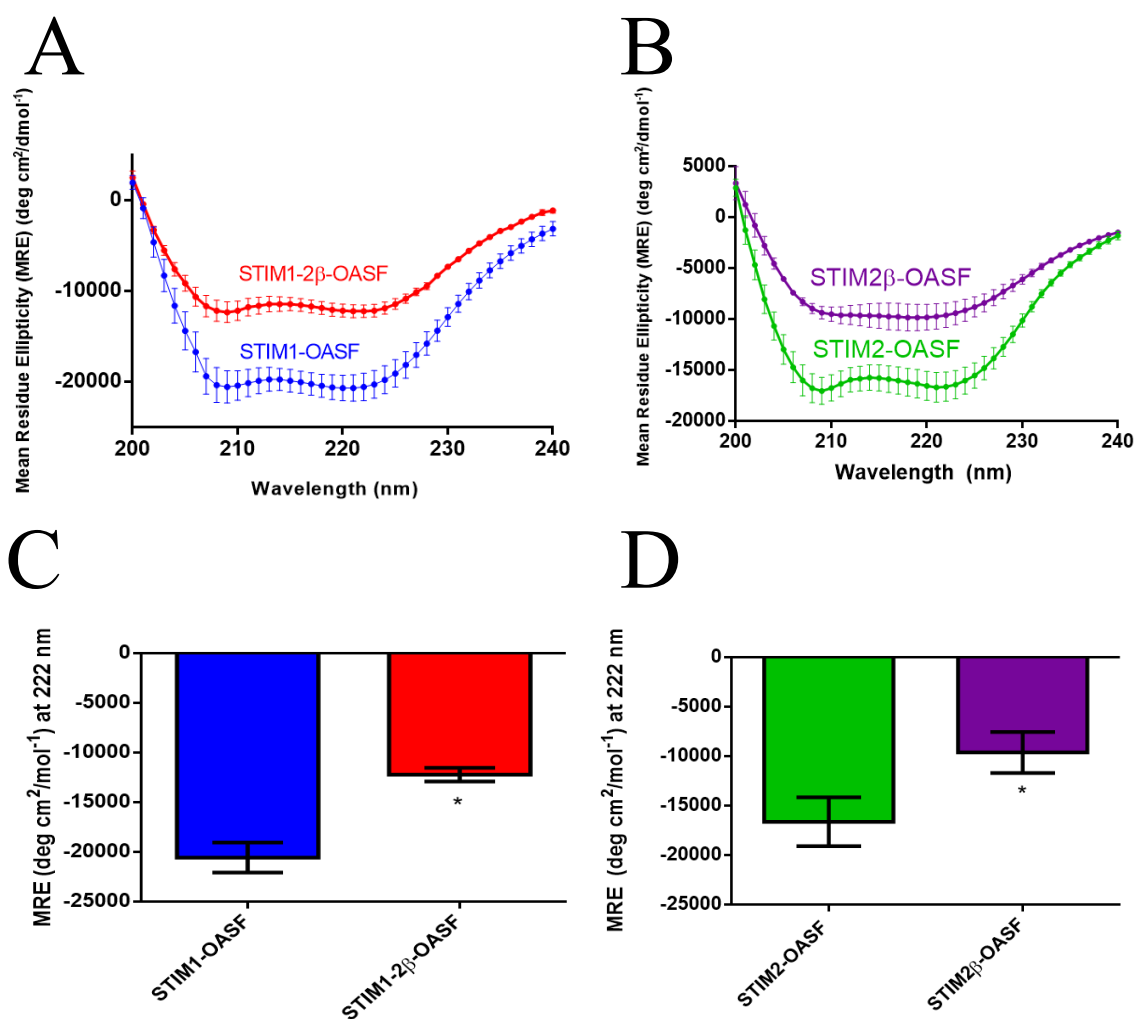


Figure 3.1. The 2 β insertion decreases α -helicity of the OASF regions of STIM1 and STIM2. Far-UV CD spectra of STIM1-OASF (A) and STIM2-OASF (B) with and without the 2 β insertions. Statistical analysis of (C) STIM1-OASF and (D) STIM2-OASF α -helicity at 222 nm using an unpaired student's t-test. All experiments were performed using 0.2 mg ml⁻¹ protein concentration. Inclusion of 2 β results in less negative ellipticity compared to unmodified STIM OASF at 208 nm and 222 nm suggesting less α -helicity. Data are means \pm SEM of n = 3 separate protein purifications (*p < 0.05 vs wildtype).

3.2 The 2 β insertion reduces the thermal stability of STIM1-OASF

Having determined that the 2 β insert affects the overall level of secondary structure within OASF, I next assessed the thermal stability by monitoring the change in far-UV CD signal at 222 nm as a function of temperature. The apparent midpoint of temperature denaturation (T_m) was taken as the temperature causing a 50 % change in the CD signal. In the STIM1-OASF context, the 2 β insert induced a systematic leftward shift in the thermal melt profile (Figure 3.2A). The apparent T_m for STIM1-2 β -OASF was 47.1 ± 0.1 °C compared to 50.5 ± 0.2 °C for STIM1-OASF. The significant reduction in T_m (i.e. $\Delta T_m = \sim -3$ °C, ****p** < 0.01) shows that the 2 β insert destabilizes the STIM1-OASF region (Figure 3.2B).

The STIM2-OASF thermal melts exhibited less well-defined folded baselines compared to the STIM1-OASF data (Figure 3.2A and Figure 3.2B), likely due to a poorer cooperativity of STIM2 CC domain unfolding. While the 2 β insert did not induce a statistically significant change in T_m as defined in this thesis (i.e. $\Delta T_m = \sim -1$ °C, $p > 0.05$, for STIM2 β -OASF compared STIM2-OASF), the first unfolding transition appeared complete at a much earlier temperature (i.e. ~ 48 °C versus ~ 58 °C, for STIM2 β versus STIM2-OASF, respectively) (Figure 3.2B and 3.2D). The second transition likely represented a protein aggregation and/or precipitation phase. Interestingly, the STIM2-OASF is markedly less stable than STIM1-OASF (i.e. $\Delta T_m = \sim -6$ °C) which may be related to its weaker ability to activate SOCE. Collectively, the thermal stability data show that the 2 β insert causes destabilization of STIM1-OASF (Table 3.1) and alters the thermal unfolding profile for STIM2-OASF such that the first unfolding transition is completed at a much lower temperature.

Table 3.1: Summary of the thermal stabilities for STIM1-OASF and STIM2-OASF with their respective 2 β insertions

Protein	Apparent T_m (°C)	ΔT_m
STIM1-OASF	50.5 \pm 0.2	
STIM1-2 β -OASF	47.1 \pm 0.1 **	-3.4 °C
STIM2-OASF	44.0 \pm 0.4	
STIM2 β -OASF	42.6 \pm 0.9	-1.4 °C

Statistical analysis was performed using an unpaired two-tailed student's t-test

****p < 0.01 vs WT STIM1-OASF and STIM2-OASF**

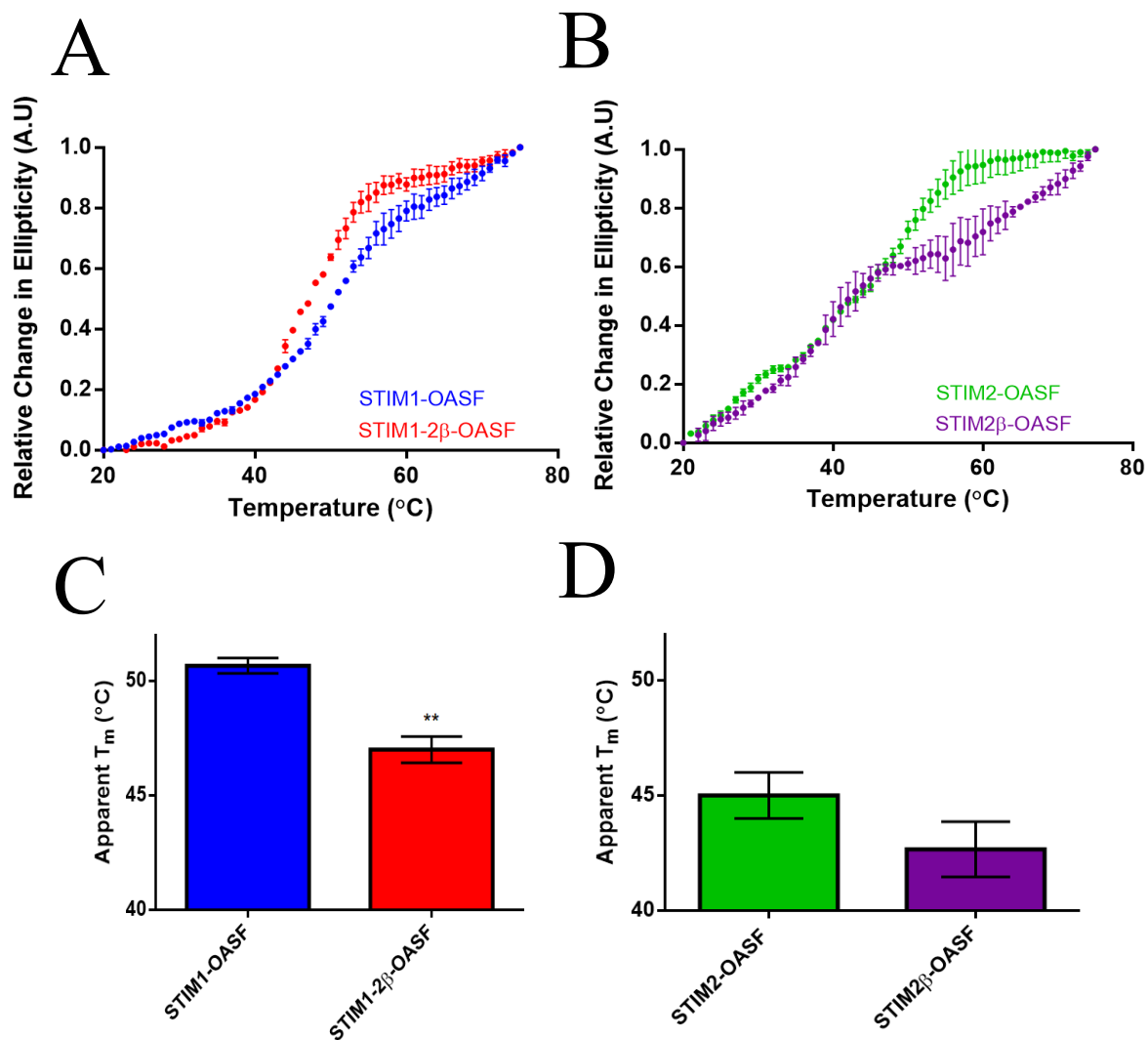


Figure 3.2. The 2 β insertion reduces the thermal stability of STIM1-OASF. Far-UV CD thermal melts of STIM1-OASF (A), STIM1 2 β -OASF (B), STIM2-OASF (C), and STIM2 β -OASF (D), The 2 β insert causes a significant thermal destabilization of STIM1-OASF. Additionally, the 2 β insert alters the unfolding profile of STIM2-OASF such that the first transition is apparently complete at a much earlier temperature for STIM2 β compared to STIM2. Data are means \pm SEM of $n = 3$ separate protein purifications (** $p < 0.01$ vs wildtype).

3.3 Calcium (Ca^{2+}) induces an increase in hydrophobic exposure which is exacerbated by 2β

Previous work showed that STIM1-OASF contains potential inhibitory Ca^{2+} binding sites which disrupt CC interactions important for mediating SOCE activity (Derler et al., 2009). This inhibitory domain contains a cluster of several negatively charged residues, conserved in both STIM1 and STIM2, which complement the positive charge of Ca^{2+} (Figure 3.3A). Having determined that the 2β insert decreases the folding and stability of OASF, I next assessed whether the insert alters how Ca^{2+} affects the conformation of OASF. I used an 8-anilinoanthracene-1-sulfonic acid (ANS) binding assay to probe OASF conformation.

I measured the ANS fluorescent intensity of STIM1-OASF, STIM1- 2β -OASF, STIM2-OASF and STIM2 β -OASF as a function of increasing Ca^{2+} concentration. The ANS fluorescence intensity for all OASF proteins showed an increase in ANS fluorescence intensity and a shift to lower wavelengths in the emission maxima, indicative of greater exposed hydrophobicity in the presence of Ca^{2+} compared to the spectra acquired with no Ca^{2+} (Figure 3.3B, Figure 3.3C, Figure 3.3D and Figure 3.3E). For STIM1-OASF and STIM2-OASF, the increase ANS fluorescence trended toward, but did not reach saturation in a titration between 0 – 40 mM CaCl_2 (Figure 3.3B and Figure 3.3C). In contrast, the fluorescence intensity of the OASF proteins containing the 2β insert reached apparent saturation over a similar 0 – 40 mM CaCl_2 concentration range (Figure 3.3D and 3.3E). The conformational sensitivity of all OASF proteins to CaCl_2 supports the existence of Ca^{2+} binding site(s) which remain accessible and intact in the 2β variants.

Interestingly, the ANS fluorescence intensity was higher with the STIM1- 2β -OASF and STIM2 β -OASF proteins compared to the STIM1-OASF samples which did not include the 2β insert (Figure 3.4). Specifically, the ANS fluorescence intensity was 392.4 ± 3.59 A.U. compared to 484.9 ± 2.61 A.U. in the presence of STIM1-OASF and STIM1- 2β -OASF, respectively (** $p < 0.01$).

This trend in ANS fluorescence was maintained at the highest CaCl_2 concentration, with the protein samples containing the 2β insert showing higher fluorescence intensity

compared to protein samples without the 2 β insert (Figure 3.4 and Table 3.2). Additionally, the magnitude of the change in ANS fluorescence as a function of CaCl₂ was smaller for both STIM1-OASF and STIM2-OASF compared to STIM1-2 β -OASF and STIM2 β -OASF (Figure 3.4 and Table 3.2).

Taken together, my ANS experiments suggests that the 2 β insert increases the exposed hydrophobicity of STIM1-OASF and STIM2-OASF, and this conformational change alters the Ca²⁺ binding properties of the domain such that the maximal change in conformation is reached at lower Ca²⁺ concentrations for OASF proteins containing the 2 β insertion. Importantly, the higher ANS fluorescence observed for protein samples containing the 2 β insert is consistent with the decreased folding and stability described above.

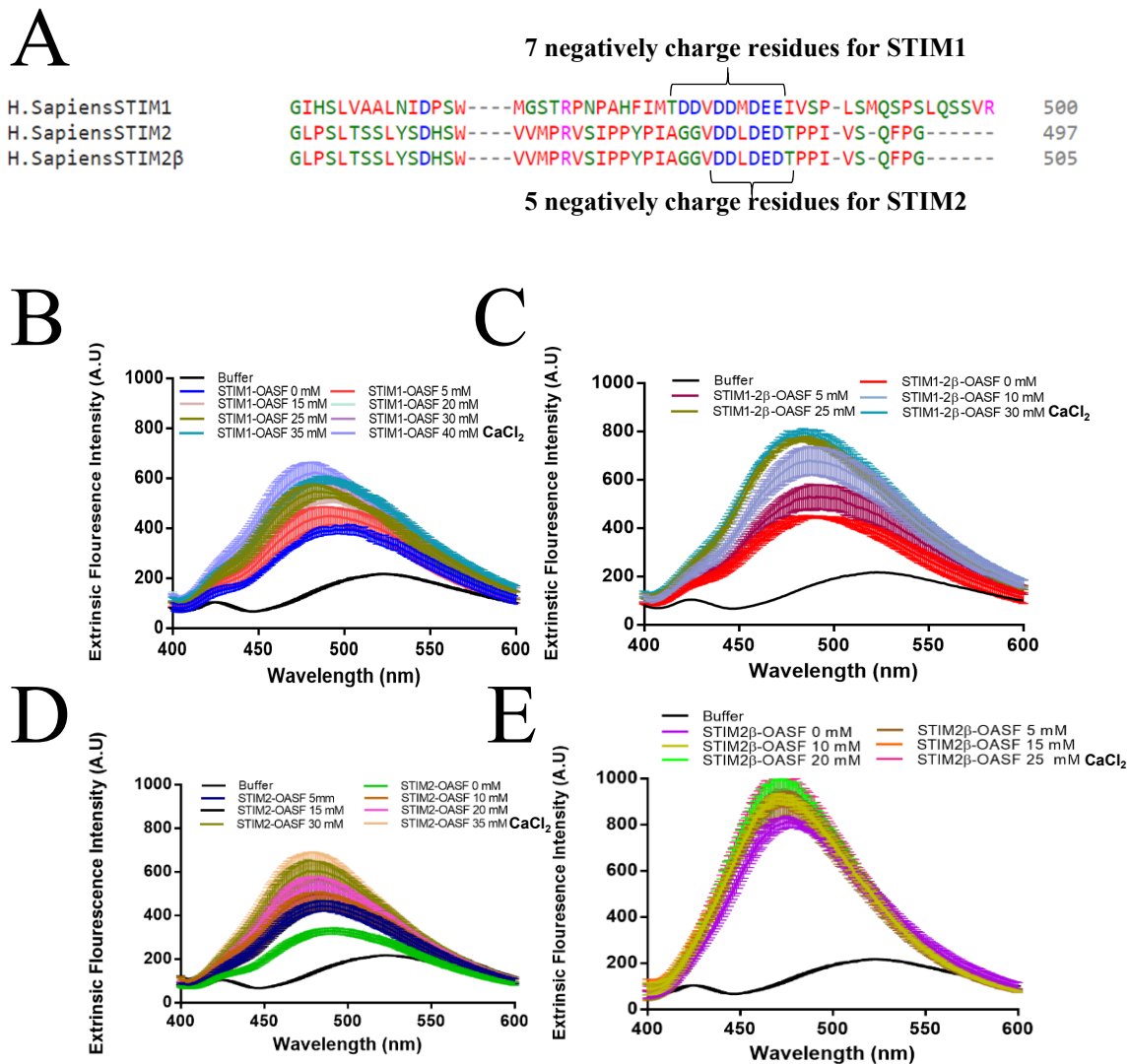


Figure 3.3. Ca^{2+} induces an increase in exposed hydrophobicity in the STIM OASF domains which is exacerbated by the 2β variation. (A) Seven and five negatively charged residues in STIM1 and STIM2, respectively, which can act as potential Ca^{2+} binding sites. Extrinsic ANS-binding induced fluorescence emission spectra of STIM1-OASF (**B**), STIM1- 2β -OASF (**C**), STIM2-OASF (**D**) and STIM2 β -OASF (**E**) as a function of increasing CaCl_2 . For all samples, fluorescence intensity increased and exhibited a concomitant blue shift in the emission maximum with increasing CaCl_2 concentrations. Data are means \pm SEM of $n = 3$ separate protein purifications.

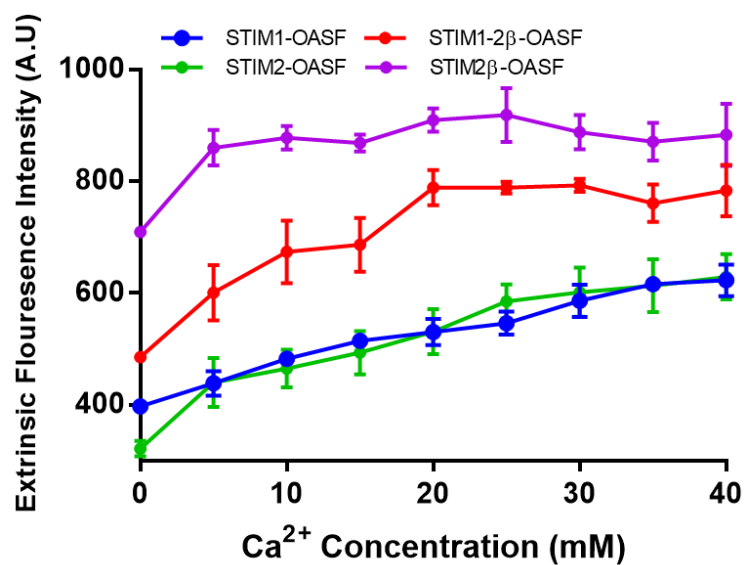


Figure 3.4. The 2β insert promotes apparently saturable Ca²⁺ binding within STIM2-OASF which enhances solvent exposed hydrophobicity. The change in maximum ANS-binding induced fluorescence emission of STIM1-OASF (blue), STIM1-2β-OASF (red), STIM2-OASF (green) and STIM2β-OASF (purple) is shown as a function of CaCl₂ concentration. At each CaCl₂ concentration, data are means ± SEM of n = 3 separate protein purifications.

Table 3.2: Summary of basal ANS fluorescence and saturated ANS fluorescence of STIM1-OASF and STIM2-OASF with their respective 2 β insertions

Protein	Basal Fluorescence^(a)	Saturated Fluorescence^(b)	ΔFluorescence^(c)
STIM1-OASF	392.4 \pm 3.59	615.8 \pm 11.65	+223
STIM1-2β-OASF	484.9 \pm 2.61 **	792.8 \pm 11.74 ***	+308
STIM2-OASF	321.4 \pm 13.72	612.9 \pm 47.14	+292
STIM2β-OASF	709.1 \pm 4.52 **	887.8 \pm 30.65 *	+179

(a) Extrinsic ANS fluorescence measured at baseline (i.e. 0 mM Ca²⁺)

(b) Extrinsic ANS fluorescence measured at the saturation point for each respective protein

(c) Change in extrinsic ANS fluorescence obtained by taking the difference between extrinsic ANS fluorescence measured at saturation and baseline

Statistical analysis was performed using an unpaired two-tailed student's t-test comparing the basal ANS fluorescence and saturated ANS fluorescence of the 2 β insertions variants to wildtype STIM1-OASF and STIM2-OASF

***p < 0.05, **p < 0.01, ***p < 0.001 vs WT STIM1-OASF and STIM2-OASF**

3.4 Ca²⁺ minimally affects the α -helicity of the OASF domains with or without 2 β

Given my ANS data which indicated that Ca²⁺ induces a conformational change in all the STIM OASF proteins, both with and without the 2 β insert, I next assessed whether this conformational change is coupled to changes in secondary structure. I used far-UV CD spectroscopy to assess α -helicity. Interestingly, the addition of 25 mM CaCl₂ to the STIM1-OASF and STIM1-2 β -OASF proteins resulted in CD spectra which showed a trend to less negative ellipticity at both the 208 and 222 nm minima (Figure 3.5A and Figure 3.5C). However, this apparent loss in α -helicity was relatively small and not statistically significant (Figure 3.5B and Figure 3.5D). Similarly, STIM2-OASF and STIM2 β -OASF protein showed no statistically significant change in negative ellipticity in the presence of 25 mM CaCl₂ (Figure 3.5E, Figure 3.5F, Figure 3.5G and Figure 3.5H).

Collectively, the far-UV CD spectra show that Ca²⁺ minimally affects the secondary structure levels of STIM1-OASF, STIM1-2 β -OASF, STIM2-OASF and STIM2 β -OASF. Thus, the Ca²⁺-induced conformational changes observed by ANS binding in all OASF proteins are not linked with major changes in α -helicity.

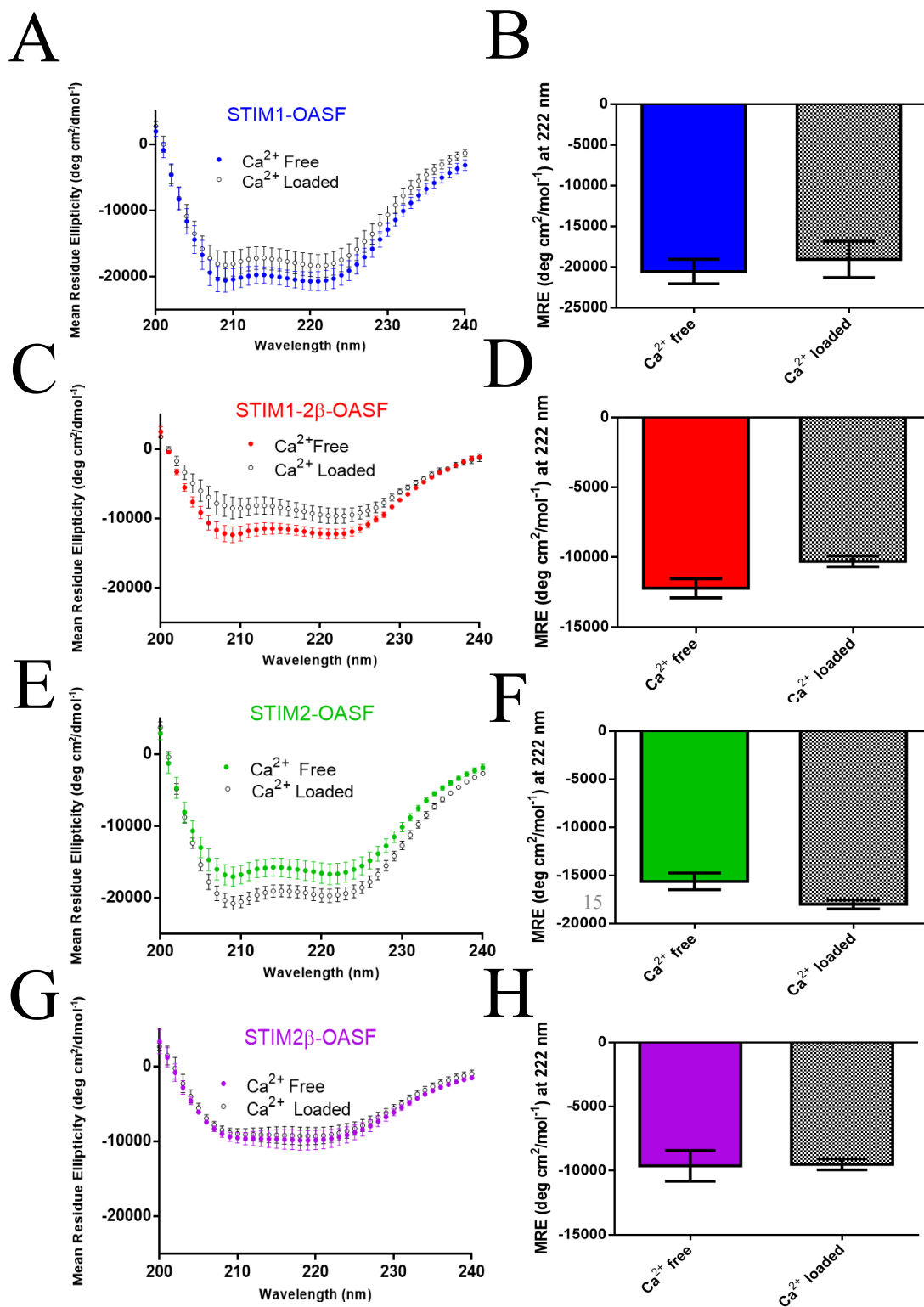


Figure 3.5: Ca²⁺ causes only minor changes in the secondary structure levels of the human OASF domains. Far-UV CD spectra of STIM1-OASF (blue circle) (**A** and **B**), STIM1-2 β -OASF (red circle) (**C** and **D**), STIM2-OASF (green circles) (**E** and **F**) and STIM2 β -OASF (purple circle) (**G** and **H**). The spectra acquired in the Ca²⁺-loaded conditions are shown as black open symbols and checkered patterns in the UV spectra and bar graphs, respectively. Data are means \pm SEM of n = 3 separate protein preparations (p > 0.05 compared Ca²⁺ free conditions for all comparisons).

3.5 Ca^{2+} thermally destabilizes STIM1-OASF and STIM1-2 β OASF

Next, I monitored changes in far-UV CD signal at 222 nm as a function of temperature to assess whether Ca^{2+} affects the thermal stability of the OASF proteins. Consistent with the trend to lower α -helicity observed for both STIM1-OASF and STIM1-2 β -OASF (see above), both these proteins exhibited decreased thermal stabilities in the presence of 25 mM CaCl_2 . STIM1-OASF showed a T_m of 47.1 ± 0.2 °C in the presence of CaCl_2 and a T_m of 50.5 ± 0.2 °C in the absence of CaCl_2 (i.e. $\Delta T_m = \sim -3$ °C, $**p < 0.01$) (Figure 3.6A and Figure 3.6B). Similarly, STIM1-2 β -OASF showed a Ca^{2+} -induced destabilization as the apparent T_m was 42.3 ± 0.6 °C in the presence of CaCl_2 compared to 46.8 ± 0.1 °C in the Ca^{2+} -free conditions (i.e. $\Delta T_m = \sim -5$ °C, $*p < 0.05$) (Figure 3.6C and Figure 3.6D) (Table 3.3).

In contrast to the STIM1 data, STIM2-OASF showed no significant differences in apparent T_m in the presence of 25 mM CaCl_2 compared to the absence of CaCl_2 . Specifically, the T_m of STIM2-OASF was 45.0 ± 0.4 °C with CaCl_2 compared to 46.6 ± 0.5 °C without CaCl_2 (i.e. $\Delta T_m = \sim +1$ °C, $p > 0.05$) (Figure 3.6E and Figure 3.6F). Similarly, the addition of CaCl_2 to the STIM2 β -OASF sample did not significantly alter the T_m . The T_m was 41.2 ± 0.9 °C for STIM2 β -OASF in presence of CaCl_2 compared to 42.6 ± 0.9 °C in the absence of CaCl_2 (i.e. $\Delta T_m = \sim +1$ °C, $p > 0.05$) (Figure 3.6G and Figure 3.6H) (Table 3.3).

Together, the thermal stability data suggest that Ca^{2+} significantly destabilizes STIM1-OASF and STIM1-2 β -OASF but does not significantly affect STIM2-OASF and STIM2 β -OASF stability. These differences could reflect discrepancies in the structures adopted by the STIM1-OASF compared to STIM2-OASF (see below).

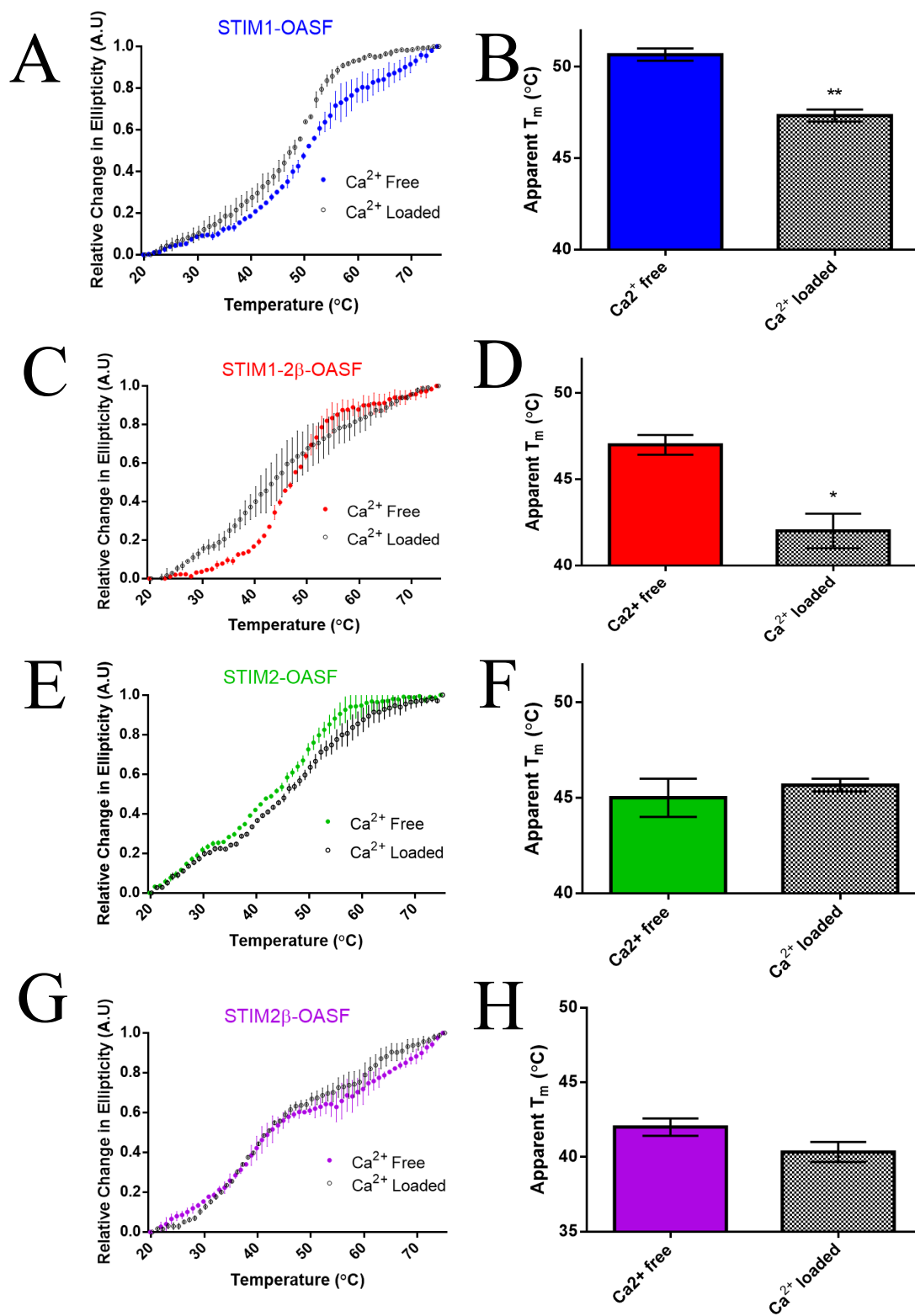


Figure 3.6: Ca²⁺ induces destabilization of STIM1-OASF and STIM1-2 β -OASF proteins. Far-UV CD thermal melts of STIM1-OASF (**A** and **B**), STIM1-2 β -OASF (**C** and **D**), STIM2-OASF (**E** and **F**) and STIM2 β -OASF (**G** and **H**) in the presence and absence of 25 mM CaCl₂. Data acquired in the presence of CaCl₂ are shown with open symbols. Data are means \pm SEM of n = 3 separate protein preparations (*p < 0.05, ** p < 0.01 vs Ca²⁺ free conditions. Ca²⁺ data points are replotted from figure 3.2.

Table 3.3: Summary of the thermal stabilities for STIM1-OASF, STIM1-2 β -OASF, STIM2-OASF and STIM2 β -OASF in the presence and absence of high Ca²⁺

Protein	Buffer Condition	Apparent T_m °C (Mean \pm SEM)	ΔT_m °C
STIM1-OASF	Ca ²⁺ free (n = 3)	50.5 \pm 0.2	-3.4 °C
	Ca ²⁺ loaded (n = 3)	47.1 \pm 0.2**	
STIM1-2β-OASF	Ca ²⁺ free (n = 3)	46.8 \pm 0.1	-4.5 °C
	Ca ²⁺ loaded (n = 3)	42.3 \pm 0.6*	
STIM2-OASF	Ca ²⁺ free (n = 3)	45.0 \pm 0.4	+1.6 °C
	Ca ²⁺ loaded (n = 3)	46.6 \pm 0.5	
STIM2β-OASF	Ca ²⁺ free (n = 3)	42.6 \pm 0.9	+1.4 °C
	Ca ²⁺ loaded (n = 3)	41.2 \pm 0.9	

Statistical analysis was performed using an unpaired two-tailed student's t-test

***p < 0.05, **p<0.01 vs Ca²⁺ free conditions**

3.6 STIM1-OASF, STIM1-2 β -OASF and STIM2 β -OASF undergo a Ca²⁺-dependent increase in aggregation propensity

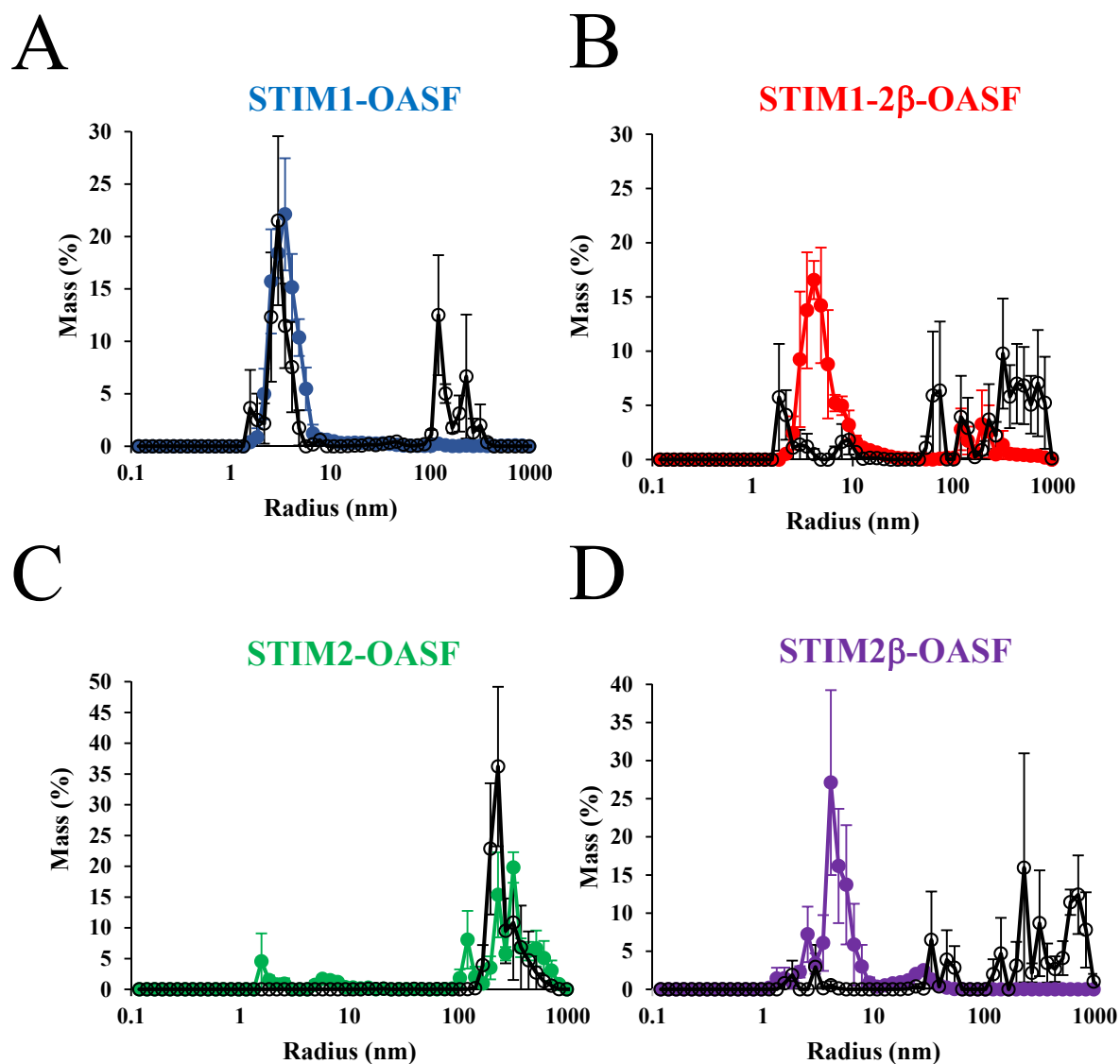
STIM-mediated activation of Orai1 channels requires oligomerization by both the N-terminal luminal domains and the cytosolic CC domains (Stathopoulos et al., 2013; Stathopoulos et al., 2009; Stathopoulos et al., 2008; Zheng et al., 2008). These oligomerization events are linked to the conformational extension within the cytosolic domains of STIM which ultimately promotes interactions with phosphoinositides and Orai1 subunits on the PM (DeHaven et al., 2007; Enomoto et al., 2017; Korzeniowski et al., 2010; Muik et al., 2009). Thus, I next assessed the oligomerization propensity of the OASF proteins by DLS.

I first assessed Ca²⁺-induced changes in oligomerization. In the absence of Ca²⁺, STIM1-OASF showed a major distribution of hydrodynamic radii (R_h) centered at \sim 3.48 nm. Similarly, the STIM1-2 β -OASF variant showed the major distribution of R_h values centered at \sim 4.10 nm. Upon addition of 25 mM CaCl₂, both STIM1-OASF and STIM1-2 β -OASF exhibited a large fraction (i.e. > 25 % by mass) of higher order oligomers with R_h greater than 100 nm (Figure 3.7A and Figure 3.7B).

Interestingly, STIM2-OASF was found to be in a largely aggregated state with most particles exhibiting R_h of > 100 nm (i.e. > 90 % by mass). Remarkably, STIM2 β -OASF showed a lower propensity for oligomerization with most particles exhibiting an R_h of 4.10 nm, similar to the distribution observed for STIM1-2 β -OASF. Upon addition of 25 mM CaCl₂, STIM2-OASF maintained its largely aggregated state, while the majority of the STIM2 β -OASF protein was converted to larger aggregates (i.e. > 100 nm) (Figure 3.7C and 3.7D).

Taken together, the DLS data show that Ca²⁺ induces and/or favours higher order oligomerization of STIM1-OASF, STIM1-2 β -OASF, STIM2-OASF and STIM2 β -OASF. Additionally, the data revealed that incorporation of the 2 β variation into either the STIM1-OASF or STIM2-OASF context promotes similar oligomerization states in the presence and absence of Ca²⁺. This effect on oligomerization is most noticeable in the STIM2-OASF

context where STIM2-OASF is largely oligomerized whereas STIM2 β -OASF shows a much smaller distribution of R_h which closely matches STIM1-2 β -OASF (Figure 3.8A and Figure 3.8B).



17

Figure 3.7. Ca²⁺ promotes aggregation of STIM1-OASF, STIM1-2β-OASF, STIM2-OASF and STIM2β-OASF. DLS analysis of STIM1-OASF (light blue) (A), STIM1-2βOASF (red) (B), STIM2-OASF (green) (C), and STIM2β-OASF (purple) (D), Data acquired in the presence of 25 mM CaCl₂ are shown as open symbols. Data are means ± SEM of n = 3 separate protein preparations.

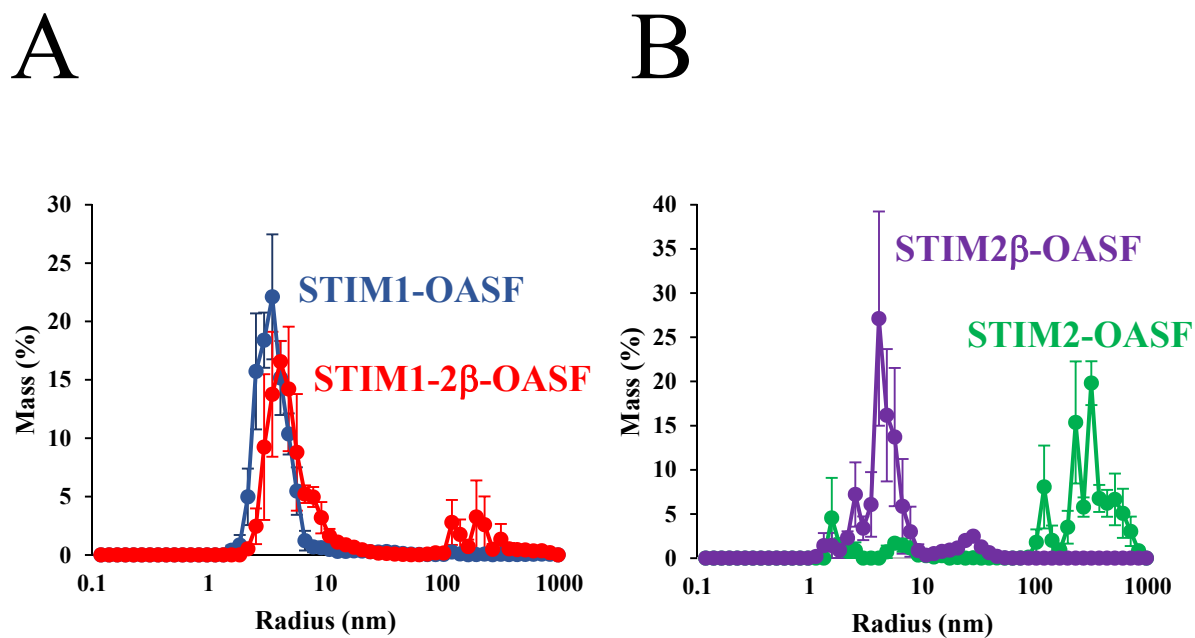


Figure 3.8. The 2 β insertion promotes similar hydrodynamic distribution as STIM1-2 β -OASF and STIM2 β -OASF conformations. Data are replotted from Figure 3.7.

3.7 The 2 β insertion does not alter OASF quaternary structure

At dilute protein concentrations and low temperatures STIM1-OASF is dimeric (Muik et al., 2011; Thompson et al., 2018). Having discovered that the 2 β insert restricts the aggregation of the STIM2 β -OASF and promotes a similar distribution of particle sizes in the STIM1-2 β -OASF and STIM2 β -OASF contexts, I next probed the quaternary structure of the smallest particle size detectable in solution using SEC-MALS experiments and the effect Ca²⁺ has on this quaternary structure. SEC-MALS showed that the elution volume of STIM1-OASF, STIM1-2 β -OASF, STIM2-OASF and STIM2 β -OASF is not altered by the presence of 25 mM CaCl₂. The MALS-determined molecular weights of all the OASF proteins indicated dimeric quaternary structures in both the presence and absence of 25 mM CaCl₂ (Figure 3.9A, Figure 3.9B, Figure 3.9C and Figure 3.9D). Specifically, based on the theoretical molecular weights of the monomer subunits, the stoichiometries of STIM1-OASF, STIM1-2 β -OASF, STIM2-OASF and STIM2 β -OASF were 2.2, 2.0, 2.0 and 2.0, respectively (Table 3.4). In the presence of Ca²⁺ the stoichiometries was 2.0 for all proteins. Interestingly, the STIM1-2 β -OASF protein showed an earlier elution volume compared to the STIM1-OASF counterpart, and this earlier elution volume was more similar to STIM2-OASF and STIM2 β -OASF (Table 3.4).

Taken together, the SEC-MALS data revealed all OASF proteins in the presence and absence of Ca²⁺ maintain a dimeric stoichiometry. However, STIM1-OASF elutes at later elution volumes suggesting a more compact (i.e. small) OASF conformation compared to STIM1-2 β -OASF, STIM2-OASF and STIM2 β -OASF.

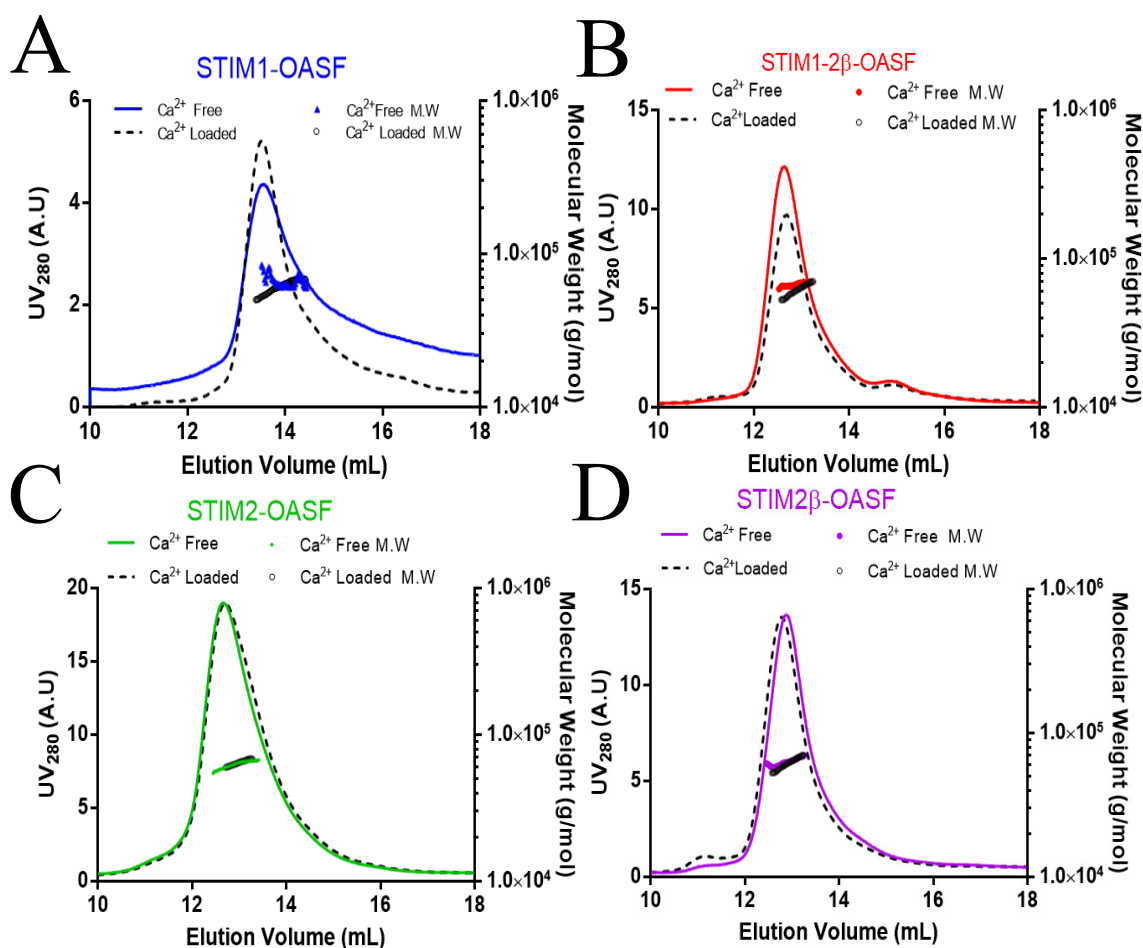


Figure 3.9. STIM1-OASF, STIM1-2β-OASF, STIM2-OASF and STIM2β-OASF form dimers in the presence and absence of Ca²⁺. SEC-MALS analysis of STIM1-OASF (A), STIM1-2β-OASF (B), STIM2-OASF (C), and STIM2β-OASF (D) The elution profiles acquired in the presence of 25 mM CaCl₂ are shown as dashed black lines in each panel. The MALS-determined molecular weights calculated for each elution peak are shown under the peaks as closed circles. A summary of the elution volumes, molecular weights and stoichiometries is given in Table 3.4. The SEC-MALS was performed using a Superdex 200 increase 10/300 GL at 10 °C.

Table 3.4: Summary of the SEC-MALS data of STIM1-OASF, STIM1-2 β -OASF, STIM2-OASF and STIM2 β -OASF proteins

Protein	Ca²⁺ (a)	Elution^(b) Volume (mL)	MALS Molecular Weight (kDa)	Stoichiometric Ratio^(c)
STIM1-OASF	-	13.59 \pm 0.14	67.6 \pm 1.4	2.18
STIM1 2β-OASF	-	12.69 \pm 0.05	64.9 \pm 1.7	2.02
STIM2-OASF	-	12.69 \pm 0.02	61.4 \pm 1.3	1.98
STIM2β-OASF	-	12.85 \pm 0.02	60.8 \pm 0.2	1.96
STIM1-OASF	+	13.55 \pm 0.01	62.3 \pm 3.7	2.00
STIM1 2β-OASF	+	13.03 \pm 0.3	63.0 \pm 1.3	1.96
STIM2-OASF	+	12.76 \pm 0.08	61.8 \pm 2.1	1.99
STIM2β-OASF	+	12.87 \pm 0.2	61.3 \pm 1.6	1.97 ⁱ

(a) represents SEC-MALS experiments were conducted in 25 mM Ca²⁺, - represents SEC-MALS experiments conducted in Ca²⁺ free conditions

(b) Superdex 200 chromatography column was used to filter and elute protein based on size

(c) Stoichiometric ratio was calculated by dividing the calculated MALS value by the theoretical monomer mass

3.8 The 2 β insertion does not alter gross OASF structure

Having discovered that the 2 β insertion decreases the level of α -helicity but does not alter the quaternary structure of STIM1-OASF or STIM2-OASF under stable and dilute conditions, I next assessed whether the 2 β variation causes gross structural changes to the domain using SAXS. The SAXS data was also acquired at 4 °C to stabilize the dimer conformation. High quality SAXS information requires high concentration and low levels of protein aggregation to yield scattering profiles which show a high level of scattering intensity after subtraction of buffer controls. Unfortunately, I found that STIM1-OASF, STIM1-2 β -OASF, STIM2-OASF and STIM2 β -OASF had a maximum achievable protein concentration of $\sim 0.8 - 1.1 \text{ mg mL}^{-1}$. Above this concentration the samples exhibited a high level of protein precipitation. Thus, all SAXS data was acquired at this relatively low concentration range, yielding noisy scattering profiles, particularly evident at higher s values (vector magnitudes).

Nevertheless, STIM1-OASF provided the SAXS profile with the least variability at higher s values (Figure 3.10A). From this data, the radius of gyration (R_g) was determined using a Guinier plot using only low s values (Figure 3.10B). The maximum particle diameter (D_{\max}) was estimated to be 11.40 nm from the Porod distance distribution plot (Figure 3.10C). Similar analyses for the STIM1-2 β -OASF protein revealed an R_g and D_{\max} of 2.94 nm and 11.10 nm, respectively (Figure 3.10D, Figure 3.10E and Figure 3.10F). The STIM2-OASF and STIM2 β -OASF proteins showed R_g values of 2.96 and 3.43 nm, respectively, and the D_{\max} values from the Porod distribution functions were 11.35 and 13.20 nm, respectively (Figure 3.11A, Figure 3.11B, Figure 3.11C, Figure 3.11D, Figure 3.11E and Figure 3.11F).

Next, I used the scattering profiles and D_{\max} from the Porod distribution plots to calculate low resolution bead models of the various OASF proteins using DAMMIF. Interestingly, for the STIM1-OASF data, two possible conformations were reconstructed. One conformation showed a single extension, which presumably corresponds to interacting CC1 domains (see Figure 1.2), while the second conformation showed two separate CC1 domains (Figure 3.12A and Figure 3.12B). The bead models for the STIM1-2 β -OASF,

STIM2-OASF and STIM2 β -OASF all exhibited very similar conformations as the STIM1-OASF model with the single extension (Figure 3.12C, Figure 3.12D and Figure 3.12E).

Overall, the SAXS data revealed R_g values in-line with the smallest distribution of R_h measured by DLS. Additionally, the 2 β insert did not cause major changes in either R_g or D_{max} , suggesting more CAD specific structural changes caused by the variation in both the STIM1-OASF and STIM2-OASF contexts. Consistent with this notion, the reconstructed bead models for all OASF proteins showed similar accessible global conformations with or without the 2 β insertion.

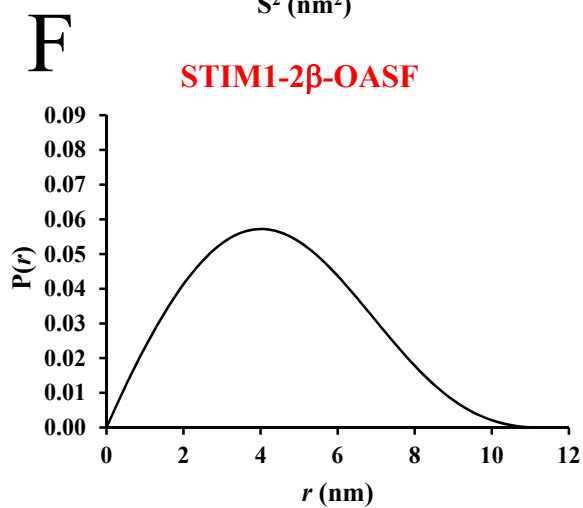
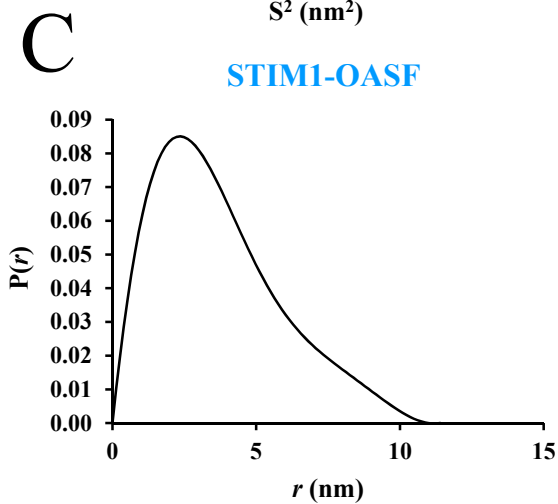
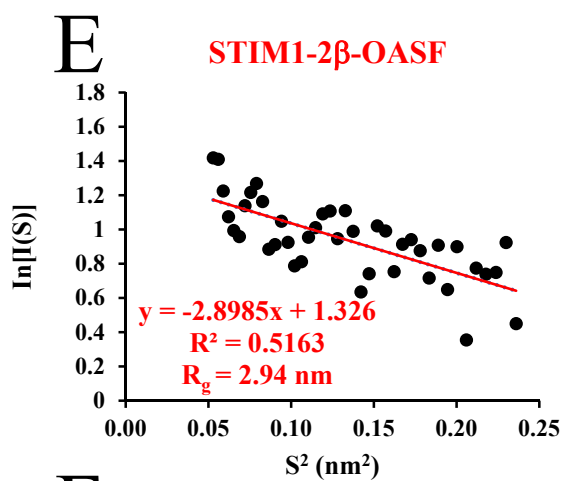
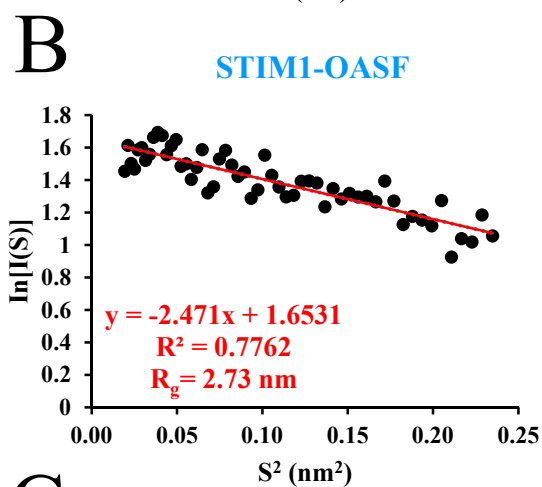
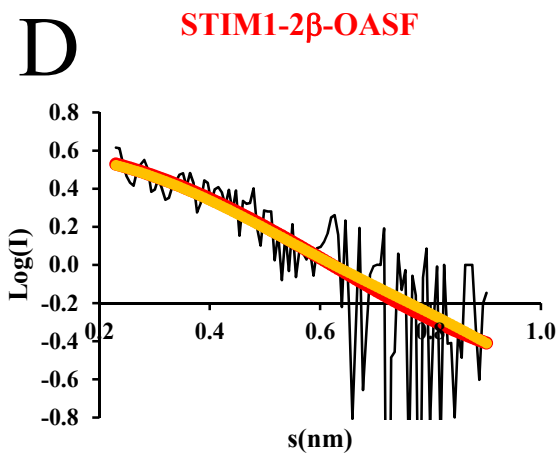
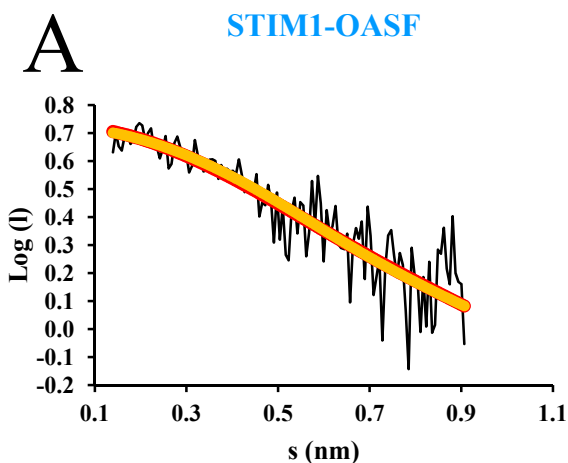


Figure 3.10: The 2 β insertion causes only minor changes to the STIM1-OASF R_g and D_{max} . (A) SAXS scattering profile of STIM1-OASF acquired at 1.04 mg mL⁻¹. (B) Guinier plot of STIM1-OASF using only low s values. (C) Porod distance distribution functions of STIM1-OASF. (D) SAXS scattering profile of STIM1-2 β -OASF acquired at 0.86 mg mL⁻¹. (E) Guinier plot of STIM1-2 β -OASF using only low s values. (F) Porod distance distribution functions of STIM1-2 β -OASF. In (A) and (D), the scattering profile reconstructed from the Porod distribution plot is shown in red while the profile reconstructed from the DAMMIF model (see Figure 3.12 below) is shown in yellow

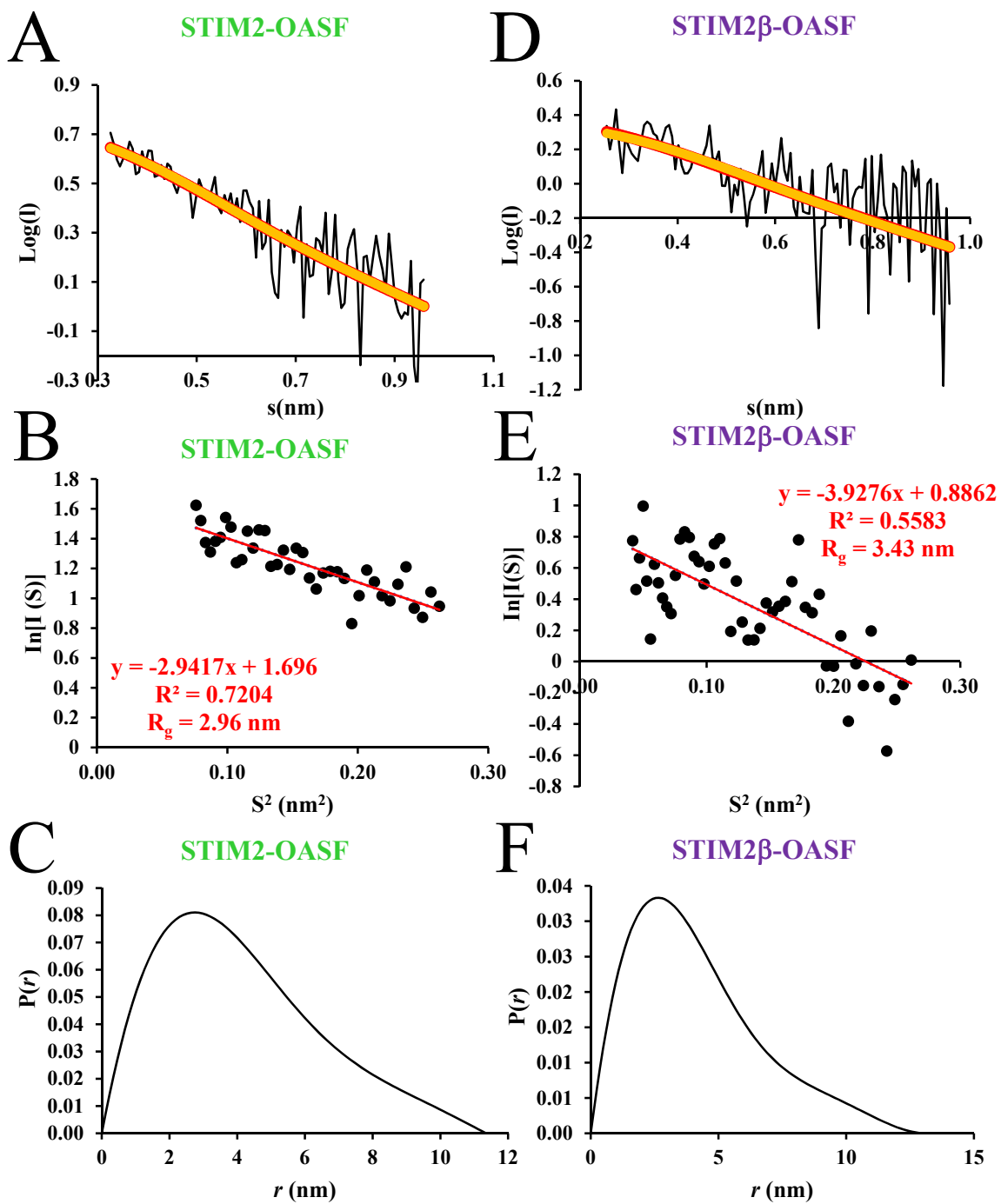


Figure 3.11: The 2 β insertion causes only minor changes to the STIM2-OASF R_g and D_{max} . (A) SAXS scattering profile of STIM2-OASF acquired at 1.05 mg mL⁻¹. (B) Guinier plot of STIM2-OASF using only low s values. (C) Porod distance distribution function of STIM2-OASF. (D) SAXS scattering profile of STIM2 β -OASF acquired at 1.10 mg mL⁻¹. (E) Guinier plot of STIM2 β -OASF using only low s values. (F) Porod distance distribution functions of STIM2 β -OASF. In (A) and (D), the scattering profile reconstructed from the Porod distribution plot is shown in red while the profile reconstructed from the DAMMIF model (see Figure 3.12 below) is shown in yellow.

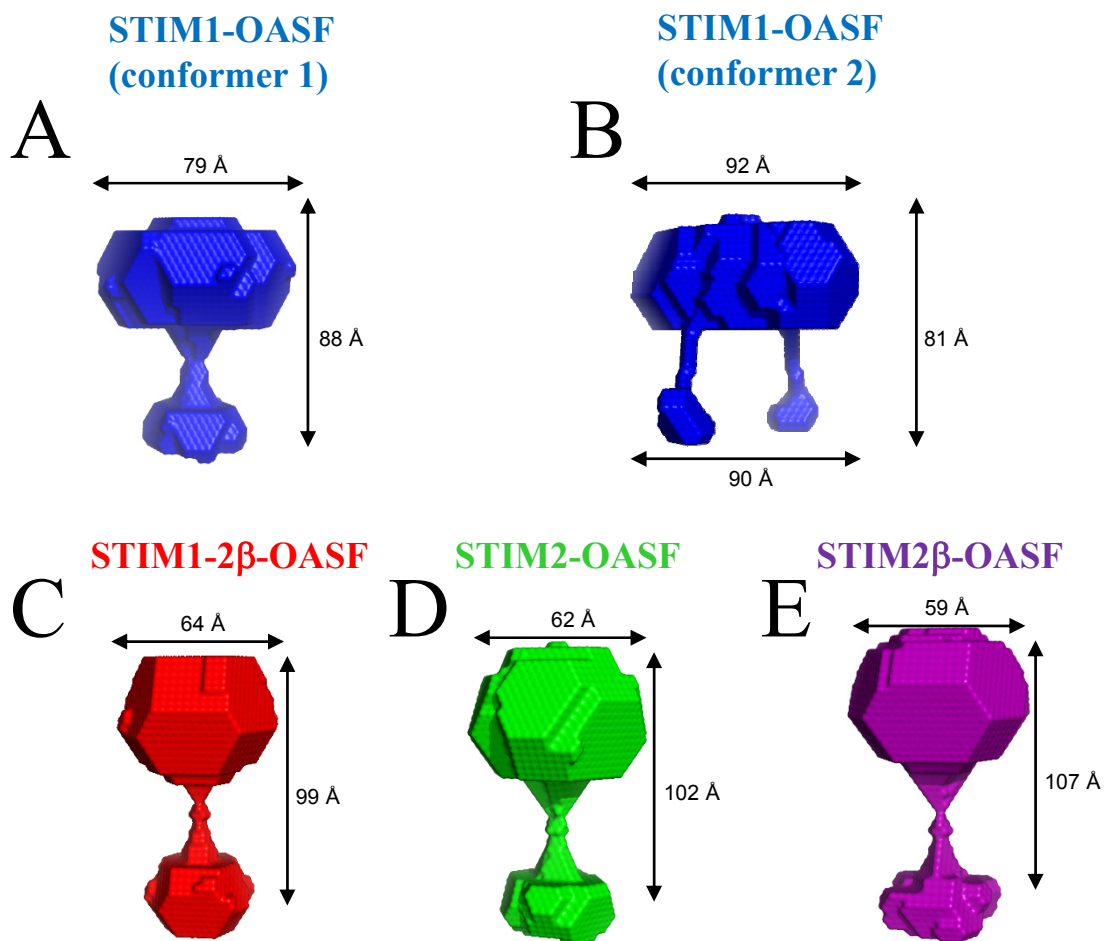


Figure 3.12. SAXS-derived bead models suggest similar global structures accessible by STIM1-OASF, STIM1-2 β -OASF, STIM2-OASF and STIM2 β -OASF. DAMMIF-derived bead of STIM1-OASF (conformation 1) (**A**), STIM1-OASF (conformation 2) (**B**), STIM1-2 β -OASF (**C**), STIM2-OASF (**D**), and STIM2 β -OASF (**E**). The reconstructed scattering curves based on the DAMMIF structures are plotted on the respective scattering profiles shown in Figure 3.10 and 3.11.

3.9 The 2 β insertion inhibits OASF function in SOCE independent of the STIM2 context

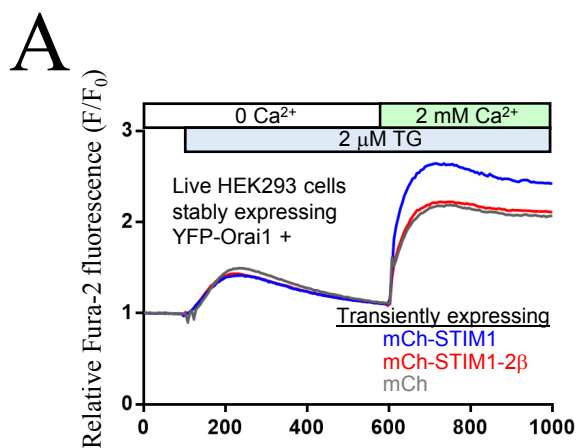
The VAASYLIQ insertion has only been identified in STIM2 homologues. Additionally, the ability of STIM2 β to inhibit Orai1 activation in SOCE has already been established by several studies (Miederer et al., 2015; Rana et al., 2015). Further, even without the 2 β insert, STIM2 is known to couple to Orai1 and activate SOCE less efficiently than STIM1 (Oh-Hora et al., 2008; Wang et al., 2014; Zhou et al., 2016). Thus, it remains unknown whether the underlying inhibitory mechanism by 2 β is a result of insertion into the context of the STIM2 which is a weak SOCE activator or whether the inhibition is due the ability to alter the intrinsic biophysical and conformational properties of OASF required for inducing SOCE.

Having shown that the 2 β insert similarly decreases the α -helicity and thermally destabilizes STIM1-OASF and STIM2-OASF and revealing that all OASF proteins access similar global structures, I next assessed whether the 2 β insert must be in the STIM2 context to exert an inhibitory effect on SOCE. First, I introduced the 2 β insert into full-length mCherry tagged STIM1 (mCh-STIM1) by site directed mutagenesis. Subsequently, HEK293 cells stably expressing YFP tagged Orai1 (YFP-Orai1) (Choi et al., 2017; Gui et al., 2018; Zhu et al., 2018) were transfected with WT mCh-STIM1 or mCh-STIM1-2 β . After loading the cells with Fura-2, SOCE was assessed using ratiometric fluorescence spectroscopy. Cells were initially bathed in HBSS medium in the absence of Ca²⁺. Upon addition of thapsigargin (TG) (2 μ M), the transient release of Ca²⁺ from the ER was not significantly different between the empty mCh-vector control, mCh-STIM1 and mCh-STIM1-2 β groups (Figure 3.13A and Figure 3.13B). After 500 s of passive ER Ca²⁺ store depletion, 2 mM of Ca²⁺ was added the cell bathing medium. As expected, cells expressing mCh-STIM1 showed a significantly higher level of SOCE than the empty vector expressing cells (i.e. Δ Fura2 ratio of 1.56 ± 0.04 compared to 1.23 ± 0.1 , respectively) (*p < 0.05) (Figure 3.13A and Figure 3.13C). When Ca²⁺ was added back to cells expressing mCh-STIM1-2 β , the Δ Fura2 ratio was not significantly different than the empty vector

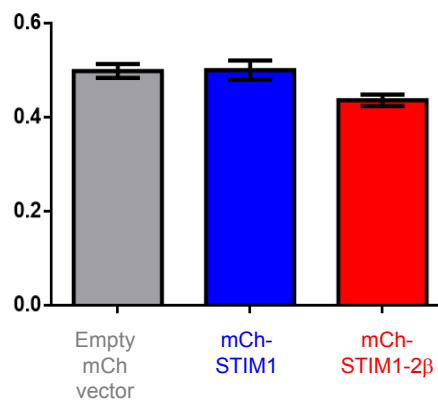
expressing cells (i.e. 1.23 ± 0.03 compared to 1.21 ± 0.1 , respectively) ($p > 0.05$) (Figure 3.13A and Figure 3.13C).

To confirm that the differences in SOCE mediated by mCh-STIM1 and mCh-STIM1-2 β were not due differences in expression levels, I obtained mCh and YFP fluorescence emission spectra of the cell suspensions used for the Fura measurements. Our laboratory has previously shown that mCh-STIM1 fluorescence correlates with proteins levels assessed by western blots (Zhu et al., 2018). As expected mCh-STIM1 and mCh-STIM1-2 β expression levels were not significantly different from one another, while the empty mCh-vector control showed higher fluorescence since it was not targeted to the ER (Figure 3.13D). Similarly, YFP fluorescence was not different among the three groups tested (Figure 3.13E).

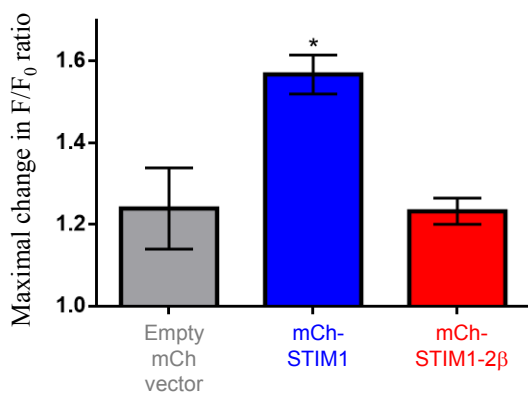
Collectively, these results show that incorporating 2 β insert into the OASF region of full length STIM1 perturbs SOCE activity, as previously observed for STIM2, suggesting that the VAASYLIQ insertion perturbs the structure, independent of the homologue-specific amino acid sequence.



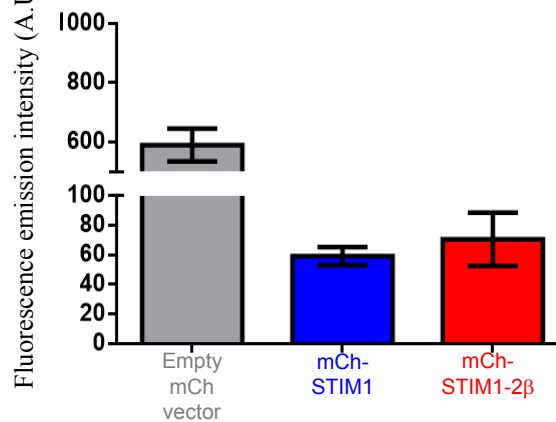
B TG-induced ER Ca^{2+} release
(between 100 – 600 s)



C SOCE after Ca^{2+} addback
(between 600 – 1000 s)



D mCh fluorescence



E YFP fluorescence

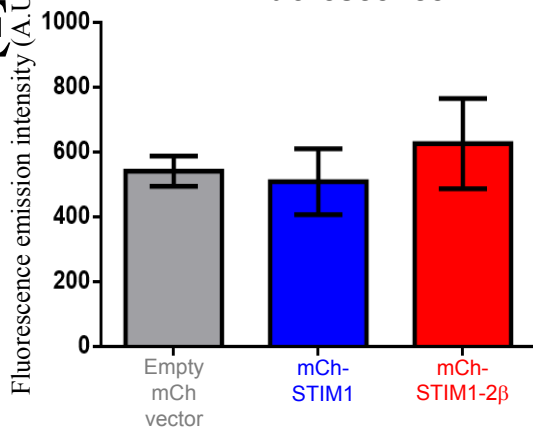


Figure 3.13: The 2 β insertion perturbs the SOCE-inducing function of STIM1 in the full-length molecular context. (A) Representative Fura-2 fluorescence traces of SOCE recorded in mCh-STIM1 (blue), mCh-STIM1-2 β insert (red) and empty mCh-vector (grey) expressing HEK293 cells also stably expressing YFP-Orai1. The data was normalized by plotting F/F_0 to determine the maximum ΔF_{ura-2} -ratio after TG addition and Ca^{2+} addback. (B) Maximal ER Ca^{2+} release taken as the maximum ΔF_{ura-2} ratio after TG addition. (C) Maximal SOCE taken as the maximum ΔF_{ura-2} ratio after Ca^{2+} addback. (D) mCh fluorescence levels of cell suspensions. (E) YFP fluorescence levels. Statistical analysis was conducted using a One-way ANOVA with Tukey's multiple comparisons test. All data are means \pm SEM of n=4 separate transfections.

Chapter 4: Discussion

4.1 Summary

The CAD domain, which is composed of CC2 and CC3 in STIM1 and STIM2, contains all the machinery required to activate Orai1-composed Ca^{2+} channels on the PM. However, CC1 is required to induce the conformational rearrangement within the STIM1 cytosolic domains which extends the protein to bridge the distance between the ER and PM and allow for direct contact between CAD and Orai. Thus, the entire OASF region is critical for intracellular Ca^{2+} homeostasis mediated by SOCE. Indeed, previous studies have demonstrated that heritable mutations in the STIM1 CAD and CC1 regions lead to disease. Disease pathologies can result from a gain of function, as is caused by R304W in CC1 which constitutively increases SOCE (Misceo et al., 2014; Morin et al., 2014) or a loss of function, as is caused by R429C in CC3 which prevents the activation of STIM1 and SOCE (Maus et al., 2015). Remarkably, cells have also evolved a mechanism to modulate CAD function through phosphorylation of T389 in CC2. The effects of this phosphorylation within CAD can be artificially mimicked through introduction of the T389E mutant which inhibits STIM1 activity (Thompson & Shuttleworth, 2015; Thompson et al., 2018).

Alternative splicing is another evolutionary mode of SOCE regulation, as the retention of an 8-amino acid residue stretch (i.e. 2 β insert) in the CAD domain of STIM2 gives rise to an inhibitory isoform known as STIM2 β . (Miederer et al., 2015; Rana et al., 2015). To elucidate how the 2 β insert converts the CAD domain into an inhibitor of SOCE, I generated site-specific mutagenic constructs to incorporate the 2 β insert into *H. sapiens* STIM1 and STIM2 OASF. I used the entire OASF region in my studies since it includes all the CC domains, each of which play an important role in the activation mechanism of STIMs. My structural studies using far-UV CD spectroscopy showed that the 2 β insert decreases the α -helicity and destabilizes OASF. I also found using ANS binding experiments that the 2 β insert increases the exposed hydrophobicity of OASF and the structural sensitivity of OASF to high concentrations of Ca^{2+} . Based on my SEC-MALS data, these changes in secondary structure and hydrophobic exposure do not affect the assembling dimer quaternary structure of OASF. Further, my low resolution SAXS

analysis suggests similar overall shapes are accessible by OASF proteins with and without the 2 β insert. Finally, using Fura-2 cytosolic Ca²⁺ measurements, I found that the 2 β insert markedly inhibits STIM1 activity and SOCE, as previously observed for STIM2. Collectively, my work demonstrates that the 2 β insert inhibits STIM activity by incorporation into the OASF structural context, independent of the STIM2-specific sequence of amino acids making up OASF.

4.2 OASF structure, variations and function

Previous studies have identified regulatory modifications in the OASF region which result in lower SOCE activity. The 2 β insert, is mutated between G379 and A380 in STIM1 which located in close proximity to T389, where the phosphorylation of this residue effectively inhibits store-dependent CRAC channel and promotes store-independent ARC channel activity (Thompson & Shuttleworth, 2015). The negatively charged properties of the phosphate group can be mimicked through a single point mutation (i.e. T389E), also inhibiting SOCE. Interestingly, the T389E mutation increases the α -helicity of STIM1-OASF (Thompson et al., 2018). Consistent with the increase in α -helicity, the phosphomimetic mutant also promotes higher thermal stability. The stabilization of STIM1-OASF is thought to be due to an extension of the CC2 helix which uniquely allows for the precise activation store-independent ARC channels and no activation of CRAC channels. Conversely, my work has shown that 2 β insert decreases α -helicity and thermal stability of STIM1-OASF (Figure 3.1 and Figure 3.2). This observation is consistent with the R429C mutation that results SCID-like syndrome which decreases the α -helicity and stability of OASF, thereby inhibiting STIM1 and SOCE activity (Maus et al., 2015).

In SOCE, dimeric STIM1 undergoes a structural change to expose the CAD region which gates Orail-composed CRAC channels at the ER-PM junctions. A previous study has shown that a concatenated CAD dimer containing the F394H point mutation in each subunit completely blocks the ability of this homodimer to induce SOCE (Zhou et al., 2015). However, if the mutation is introduced into only one of the monomers, Orail binding and activation remains unaffected, suggesting unimolecular coupling between STIM1 and Orail (Zhou et al., 2015). Using HEK cells, Zhou et al. also compared the

Orai1 activation using a STIM1/STIM2 β heterodimers and found that they were able to couple with activate Orai1 channels. This finding suggests that homodimers of STIM2 β are necessary to induce complete SOCE inhibition. However, this work by Zhou et al. is inconsistent with the data presented by Rana et al. and Miederer et al., where both groups independently found STIM1/STIM2 β and STIM2/STIM2 β heterodimers were unable to activate Orai1-composed CRAC channels(Miederer et al., 2015; Rana et al., 2015). It should also be noted that Zhou et al. speculated that the 2 β insert induces an α -helical extension (Zhou et al., 2015); however, my work clearly shows that incorporating the 2 β insert into OASF significantly reduces α -helicity in both the STIM1 and STIM2 context (Figure 3.1).

One of the steps in SOCE is the conformational change of OASF from a compact inactive state to an extended activated state (Muik et al., 2011). This transition exposes the CC2-CC3 (i.e. CAD) region to the PM where interactions can occur with Orai1 subunits resulting in CRAC gating and activation. Based on my SEC data, the extended conformation was adopted by STIM1-2 β insert and STIM2 β -OASF (Figure 3.9). Interestingly, STIM2-OASF, but not STIM1-OASF, was also in the extended conformation, as indicated by the earlier elution volumes. Therefore, SOCE inhibition by the 2 β insert is likely not attributable to the inability for STIM1 to transition to the extended state; rather, the inhibition occurs downstream of the conformational extension.

Several models of SOCE inhibition by the 2 β insert have been suggested. Homology modeling has suggested that the 2 β insert alters the self-association of CAD such that it cannot form stable dimers, and this deficiency may underlie the inability to interact with Orai1 channels (Miederer et al., 2015). However, my data shows that the dimer nature of OASF remains intact (Figure 3.9). Another model suggests that STIM2 β precludes binding of STIM1 or STIM2 to Orai1 subunits through steric hinderance when cytosolic Ca²⁺ ions are present essentially inducing a negative feedback process to halt SOCE (Miederer et al., 2015). My findings show that Ca²⁺ may be driving a state of aggregation (Figure 3.7) through promoting greater exposed hydrophobicity (Figure 3.3) within OASF. The aggregation of STIM1 and STIM2 in the presence of Ca²⁺ may prevent coupling between

CAD and Orai1 by burying Orai1 binding site. Interestingly, Rana et al. showed that SOCE inhibition by the 2 β insert is sensitive to variations in the 8-residue insert sequence (Rana et al., 2015). Thus, another possible mechanism is a more active inhibition, whereby STIM2 β adopts a conformation which delivers inhibitory signals through interactions with Orai1 (Rana et al., 2015). This type of inhibition would be sequence-specific, consistent with the ability of mutations in this region to reduce the effects of inhibition.

The 2 β insert is found at residues 383 - 391 in STIM2 β ; however, it would be found at residues 379 - 387 when/if naturally incorporated into STIM1 (Figure 1.3). There has been extensive structural characterization in the STIM1 CC1-CC2 region using solution NMR spectroscopy and SAXS. Previous studies showed that the CC1-CC2 structure exhibits two extended helices called α 1 (residues 313 - 340) and α 2 (residues 344 - 382) that are linked together by a short loop called L1 (residues 341 - 343) (Stathopoulos et al., 2013; X. Yang et al., 2012). This CC1-CC2 structure showed that monomers form an antiparallel symmetric dimer through α 1: α 1', α 2: α 2' and C-terminal α 2:L1' interactions. An additional solution structure of CC1-CC2 in complex with the human Orai1 C-terminal domain revealed that many of the CC2 (i.e. α 2) residues play vital roles in directly interacting with Orai1. These α 2 residues form hydrophobic cleft which is encircled by an electropositive surface potential. Both hydrophobic and electrostatic interactions are required for binding to Orai1 C-terminal domain. The Orai1 binding region on STIM1 formed by the CC2 helices is termed the STIM-Orai association pocket (SOAP). Based on the solution NMR structure of the STIM1 CC1-CC2:Orai1 C-terminal domain complex, the 2 β insert is localized just upstream of residues intimately involved in forming the electropositive potential. Thus, 2 β insert may, at least in part, prevent binding to Orai1 by disrupting the electropositive potential of this region in STIM molecules.

4.3 Ca²⁺ and OASF function

To regulate Ca²⁺ influx and minimize risk of toxicity associated with diseases, STIM1 contains 7 highly conserved negatively charged residues (i.e. DDVDDMDEE) called the CRAC modulatory domain (CMD). This sequence is located downstream of the CC domains (i.e. 474 - 485) and is the first putative Ca²⁺ binding site identified in the STIM1-

C terminus (Derler et al., 2009). Interestingly, Derler et al. showed that STIM1 mutants that lacked the CMD region exhibited a significantly reduced inactivation of Orai/CRAC by Ca^{2+} . They proposed that Ca^{2+} binding induces a conformational change within the STIM1 cytosolic domain that perturbs the interaction with Orai1 and promotes Ca^{2+} -binding-dependent inactivation. Consistent with the Derler et al. work, another study that neutralized CMD by converting the Glu and Asp residues to Ala showed a marked reduction in Ca^{2+} -dependent inactivation not only when coupled to Orai1, but also when bound to Orai2 and Orai3 (Lee et al., 2009). These two studies conclude that the inactivation of Orai1 currents is preserved so long as the negatively charged residues in this region are present. Thus, the CMD play a role in providing a negative signal to Ca^{2+} entry through promoting fast Ca^{2+} -dependent inactivation of CRAC channels. Remarkably, my ANS data shows that incorporating 2 β insert results in greater exposed hydrophobicity (Figure 3.3). Importantly, the marked increase in exposed hydrophobicity is further exacerbated with the subsequent addition of Ca^{2+} which drives a conformational change associated with more exposed hydrophobic regions for STIM1-OASF and STIM2-OASF. My findings support the notion put forward by Derler et al. that Ca^{2+} induces a conformational change.

The oligomerization of the STIM cytosolic domains is one of the crucial steps of SOCE activation as it leads to the formation of discrete puncta, allowing for Orai co-clustering. Previous studies have shown that the STIM1 cytosolic C-terminal domains are sufficient to activate Orai1 currents, independent of store-depletion. Interestingly, confocal FRET analysis has shown that the STIM1 fragments (i.e. 233-450/474) exhibited the highest level of self-association and co-clustering with Orai1 in HEK293 cells (Zhou et al., 2015). This finding lead to the identification of residues 420-474 playing an important in the homomerization of the STIM1 cytosolic domains (Muik et al., 2009). This 420-474 region is located upstream of the putative Ca^{2+} binding site (i.e. residue 474-485). Thus, I speculate that Ca^{2+} binding to the negatively charged residues could result in a conformational change which affects the exposure of this homomerization domain. An independent study confirmed the CC regions play a role in mediating STIM1 oligomerization (Covington et al., 2010). By using coimmunoprecipitation, fluorescence

photobleaching and energy transfer techniques, they showed that STIM1 mutants lacking the cytosolic domains could not form stable oligomers in response to ER Ca^{2+} store depletion. Furthermore, they demonstrated that truncating STIM1 at CC2 resulted in no puncta formation or Orai1 recruitment after ER Ca^{2+} store depletion. However, adding back the residues making up CC3 (i.e. residues 392-448) permitted the formation of stable, higher-order STIM1 oligomers in response ER Ca^{2+} store-depletion. Thus, CC2 acting as the mediator and CC3 acting as the homomerization domain were shown to be important factors which function in tandem to mediate the formation STIM1 oligomers and promote SOCE.

My data shows that increased ANS binding at higher Ca^{2+} concentrations could be due to a Ca^{2+} -binding induced conformational change to OASF. Based on the findings presented by Covington et al. and Muik et al., these Ca^{2+} binding induces structural changes in OASF are likely to affect oligomerization and Orai1 binding due to the close proximity to CC3 (required for homomerization) and the proximity to CAD which is necessary for Orai1 binding. Therefore, the Ca^{2+} binding induced aggregation I observed for all constructs (Figure 3.7) is consistent with the conformational change induced by Ca^{2+} binding affecting the homomerization domain (i.e. CC3). It is important to note that the increased aggregation is counterintuitive given that oligomerization promotes STIM1 activation; however, I speculate that the Ca^{2+} induced aggregated state of OASF is different than the conformation required for Orai1 activation.

In the absence of Ca^{2+} , my data shows increased ANS binding in the OASF proteins containing 2 β . This increased ANS binding may be associated with the reduced α -helicity observed when the 2 β is incorporated into STIM1-OASF and STIM2-OASF (Figure 3.1). Thus, the 2 β insert may promote a localized unfolding in OASF which would lead to more ANS binding sites. The idea of a localized structural change induced by 2 β insert on both STIM1 and STIM2 is consistent the SEC-MALS data where all OASF proteins remained dimeric (Figure 3.9). Furthermore, for STIM1-OASF, there also appears to be a marked change in elution volume, even though the protein remains dimeric. This suggests that for STIM1-OASF the localized unfolding may promote the extended conformation as has been observed in previous studies (Muik et al., 2011). Since the elution volume of STIM1-2 β -

OASF is the same as STIM2-OASF and STIM2 β -OASF, both STIM2-OASF and STIM2 β -OASF may already adopt the extended conformation.

My SAXS data supports the notion that the STIM1-OASF conformation may be subtly different than STIM1-2 β -OASF, STIM2-OASF and STIM2 β -OASF since the bead model reconstruction shows two distinct conformations for STIM1-OASF: one with the CC1 domains separated and one conformation where the CC1 domains are interacting (Figure 3.12). After the 2 β insertion, the STIM1-2 β -OASF bead model exhibits a conformation similar to STIM2-OASF and STIM2 β -OASF. Interestingly, my STIM1-OASF reconstructed bead model with the CC1 regions separated bears a striking resemblance to the SAXS model reconstructed from STIM1 in a previous study (Cui et al., 2013). The STIM1-OASF (i.e. 234-491) used in my study spanned all three CC regions, while the previous study used a cytosolic STIM1 protein composed of residues 254-504. Despite this reassuring similarity between my work and the previously published SAXS data, my SAXS data overall was poor quality and further structural studies are required to more precisely compare the gross structures of OASF and perturbations caused by the 2 β insert (see below).

4.4 The 2 β insert inhibits SOCE in the context of the OASF structure

STIM2 β has been demonstrated in past studies to be inhibitory to SOCE which has been proposed to act through heterodimerization with STIM1 and STIM2 (i.e. STIM1/STIM2 β and STIM2/STIM2 β , respectively). Using total internal reflection fluorescence (TIRF) microscopy, Miederer et al. showed that STIM2 β exhibited impaired interactions with Orai1 as there was reduced co-localization between STIM2 β and Orai1 in HEK239 cells (Miederer et al., 2015). Furthermore, Rana et al. showed that while overexpression of STIM2 increases NFAT-translocation to the nucleus even in the absence of TG, overexpressed STIM2 β with Orai1 strongly inhibited TG-mediated NFAT translocation, consistent with an inhibitory role in SOCE. NFAT translocation to the nucleus is dependent on SOCE activation. Remarkably, both groups showed that STIM2 β can heterodimerize with STIM1 and STIM2 and postulated that inhibition is occurring due to interactions with

the STIM homologues. To test for heterodimerization, Rana et al. co-transfected STIM1 and STIM2 β lacking the polybasic domain such that trapping at the PM was dependent on CAD interactions with Orai1. They showed that when co-expressed, STIM2 β was recruited to Orai1 through sufficient interactions with STIM1. Similarly, Miederer et al. co-expressed STIM2 with STIM2 β in HEK293 cells and found a significant reduction in Ca²⁺ inward currents (Miederer et al., 2015).

STIM2 is a slower activator of SOCE and has a weaker efficacy of Orai1 activation (Brandman et al., 2007; Wang et al., 2014; Zhou et al., 2009). In relation to the kinetics of STIM2, to determine whether the 2 β insert is inhibitory because it is already found in the context of a weak SOCE activator (i.e. STIM2), I tested the inhibition in the context of STIM1, a robust SOCE activator. Remarkably, introducing the 2 β insert into full length STIM1 resulted in a significant reduction in SOCE activity as apparent in the reduced Fura-2 ratio (Figure 3.13). My findings suggest that the 2 β insert perturbs OASF conformation and function making OASF incapable of activating SOCE, independent of the STIM2 context of weaker Orai1 binding affinity and SOCE activation efficiency.

4.5 Conclusions

Ca²⁺ is an important regulatory ion in nearly all physiological processes. Regulation of cellular Ca²⁺ through the actions of STIM1 and STIM2 proteins maintains basal Ca²⁺ levels and allows cells to signal fluxes required for life and death processes. Mutations within the cytosolic domain of STIM1 affect SOCE activity by overactivation of CRAC channels such as via the R304W which leads to Stormorken Syndrome (Misceo et al., 2014; Morin et al., 2014). Disease can also be caused by mutations in STIM1 such as R429C which result in a SCID-like pathophysiology. Alternative splicing is a mechanism of Ca²⁺ regulation which is introduced in cells at the transcriptional level. STIM2 β is a splice isoform which inhibits SOCE (Miederer et al., 2015; Rana et al., 2015). Collectively, my biophysical data revealed that the 2 β insert reduces the α -helicity of the OASF region, promotes an alternative conformation with greater exposed hydrophobicity and increases the sensitivity of the region to Ca²⁺. Furthermore, the insertion into the robust SOCE activator of STIM1 results in complete inability to activate SOCE, as was previously

observed for the milder SOCE activator STIM2, suggesting that this 8-amino acid insert is inhibitory outside of the STIM2 context (Figure 4.1).

It is interesting to speculate that STIM2 β heterodimerization with STIM1 or STIM2 may add an additional layer of regulation to this complex, but physiologically vital process. Alternative splicing is a phenomenon that can give rise a plethora of isoforms from a single gene. My work shows that understanding the differences in the structural mechanisms of function between isoforms may provide a foundation for the future development of new therapies for disease.

4.6 Future Directions and Limitations

Solution SAXS experiments on STIM1-OASF, STIM1-2 β -OASF, STIM2 β -OASF and STIM2-OASF were unable to reveal precise structural differences between the OASF due to the low-resolution technique which was also exacerbated by poor quality data. However, my work showed that the 2 β insert decreases the overall OASF α -helicity and induces a conformation with greater exposed hydrophobicity (Figure 3.1, Figure 3.3 and Figure 3.4). Thus, future studies should work toward increasing the resolution of the structural data to provide new insights on the basis for 2 β insert-mediated inhibition at the atomic level. Previous studies have used solution NMR spectroscopy to assess various structural aspects of the CC region of STIM1-OASF (Fahrner et al., 2018; Rathner et al., 2018; Stathopoulos et al., 2013), and this approach may be useful to assess the structural effects of the 2 β insert with higher precision.

In Stromorken syndrome, the R304W in CC1 results in an overactivation of SOCE leading to symptoms such as muscle fatigue and thrombocytopenia (Fahrner et al., 2018; Morin et al., 2014). On other hand, STIM2 β robustly inhibits SOCE (Miederer et al., 2015; Rana et al., 2015). My functional data using HEK293 cells have shown incorporation of the 2 β insert into STIM1 renders STIM1 incapable of eliciting SOCE. To gain additional insight into the inhibitory mechanisms of the 2 β insert, it would be interesting to determine if incorporating the 2 β insert into a STIM1-OASF containing the R304W can abolish the constitutive activation of SOCE. Inhibition of SOCE in the STIM1-R304W context by the

2 β insert may help in the development of a new treatment strategy for Stormorken syndrome patients through exploiting the 2 β inhibition mechanism on OASF. To determine whether the 2 β heterodimers are dominant SOCE inhibitors, one could attempt to overexpress STIM2 β heterodimers in an *in vivo* mouse model of Stormorken syndrome. The ability of STIM2 β to inhibit the constitutive SOCE in Stormorken model mice would open the door to potentially treating Stormorken syndrome by altering (i.e. upregulating) the STIM2 β expression already endogenous to vertebrates.

There are limitations associated with biophysical aspects of this study. First, my experiments use isolated STIM1-OASF and STIM2-OASF outside the normal cellular milieu which could affect both structure and stability of the domain. There are STIM binding partners such as the microtubule plus-end-tracking protein-1 (EB1) (Honnappa et al., 2009), calnexin and two other transporters, exportin1 and transportin1 (Saitoh et al., 2011), and many others, which can associate with STIM1 and STIM2 and possibly affect how the 2 β insert exerts its effects. Furthermore, my biophysical studies used a segregated portion, OASF, from STIM otherwise composed of several other important regions which play a role in SOCE such as the EF-SAM domain that acts as the ER Ca²⁺ sensor and the polybasic region that interacts with the PM after conformational extension (Figure 1.2). These other domains may play a role in mediating stability and structure via allosteric and/or direct interactions.

The basal physiological concentration of Ca²⁺ in the cytosol is ~100 nM and can reach as high as ~1-2 μ M during a signaling cascade (Clapham, 2007; Kurosaki et al., 2010). I used 25 mM Ca²⁺ in my ANS binding assay, far-UV CD and SEC-MALS experiments. While this high Ca²⁺ concentration promoted a maximal Ca²⁺ response in our *in vitro* experiments, this concentration far exceeds the upper known boundaries of Ca²⁺ within cells and may not be representative of STIM protein behavior in a physiological state.

SAXS is a powerful tool that can be used to determine certain biophysical characteristics such as R_g and, importantly, reconstruct a low-resolution structure using the SAX scattering profile. However, SAXS often requires a highly concentrated and pure protein which proved challenging using my OASF proteins. High concentrations (i.e. > ~ mg mL⁻¹)

resulted in aggregation and precipitation with my OASF proteins. Due to the relatively low protein concentrations of all OASF proteins and the home source SAXS instrument used in the data acquisition (see Materials and Methods), the SAXS data suffered from low signal to noise and was, overall, of poor quality. The data was further negatively affected by the aggregation propensity of all samples.

Finally, in my functional Fura 2 assay, I was working with a population of HEK293 cells that were stably expressing YFP-Orai1 subunits. To test SOCE, I transfected my HEK293 cells to transiently express mCh-STIM1 and mCh-STIM1-2 β ; however, it was not ascertained whether the 2 β insert altered the localization of the STIM1 protein. Thus, future studies should assess the localization of the mCh-STIM1-2 β before and after ER Ca²⁺ store depletion, using TIRF microscopy.

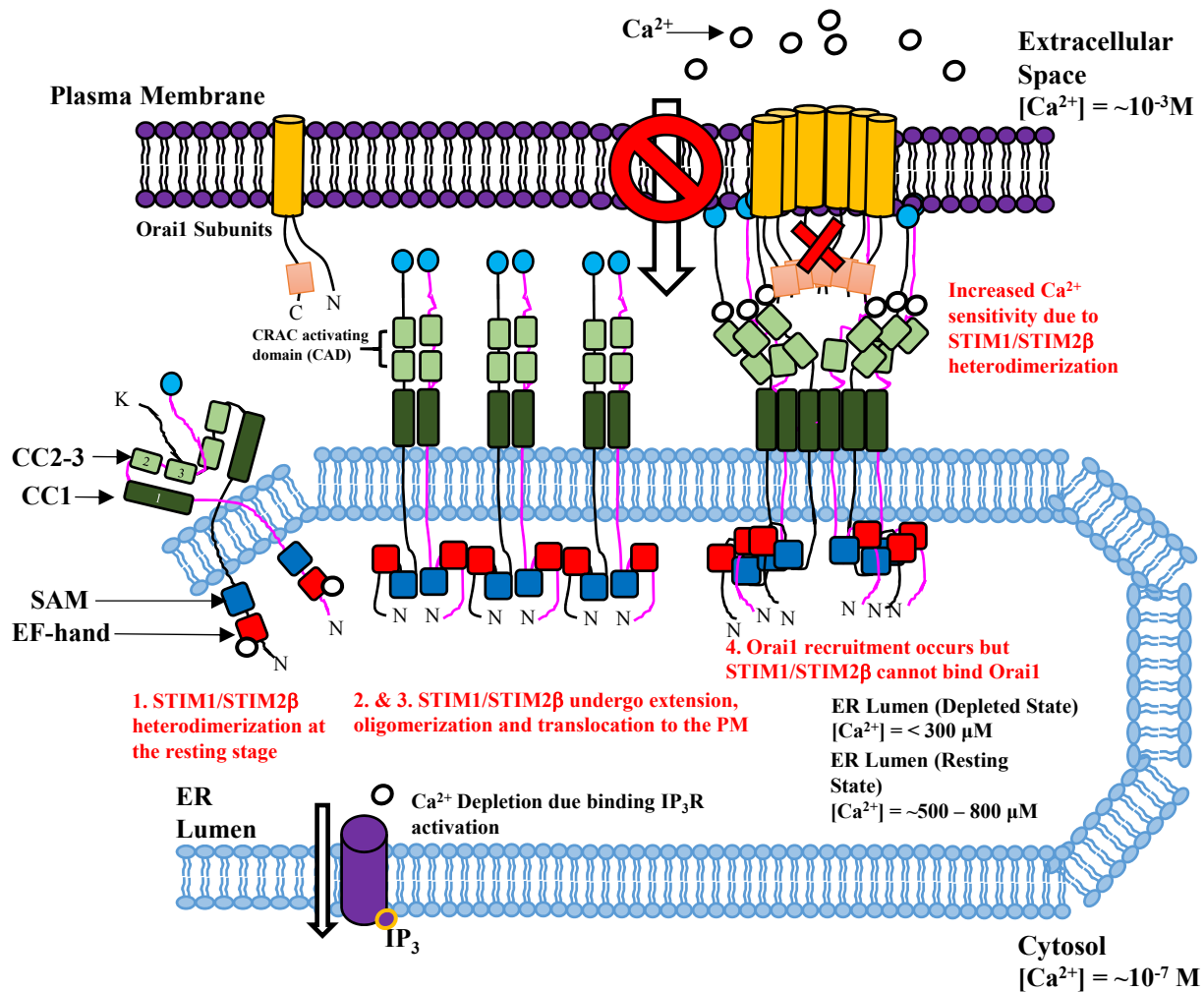


Figure 4.1. Proposed model of the STIM2 β mechanism of SOCE inhibition based on the data presented in this thesis. (1) STIM1 dimer undergoes conformational change and translocation towards the PM. (2) STIM2 β forms a heterodimer with STIM1. (3) STIM1/STIM2 β heterodimers oligomerize. (4) Orai1 subunits are recruited but no SOCE occurs.

Bibliography

- Alonso, M. T., Villalobos, C., Chamero, P., Alvarez, J., & Garcia-Sancho, J. (2006). Calcium microdomains in mitochondria and nucleus. *Cell Calcium*, *40*(5-6), 513-525. doi: 10.1016/j.ceca.2006.08.013
- Ando, S., Sarlis, N. J., Krishnan, J., Feng, X., Refetoff, S., Zhang, M. Q., . . . Yen, P. M. (2001). Aberrant alternative splicing of thyroid hormone receptor in a TSH-secreting pituitary tumor is a mechanism for hormone resistance. *Mol Endocrinol*, *15*(9), 1529-1538. doi: 10.1210/mend.15.9.0687
- Augustine, G. J. (2001). How does calcium trigger neurotransmitter release? *Current Opinion in Neurobiology*, *11*(3), 320-326. doi: 10.1016/s0959-4388(00)00214-2
- Baba, Y., Hayashi, K., Fujii, Y., Mizushima, A., Watarai, H., Wakamori, M., . . . Kurosaki, T. (2006). Coupling of STIM1 to store-operated Ca²⁺ entry through its constitutive and inducible movement in the endoplasmic reticulum. *Proc Natl Acad Sci U S A*, *103*(45), 16704-16709. doi: 10.1073/pnas.0608358103
- Baba, Y., Matsumoto, M., & Kurosaki, T. (2014). Calcium signaling in B cells: regulation of cytosolic Ca²⁺ increase and its sensor molecules, STIM1 and STIM2. *Mol Immunol*, *62*(2), 339-343. doi: 10.1016/j.molimm.2013.10.006
- Bauer, M. C., O'Connell, D., Cahill, D. J., & Linse, S. (2008). Calmodulin binding to the polybasic C-termini of STIM proteins involved in store-operated calcium entry. *Biochemistry*, *47*(23), 6089-6091. doi: 10.1021/bi800496a
- Bergmeier, W., Weidinger, C., Zee, I., & Feske, S. (2013). Emerging roles of store-operated Ca²⁺(+) entry through STIM and ORAI proteins in immunity, hemostasis and cancer. *Channels (Austin)*, *7*(5), 379-391. doi: 10.4161/chan.24302
- Berridge, M. J., Bootman, M. D., & Roderick, H. L. (2003). Calcium signalling: dynamics, homeostasis and remodelling. *Nat Rev Mol Cell Biol*, *4*(7), 517-529. doi: 10.1038/nrm1155
- Bertero, E., & Maack, C. (2018). Calcium Signaling and Reactive Oxygen Species in Mitochondria. *Circ Res*, *122*(10), 1460-1478. doi: 10.1161/CIRCRESAHA.118.310082
- Boldon, L., Laliberte, F., & Liu, L. (2015). Review of the fundamental theories behind small angle X-ray scattering, molecular dynamics simulations, and relevant integrated application. *Nano Rev*, *6*, 25661. doi: 10.3402/nano.v6.25661
- Braakman, I., & Hebert, D. N. (2013). Protein folding in the endoplasmic reticulum. *Cold Spring Harb Perspect Biol*, *5*(5), a013201. doi: 10.1101/cshperspect.a013201

- Brandman, O., Liou, J., Park, W. S., & Meyer, T. (2007). STIM2 is a feedback regulator that stabilizes basal cytosolic and endoplasmic reticulum Ca²⁺ levels. *Cell*, *131*(7), 1327-1339. doi: 10.1016/j.cell.2007.11.039
- Brauchi, S., Orta, G., Salazar, M., Rosenmann, E., & Latorre, R. (2006). A hot-sensing cold receptor: C-terminal domain determines thermosensation in transient receptor potential channels. *J Neurosci*, *26*(18), 4835-4840. doi: 10.1523/JNEUROSCI.5080-05.2006
- Cahalan, M. D. (2009). STIMulating store-operated Ca²⁺ entry. *Nat Cell Biol*, *11*(6), 669-677. doi: 10.1038/ncb0609-669
- Cai, X. (2007). Molecular evolution and structural analysis of the Ca²⁺ release-activated Ca²⁺ channel subunit, Orai. *J Mol Biol*, *368*(5), 1284-1291. doi: 10.1016/j.jmb.2007.03.022
- Calloway, N., Owens, T., Corwith, K., Rodgers, W., Holowka, D., & Baird, B. (2011). Stimulated association of STIM1 and Orai1 is regulated by the balance of PtdIns(4,5)P₂ between distinct membrane pools. *J Cell Sci*, *124*(Pt 15), 2602-2610. doi: 10.1242/jcs.084178
- Chan, W. Y., Soloviev, M. M., Ciruela, F., & McIlhinney, R. A. (2001). Molecular determinants of metabotropic glutamate receptor 1B trafficking. *Mol Cell Neurosci*, *17*(3), 577-588. doi: 10.1006/mcne.2001.0965
- Chin, D., & Means, A. R. (2000). Calmodulin: a prototypical calcium sensor. *Trends in Cell Biology*, *10*(8), 322-328. doi: 10.1016/s0962-8924(00)01800-6
- Choi, Y. J., Zhao, Y., Bhattacharya, M., & Stathopoulos, P. B. (2017). Structural perturbations induced by Asn131 and Asn171 glycosylation converge within the EFSAM core and enhance stromal interaction molecule-1 mediated store operated calcium entry. *Biochim Biophys Acta*, *1864*(6), 1054-1063. doi: 10.1016/j.bbamcr.2016.11.015
- Clapham, D. E. (2007). Calcium signaling. *Cell*, *131*(6), 1047-1058. doi: 10.1016/j.cell.2007.11.028
- Collins, H. E., Zhu-Mauldin, X., Marchase, R. B., & Chatham, J. C. (2013). STIM1/Orai1-mediated SOCE: current perspectives and potential roles in cardiac function and pathology. *Am J Physiol Heart Circ Physiol*, *305*(4), H446-458. doi: 10.1152/ajpheart.00104.2013
- Collins, S. R., & Meyer, T. (2011). Evolutionary origins of STIM1 and STIM2 within ancient Ca²⁺ signaling systems. *Trends Cell Biol*, *21*(4), 202-211. doi: 10.1016/j.tcb.2011.01.002

- Covington, E. D., Wu, M. M., & Lewis, R. S. (2010). Essential role for the CRAC activation domain in store-dependent oligomerization of STIM1. *Mol Biol Cell*, *21*(11), 1897-1907. doi: 10.1091/mbc.E10-02-0145
- Cui, B., Yang, X., Li, S., Lin, Z., Wang, Z., Dong, C., & Shen, Y. (2013). The inhibitory helix controls the intramolecular conformational switching of the C-terminus of STIM1. *PLoS One*, *8*(9), e74735. doi: 10.1371/journal.pone.0074735
- Cui, X., Song, L., Bai, Y., Wang, Y., Wang, B., & Wang, W. (2017). Stromal interaction molecule 1 regulates growth, cell cycle, and apoptosis of human tongue squamous carcinoma cells. *Biosci Rep*, *37*(2). doi: 10.1042/BSR20160519
- Darbellay, B., Arnaudeau, S., Bader, C. R., Konig, S., & Bernheim, L. (2011). STIM1L is a new actin-binding splice variant involved in fast repetitive Ca²⁺ release. *J Cell Biol*, *194*(2), 335-346. doi: 10.1083/jcb.201012157
- DeHaven, W. I., Smyth, J. T., Boyles, R. R., & Putney, J. W., Jr. (2007). Calcium inhibition and calcium potentiation of Orai1, Orai2, and Orai3 calcium release-activated calcium channels. *J Biol Chem*, *282*(24), 17548-17556. doi: 10.1074/jbc.M611374200
- Derler, I., Fahrner, M., Carugo, O., Muik, M., Bergsmann, J., Schindl, R., . . . Romanin, C. (2009a). Increased hydrophobicity at the N terminus/membrane interface impairs gating of the severe combined immunodeficiency-related ORAI1 mutant. *J Biol Chem*, *284*(23), 15903-15915. doi: 10.1074/jbc.M808312200
- Derler, I., Fahrner, M., Muik, M., Lackner, B., Schindl, R., Groschner, K., & Romanin, C. (2009b). A Ca²⁺ release-activated Ca²⁺ (CRAC) modulatory domain (CMD) within STIM1 mediates fast Ca²⁺-dependent inactivation of ORAI1 channels. *J Biol Chem*, *284*(37), 24933-24938. doi: 10.1074/jbc.C109.024083
- Enomoto, M., Nishikawa, T., Siddiqui, N., Chung, S., Ikura, M., & Stathopoulos, P. B. (2017). From Stores to Sinks: Structural Mechanisms of Cytosolic Calcium Regulation. *Adv Exp Med Biol*, *981*, 215-251. doi: 10.1007/978-3-319-55858-5_10
- Fahrner, M., Muik, M., Derler, I., Schindl, R., Fritsch, R., Frischauf, I., & Romanin, C. (2009). Mechanistic view on domains mediating STIM1-Orai coupling. *Immunol Rev*, *231*(1), 99-112. doi: 10.1111/j.1600-065X.2009.00815.x
- Fahrner, M., Stadlbauer, M., Muik, M., Rathner, P., Stathopoulos, P., Ikura, M., . . . Romanin, C. (2018). A dual mechanism promotes switching of the Stormorken STIM1 R304W mutant into the activated state. *Nat Commun*, *9*(1), 825. doi: 10.1038/s41467-018-03062-w
- Feske, S., Gwack, Y., Prakriya, M., Srikanth, S., Puppel, S. H., Tanasa, B., . . . Rao, A. (2006). A mutation in Orai1 causes immune deficiency by abrogating CRAC channel function. *Nature*, *441*(7090), 179-185. doi: 10.1038/nature04702

- Franke, D., & Svergun, D. I. (2009). DAMMIF, a program for rapid ab-initio shape determination in small-angle scattering. *J Appl Crystallogr*, 42(Pt 2), 342-346. doi: 10.1107/S0021889809000338
- Frischauf, I., Muik, M., Derler, I., Bergsmann, J., Fahrner, M., Schindl, R., . . . Romanin, C. (2009). Molecular determinants of the coupling between STIM1 and Orai channels: differential activation of Orai1-3 channels by a STIM1 coiled-coil mutant. *J Biol Chem*, 284(32), 21696-21706. doi: 10.1074/jbc.M109.018408
- Gidalevitz, T., Stevens, F., & Argon, Y. (2013). Orchestration of secretory protein folding by ER chaperones. *Biochim Biophys Acta*, 1833(11), 2410-2424. doi: 10.1016/j.bbamcr.2013.03.007
- Graham, S. J., Dziadek, M. A., & Johnstone, L. S. (2011). A cytosolic STIM2 preprotein created by signal peptide inefficiency activates ORAI1 in a store-independent manner. *J Biol Chem*, 286(18), 16174-16185. doi: 10.1074/jbc.M110.206946
- Graveley, B. R. (2001). Alternative splicing: increasing diversity in the proteomic world. *Trends Genet*, 17(2), 100-107.
- Gudlur, A., Zhou, Y., & Hogan, P. G. (2013). STIM-ORAI interactions that control the CRAC channel. *Curr Top Membr*, 71, 33-58. doi: 10.1016/B978-0-12-407870-3.00002-0
- Gui, L., Zhu, J., Lu, X., Sims, S. M., Lu, W. Y., Stathopoulos, P. B., & Feng, Q. (2018). S-Nitrosylation of STIM1 by Neuronal Nitric Oxide Synthase Inhibits Store-Operated Ca(2+) Entry. *J Mol Biol*, 430(12), 1773-1785. doi: 10.1016/j.jmb.2018.04.028
- Haller, T., Dietl, P., Deetjen, P., & Volkl, H. (1996). The lysosomal compartment as intracellular calcium store in MDCK cells: a possible involvement in InsP3-mediated Ca²⁺ release. *Cell Calcium*, 19(2), 157-165.
- Halperin, L., Jung, J., & Michalak, M. (2014). The many functions of the endoplasmic reticulum chaperones and folding enzymes. *IUBMB Life*, 66(5), 318-326. doi: 10.1002/iub.1272
- Herzberg, O., Moulton, J., & James, M. N. (1986). Calcium binding to skeletal muscle troponin C and the regulation of muscle contraction. *Ciba Found Symp*, 122, 120-144.
- Hilden, S. A., & Madias, N. E. (1989). H⁺/Ca²⁺ exchange in rabbit renal cortical endosomes. *J Membr Biol*, 112(2), 131-138.
- Honnappa, S., Gouveia, S. M., Weisbrich, A., Damberger, F. F., Bhavesh, N. S., Jawhari, H., . . . Steinmetz, M. O. (2009). An EB1-binding motif acts as a microtubule tip localization signal. *Cell*, 138(2), 366-376. doi: 10.1016/j.cell.2009.04.065

- Hooper, R., Samakai, E., Kedra, J., & Soboloff, J. (2013). Multifaceted roles of STIM proteins. *Pflugers Arch*, *465*(10), 1383-1396. doi: 10.1007/s00424-013-1270-8
- Horinouchi, T., Higashi, T., Higa, T., Terada, K., Mai, Y., Aoyagi, H., . . . Miwa, S. (2012). Different binding property of STIM1 and its novel splice variant STIM1L to Orai1, TRPC3, and TRPC6 channels. *Biochem Biophys Res Commun*, *428*(2), 252-258. doi: 10.1016/j.bbrc.2012.10.034
- Hou, X., Pedi, L., Diver, M. M., & Long, S. B. (2012). Crystal structure of the calcium release-activated calcium channel Orai. *Science*, *338*(6112), 1308-1313. doi: 10.1126/science.1228757
- Ikura, M. (1996). Calcium binding and conformational response in EF-hand proteins. *Trends Biochem Sci*, *21*(1), 14-17.
- Jewell, B. R. (1977). A reexamination of the influence of muscle length on myocardial performance. *Circ Res*, *40*(3), 221-230.
- Ji, W., Xu, P., Li, Z., Lu, J., Liu, L., Zhan, Y., . . . Chen, L. (2008). Functional stoichiometry of the unitary calcium-release-activated calcium channel. *Proc Natl Acad Sci U S A*, *105*(36), 13668-13673. doi: 10.1073/pnas.0806499105
- Joseph, N., Reicher, B., & Barda-Saad, M. (2014). The calcium feedback loop and T cell activation: how cytoskeleton networks control intracellular calcium flux. *Biochim Biophys Acta*, *1838*(2), 557-568. doi: 10.1016/j.bbamem.2013.07.009
- Kawasaki, T., Lange, I., & Feske, S. (2009). A minimal regulatory domain in the C terminus of STIM1 binds to and activates ORAI1 CRAC channels. *Biochem Biophys Res Commun*, *385*(1), 49-54. doi: 10.1016/j.bbrc.2009.05.020
- Kelemen, O., Convertini, P., Zhang, Z., Wen, Y., Shen, M., Falaleeva, M., & Stamm, S. (2013). Function of alternative splicing. *Gene*, *514*(1), 1-30. doi: 10.1016/j.gene.2012.07.083
- Kim, M. S., Pinto, S. M., Getnet, D., Nirujogi, R. S., Manda, S. S., Chaerkady, R., . . . Pandey, A. (2014). A draft map of the human proteome. *Nature*, *509*(7502), 575-581. doi: 10.1038/nature13302
- Kondratska, K., Kondratskyi, A., Yassine, M., Lemonnier, L., Lepage, G., Morabito, A., . . . Prevarskaya, N. (2014). Orai1 and STIM1 mediate SOCE and contribute to apoptotic resistance of pancreatic adenocarcinoma. *Biochim Biophys Acta*, *1843*(10), 2263-2269. doi: 10.1016/j.bbamcr.2014.02.012
- Korzeniowski, M. K., Manjarres, I. M., Varnai, P., & Balla, T. (2010). Activation of STIM1-Orai1 involves an intramolecular switching mechanism. *Sci Signal*, *3*(148), ra82. doi: 10.1126/scisignal.2001122

- Kurosaki, T., & Baba, Y. (2010). Ca²⁺ signaling and STIM1. *Prog Biophys Mol Biol*, *103*(1), 51-58. doi: 10.1016/j.pbiomolbio.2010.02.004
- Le Deist, F., Hivroz, C., Partiseti, M., Thomas, C., Buc, H. A., Oleastro, M., . . . Fischer, A. (1995). A primary T-cell immunodeficiency associated with defective transmembrane calcium influx. *Blood*, *85*(4), 1053-1062.
- Lee, K. P., Yuan, J. P., Zeng, W., So, I., Worley, P. F., & Muallem, S. (2009). Molecular determinants of fast Ca²⁺-dependent inactivation and gating of the Orai channels. *Proc Natl Acad Sci U S A*, *106*(34), 14687-14692. doi: 10.1073/pnas.0904664106
- Levine, J. D., & Alessandri-Haber, N. (2007). TRP channels: targets for the relief of pain. *Biochim Biophys Acta*, *1772*(8), 989-1003. doi: 10.1016/j.bbadis.2007.01.008
- Liou, J., Kim, M. L., Heo, W. D., Jones, J. T., Myers, J. W., Ferrell, J. E., Jr., & Meyer, T. (2005). STIM is a Ca²⁺ sensor essential for Ca²⁺-store-depletion-triggered Ca²⁺ influx. *Curr Biol*, *15*(13), 1235-1241. doi: 10.1016/j.cub.2005.05.055
- Luik, R. M., Wang, B., Prakriya, M., Wu, M. M., & Lewis, R. S. (2008). Oligomerization of STIM1 couples ER calcium depletion to CRAC channel activation. *Nature*, *454*(7203), 538-542. doi: 10.1038/nature07065
- Luik, R. M., Wu, M. M., Buchanan, J., & Lewis, R. S. (2006). The elementary unit of store-operated Ca²⁺ entry: local activation of CRAC channels by STIM1 at ER-plasma membrane junctions. *J Cell Biol*, *174*(6), 815-825. doi: 10.1083/jcb.200604015
- Maruyama, Y., Ogura, T., Mio, K., Kato, K., Kaneko, T., Kiyonaka, S., . . . Sato, C. (2009). Tetrameric Orai1 is a teardrop-shaped molecule with a long, tapered cytoplasmic domain. *J Biol Chem*, *284*(20), 13676-13685. doi: 10.1074/jbc.M900812200
- Maus, M., Jairaman, A., Stathopulos, P. B., Muik, M., Fahrner, M., Weidinger, C., . . . Feske, S. (2015). Missense mutation in immunodeficient patients shows the multifunctional roles of coiled-coil domain 3 (CC3) in STIM1 activation. *Proc Natl Acad Sci U S A*, *112*(19), 6206-6211. doi: 10.1073/pnas.1418852112
- McDonald, T. F., Pelzer, S., Trautwein, W., & Pelzer, D. J. (1994). Regulation and modulation of calcium channels in cardiac, skeletal, and smooth muscle cells. *Physiol Rev*, *74*(2), 365-507. doi: 10.1152/physrev.1994.74.2.365
- McGuffin, L. J., Bryson, K., & Jones, D. T. (2000). The PSIPRED protein structure prediction server. *Bioinformatics*, *16*(4), 404-405.
- Miederer, A. M., Alansary, D., Schwar, G., Lee, P. H., Jung, M., Helms, V., & Niemeyer, B. A. (2015). A STIM2 splice variant negatively regulates store-operated calcium entry. *Nat Commun*, *6*, 6899. doi: 10.1038/ncomms7899

- Miki, T., Bottaro, D. P., Fleming, T. P., Smith, C. L., Burgess, W. H., Chan, A. M., & Aaronson, S. A. (1992). Determination of ligand-binding specificity by alternative splicing: two distinct growth factor receptors encoded by a single gene. *Proc Natl Acad Sci U S A*, *89*(1), 246-250.
- Misceo, D., Holmgren, A., Louch, W. E., Holme, P. A., Mizobuchi, M., Morales, R. J., . . . Frengen, E. (2014). A dominant STIM1 mutation causes Stormorken syndrome. *Hum Mutat*, *35*(5), 556-564. doi: 10.1002/humu.22544
- Morin, G., Bruechle, N. O., Singh, A. R., Knopp, C., Jedraszak, G., Elbracht, M., . . . Rochette, J. (2014). Gain-of-Function Mutation in STIM1 (P.R304W) Is Associated with Stormorken Syndrome. *Hum Mutat*, *35*(10), 1221-1232. doi: 10.1002/humu.22621
- Muik, M., Fahrner, M., Derler, I., Schindl, R., Bergsmann, J., Frischauf, I., . . . Romanin, C. (2009). A Cytosolic Homomerization and a Modulatory Domain within STIM1 C Terminus Determine Coupling to ORAI1 Channels. *J Biol Chem*, *284*(13), 8421-8426. doi: 10.1074/jbc.C800229200
- Muik, M., Fahrner, M., Schindl, R., Stathopoulos, P., Frischauf, I., Derler, I., . . . Romanin, C. (2011). STIM1 couples to ORAI1 via an intramolecular transition into an extended conformation. *EMBO J*, *30*(9), 1678-1689. doi: 10.1038/emboj.2011.79
- Mullins, F. M., Park, C. Y., Dolmetsch, R. E., & Lewis, R. S. (2009). STIM1 and calmodulin interact with Orail to induce Ca²⁺-dependent inactivation of CRAC channels. *Proc Natl Acad Sci U S A*, *106*(36), 15495-15500. doi: 10.1073/pnas.0906781106
- Niccoli-Sire, P., Fayadat, L., Siffroi-Fernandez, S., Malthierry, Y., & Franc, J. L. (2001). Alternatively spliced form of human thyroperoxidase, TPOzanelli: activity, intracellular trafficking, and role in hormonogenesis. *Biochemistry*, *40*(8), 2572-2579.
- Noury, J. B., Bohm, J., Peche, G. A., Guyant-Marechal, L., Bedat-Millet, A. L., Chiche, L., . . . Stojkovic, T. (2017). Tubular aggregate myopathy with features of Stormorken disease due to a new STIM1 mutation. *Neuromuscul Disord*, *27*(1), 78-82. doi: 10.1016/j.nmd.2016.10.006
- Oh-Hora, M., Yamashita, M., Hogan, P. G., Sharma, S., Lamperti, E., Chung, W., . . . Rao, A. (2008). Dual functions for the endoplasmic reticulum calcium sensors STIM1 and STIM2 in T cell activation and tolerance. *Nat Immunol*, *9*(4), 432-443. doi: 10.1038/ni1574
- Palty, R., Silverman, W. F., Hershinkel, M., Caporale, T., Sensi, S. L., Parnis, J., . . . Sekler, I. (2010). NCLX is an essential component of mitochondrial Na⁺/Ca²⁺ exchange. *Proc Natl Acad Sci U S A*, *107*(1), 436-441. doi: 10.1073/pnas.0908099107

- Park, C. Y., Hoover, P. J., Mullins, F. M., Bachhawat, P., Covington, E. D., Raunser, S., . . . Lewis, R. S. (2009). STIM1 clusters and activates CRAC channels via direct binding of a cytosolic domain to Orai1. *Cell*, *136*(5), 876-890. doi: 10.1016/j.cell.2009.02.014
- Partiseti, M., Le Deist, F., Hivroz, C., Fischer, A., Korn, H., & Choquet, D. (1994). The calcium current activated by T cell receptor and store depletion in human lymphocytes is absent in a primary immunodeficiency. *J Biol Chem*, *269*(51), 32327-32335.
- Parvez, S., Beck, A., Peinelt, C., Soboloff, J., Lis, A., Monteilh-Zoller, M., . . . Penner, R. (2008). STIM2 protein mediates distinct store-dependent and store-independent modes of CRAC channel activation. *FASEB J*, *22*(3), 752-761. doi: 10.1096/fj.07-9449com
- Penna, A., Demuro, A., Yeromin, A. V., Zhang, S. L., Safrina, O., Parker, I., & Cahalan, M. D. (2008). The CRAC channel consists of a tetramer formed by Stim-induced dimerization of Orai dimers. *Nature*, *456*(7218), 116-120. doi: 10.1038/nature07338
- Petoukhov, M. V., Franke, D., Shkumatov, A. V., Tria, G., Kikhney, A. G., Gajda, M., . . . Svergun, D. I. (2012). New developments in the ATSAS program package for small-angle scattering data analysis. *J Appl Crystallogr*, *45*(Pt 2), 342-350. doi: 10.1107/S0021889812007662
- Petoukhov, M. V., Konarev, P. V., Kikhney, A. G., & Svergun, D. I. (2007). ATSAS 2.1 – towards automated and web-supported small-angle scattering data analysis. *J Appl Crystallogr*, *40*(s1), s223-s228. doi: doi:10.1107/S0021889807002853
- Pinton, P., Pozzan, T., & Rizzuto, R. (1998). The Golgi apparatus is an inositol 1,4,5-trisphosphate-sensitive Ca²⁺ store, with functional properties distinct from those of the endoplasmic reticulum. *EMBO J*, *17*(18), 5298-5308. doi: 10.1093/emboj/17.18.5298
- Prakriya, M., Feske, S., Gwack, Y., Srikanth, S., Rao, A., & Hogan, P. G. (2006). Orai1 is an essential pore subunit of the CRAC channel. *Nature*, *443*(7108), 230-233. doi: 10.1038/nature05122
- Putnam, C. D. (2016). Guinier peak analysis for visual and automated inspection of small-angle X-ray scattering data. *J Appl Crystallogr*, *49*(Pt 5), 1412-1419. doi: 10.1107/S1600576716010906
- Putney, J. W. (1986). A model for receptor-regulated calcium entry. *Cell Calcium*, *7*(1), 1-12. doi: 10.1016/0143-4160(86)90026-6
- Rana, A., Yen, M., Sadaghiani, A. M., Malmersjo, S., Park, C. Y., Dolmetsch, R. E., & Lewis, R. S. (2015). Alternative splicing converts STIM2 from an activator to an

- inhibitor of store-operated calcium channels. *J Cell Biol*, 209(5), 653-669. doi: 10.1083/jcb.201412060
- Rathner, P., Stadlbauer, M., Romanin, C., Fahrner, M., Derler, I., & Muller, N. (2018). Rapid NMR-scale purification of (15)N,(13)C isotope-labeled recombinant human STIM1 coiled coil fragments. *Protein Expr Purif*, 146, 45-50. doi: 10.1016/j.pep.2018.01.013
- Razzell, W., Evans, I. R., Martin, P., & Wood, W. (2013). Calcium flashes orchestrate the wound inflammatory response through DUOX activation and hydrogen peroxide release. *Curr Biol*, 23(5), 424-429. doi: 10.1016/j.cub.2013.01.058
- Rong, Y., & Distelhorst, C. W. (2008). Bcl-2 protein family members: versatile regulators of calcium signaling in cell survival and apoptosis. *Annu Rev Physiol*, 70, 73-91. doi: 10.1146/annurev.physiol.70.021507.105852
- Roos, J., DiGregorio, P. J., Yeromin, A. V., Ohlsen, K., Liudyno, M., Zhang, S., . . . Stauderman, K. A. (2005). STIM1, an essential and conserved component of store-operated Ca²⁺ channel function. *J Cell Biol*, 169(3), 435-445. doi: 10.1083/jcb.200502019
- Saitoh, N., Oritani, K., Saito, K., Yokota, T., Ichii, M., Sudo, T., . . . Kanakura, Y. (2011). Identification of functional domains and novel binding partners of STIM proteins. *J Cell Biochem*, 112(1), 147-156. doi: 10.1002/jcb.22910
- Sauc, S., Bulla, M., Nunes, P., Orci, L., Marchetti, A., Antigny, F., . . . Demaurex, N. (2015). STIM1L traps and gates Orail channels without remodeling the cortical ER. *J Cell Sci*, 128(8), 1568-1579. doi: 10.1242/jcs.164228
- Schulman, I. H., Zachariah, M., & Rajj, L. (2005). Calcium channel blockers, endothelial dysfunction, and combination therapy. *Aging Clin Exp Res*, 17(4 Suppl), 40-45.
- Selliah, N., Brooks, W. H., & Roszman, T. L. (1996). Proteolytic cleavage of alpha-actinin by calpain in T cells stimulated with anti-CD3 monoclonal antibody. *J Immunol*, 156(9), 3215-3221.
- Shaw, P. J., & Feske, S. (2012). Regulation of lymphocyte function by ORAI and STIM proteins in infection and autoimmunity. *J Physiol*, 590(17), 4157-4167. doi: 10.1113/jphysiol.2012.233221
- Shen, W. W., & Demaurex, N. (2012). Morphological and functional aspects of STIM1-dependent assembly and disassembly of store-operated calcium entry complexes. *Biochem Soc Trans*, 40(1), 112-118. doi: 10.1042/BST20110620
- Singh, B. B., Liu, X., Tang, J., Zhu, M. X., & Ambudkar, I. S. (2002). Calmodulin regulates Ca(2+)-dependent feedback inhibition of store-operated Ca(2+) influx by interaction with a site in the C terminus of TrpC1. *Mol Cell*, 9(4), 739-750.

- Slusarski, D. C., & Pelegri, F. (2007). Calcium signaling in vertebrate embryonic patterning and morphogenesis. *Dev Biol*, *307*(1), 1-13. doi: 10.1016/j.ydbio.2007.04.043
- Soboloff, J., Rothberg, B. S., Madesh, M., & Gill, D. L. (2012). STIM proteins: dynamic calcium signal transducers. *Nat Rev Mol Cell Biol*, *13*(9), 549-565. doi: 10.1038/nrm3414
- Soboloff, J., Spassova, M. A., Tang, X. D., Hewavitharana, T., Xu, W., & Gill, D. L. (2006). Orai1 and STIM reconstitute store-operated calcium channel function. *J Biol Chem*, *281*(30), 20661-20665. doi: 10.1074/jbc.C600126200
- Spira, M. E., Oren, R., Dormann, A., Ilouz, N., & Lev, S. (2001). Calcium, protease activation, and cytoskeleton remodeling underlie growth cone formation and neuronal regeneration. *Cell Mol Neurobiol*, *21*(6), 591-604.
- Stathopulos, P. B., & Ikura, M. (2010). Partial unfolding and oligomerization of stromal interaction molecules as an initiation mechanism of store operated calcium entry. *Biochem Cell Biol*, *88*(2), 175-183. doi: 10.1139/o09-125
- Stathopulos, P. B., Li, G. Y., Plevin, M. J., Ames, J. B., & Ikura, M. (2006). Stored Ca²⁺ depletion-induced oligomerization of stromal interaction molecule 1 (STIM1) via the EF-SAM region: An initiation mechanism for capacitive Ca²⁺ entry. *J Biol Chem*, *281*(47), 35855-35862. doi: 10.1074/jbc.M608247200
- Stathopulos, P. B., Schindl, R., Fahrner, M., Zheng, L., Gasmi-Seabrook, G. M., Muik, M., . . . Ikura, M. (2013). STIM1/Orai1 coiled-coil interplay in the regulation of store-operated calcium entry. *Nat Commun*, *4*, 2963. doi: 10.1038/ncomms3963
- Stathopulos, P. B., Zheng, L., & Ikura, M. (2009). Stromal interaction molecule (STIM) 1 and STIM2 calcium sensing regions exhibit distinct unfolding and oligomerization kinetics. *J Biol Chem*, *284*(2), 728-732. doi: 10.1074/jbc.C800178200
- Stathopulos, P. B., Zheng, L., Li, G. Y., Plevin, M. J., & Ikura, M. (2008). Structural and mechanistic insights into STIM1-mediated initiation of store-operated calcium entry. *Cell*, *135*(1), 110-122. doi: 10.1016/j.cell.2008.08.006
- Stefan, C. J., Manford, A. G., & Emr, S. D. (2013). ER-PM connections: sites of information transfer and inter-organellar communication. *Curr Opin Cell Biol*, *25*(4), 434-442. doi: 10.1016/j.ceb.2013.02.020
- Ter Keurs, H. E., & Boyden, P. A. (2007). Calcium and arrhythmogenesis. *Physiol Rev*, *87*(2), 457-506. doi: 10.1152/physrev.00011.2006
- Thebault, S., Hoenderop, J. G., & Bindels, R. J. (2006). Epithelial Ca²⁺ and Mg²⁺ channels in kidney disease. *Adv Chronic Kidney Dis*, *13*(2), 110-117. doi: 10.1053/j.ackd.2006.01.002

- Thompson, J. L., & Shuttleworth, T. J. (2015). Anchoring protein AKAP79-mediated PKA phosphorylation of STIM1 determines selective activation of the ARC channel, a store-independent Orai channel. *J Physiol*, *593*(3), 559-572. doi: 10.1113/jphysiol.2014.284182
- Thompson, J. L., Zhao, Y., Stathopoulos, P. B., Grossfield, A., & Shuttleworth, T. J. (2018). Phosphorylation-mediated structural changes within the SOAR domain of stromal interaction molecule 1 enable specific activation of distinct Orai channels. *J Biol Chem*, *293*(9), 3145-3155. doi: 10.1074/jbc.M117.819078
- Tu, H., Nelson, O., Bezprozvanny, A., Wang, Z., Lee, S. F., Hao, Y. H., . . . Bezprozvanny, I. (2006). Presenilins form ER Ca²⁺ leak channels, a function disrupted by familial Alzheimer's disease-linked mutations. *Cell*, *126*(5), 981-993. doi: 10.1016/j.cell.2006.06.059
- Vig, M., Beck, A., Billingsley, J. M., Lis, A., Parvez, S., Peinelt, C., . . . Penner, R. (2006). CRACM1 multimers form the ion-selective pore of the CRAC channel. *Curr Biol*, *16*(20), 2073-2079. doi: 10.1016/j.cub.2006.08.085
- Vriens, J., Nilius, B., & Voets, T. (2014). Peripheral thermosensation in mammals. *Nat Rev Neurosci*, *15*(9), 573-589. doi: 10.1038/nrn3784
- Walsh, C. M., Chvanov, M., Haynes, L. P., Petersen, O. H., Tepikin, A. V., & Burgoyne, R. D. (2009). Role of phosphoinositides in STIM1 dynamics and store-operated calcium entry. *Biochem J*, *425*(1), 159-168. doi: 10.1042/BJ20090884
- Wang, X., Wang, Y., Zhou, Y., Hendron, E., Mancarella, S., Andrade, M. D., . . . Gill, D. L. (2014). Distinct Orai-coupling domains in STIM1 and STIM2 define the Orai-activating site. *Nat Commun*, *5*, 3183. doi: 10.1038/ncomms4183
- Wu, M. M., Buchanan, J., Luik, R. M., & Lewis, R. S. (2006). Ca²⁺ store depletion causes STIM1 to accumulate in ER regions closely associated with the plasma membrane. *J Cell Biol*, *174*(6), 803-813. doi: 10.1083/jcb.200604014
- Yamamoto, K., Nakayama, H., Nunoi, K., & Fujishima, M. (1987). Interaction of calmodulin with troponin I and the troponin-tropomyosin-actin complex. Effect of Ca²⁺ and Sr²⁺ ions. *Biochem J*, *241*(3), 905-909.
- Yang, X., Jin, H., Cai, X., Li, S., & Shen, Y. (2012). Structural and mechanistic insights into the activation of Stromal interaction molecule 1 (STIM1). *Proc Natl Acad Sci U S A*, *109*(15), 5657-5662. doi: 10.1073/pnas.1118947109
- Yang, Z., Kirton, H. M., MacDougall, D. A., Boyle, J. P., Deuchars, J., Frater, B., . . . Steele, D. S. (2015). The Golgi apparatus is a functionally distinct Ca²⁺ store regulated by the PKA and Epac branches of the beta1-adrenergic signaling pathway. *Sci Signal*, *8*(398), ra101. doi: 10.1126/scisignal.aaa7677

- Yeromin, A. V., Zhang, S. L., Jiang, W., Yu, Y., Safrina, O., & Cahalan, M. D. (2006). Molecular identification of the CRAC channel by altered ion selectivity in a mutant of Orai. *Nature*, *443*(7108), 226-229. doi: 10.1038/nature05108
- Yuan, J. P., Zeng, W., Dorwart, M. R., Choi, Y. J., Worley, P. F., & Muallem, S. (2009). SOAR and the polybasic STIM1 domains gate and regulate Orai channels. *Nat Cell Biol*, *11*(3), 337-343. doi: 10.1038/ncb1842
- Zhang, S. L., Yu, Y., Roos, J., Kozak, J. A., Deerinck, T. J., Ellisman, M. H., . . . Cahalan, M. D. (2005). STIM1 is a Ca²⁺ sensor that activates CRAC channels and migrates from the Ca²⁺ store to the plasma membrane. *Nature*, *437*(7060), 902-905. doi: 10.1038/nature04147
- Zheng, L., Stathopoulos, P. B., Li, G. Y., & Ikura, M. (2008). Biophysical characterization of the EF-hand and SAM domain containing Ca²⁺ sensory region of STIM1 and STIM2. *Biochem Biophys Res Commun*, *369*(1), 240-246. doi: 10.1016/j.bbrc.2007.12.129
- Zheng, L., Stathopoulos, P. B., Schindl, R., Li, G. Y., Romanin, C., & Ikura, M. (2011). Auto-inhibitory role of the EF-SAM domain of STIM proteins in store-operated calcium entry. *Proc Natl Acad Sci U S A*, *108*(4), 1337-1342. doi: 10.1073/pnas.1015125108
- Zhou, Y., Cai, X., Loktionova, N. A., Wang, X., Nwokonko, R. M., Wang, X., . . . Gill, D. L. (2016). The STIM1-binding site nexus remotely controls Orai1 channel gating. *Nat Commun*, *7*, 13725. doi: 10.1038/ncomms13725
- Zhou, Y., Mancarella, S., Wang, Y., Yue, C., Ritchie, M., Gill, D. L., & Soboloff, J. (2009). The short N-terminal domains of STIM1 and STIM2 control the activation kinetics of Orai1 channels. *J Biol Chem*, *284*(29), 19164-19168. doi: 10.1074/jbc.C109.010900
- Zhou, Y., Wang, X., Wang, X., Loktionova, N. A., Cai, X., Nwokonko, R. M., . . . Gill, D. L. (2015). STIM1 dimers undergo unimolecular coupling to activate Orai1 channels. *Nat Commun*, *6*, 8395. doi: 10.1038/ncomms9395
- Zhu, J., Lu, X., Feng, Q., & Stathopoulos, P. B. (2018). A charge sensing region in the stromal interaction molecule-1 luminal domain confers stabilization-mediated inhibition of SOCE in response to S-nitrosylation. *J Biol Chem*. doi: 10.1074/jbc.RA117.000503
- Zot, A. S., & Potter, J. D. (1987). Structural aspects of troponin-tropomyosin regulation of skeletal muscle contraction. *Annu Rev Biophys Biophys Chem*, *16*, 535-559. doi: 10.1146/annurev.bb.16.060187.002535

Curriculum Vitae

Name: Steve Chung

Post-secondary Education and Degrees: University of Toronto
University of Toronto, Ontario, Canada
Honours B.Sc 2012-2016

Honours and Awards: Western Graduate Research Scholarship
2016-2018

Related Work Experience

Research Assistant
University of Toronto
2015 - 2016

Teaching Assistant
Physiology 3120
The University of Western Ontario
2016-2017

Physiology 3000e
The University of Western Ontario
2017-2018

Publications:

Chung, S., & Stathopoulos, P.B. (2018). Stromal interaction molecule (STIM) 2 β insert perturbs folding, stability and hydrophobic exposure of OASF. Ion Channel and Ion-Related Signaling. *Interactional Journal of Molecular Sciences* (in press).

Enomoto, M., Nishikawa, T., Siddiqui, N., **Chung, S.**, Ikura, M., & Stathopoulos, P. B. (2017). From Stores to Sinks: Structural Mechanisms of Cytosolic Calcium Regulation. In *Membrane Dynamics and Calcium Signaling* (pp. 215-251). Springer, Cham.

Choi, Y. J., Zhu, J., **Chung, S.**, Siddiqui, N., Feng, Q., & Stathopoulos, P. B. (2017). Targeting Cysteine Thiols for in Vitro Site-specific Glycosylation of Recombinant Proteins. *Journal of visualized experiments: JoVE*, (128).

Presentations:

The 10th Annual Department of Physiology and Pharmacology Research Day, Western University, London, ON, 2016.

Title: Mechanisms by which variations in STIM coil-coil domains contribute to store operated Ca²⁺ entry (SOCE)

London Health Research Day, London, ON 2016

Title: Mechanisms by which variations in STIM coil-coil domains contribute to store operated Ca²⁺ entry (SOCE)

Cardiovascular Journal Club, Western University, London ON, 2017

Title: The effects of the 2 β insert on the Stromal Interaction Molecule (STIM) coiled-coil mechanisms of function

The 11th Annual Department of Physiology and Pharmacology Research Day, Western University, London, ON, 2017.

Title: The effects of the 2 β insert on the Stromal Interaction Molecule (STIM) coiled-coil mechanisms of function

London Health Research Day, London, ON 2017

Title: Stromal interaction molecule (STIM) 2 β insert perturbs folding, stability and hydrophobic exposure of OASF

-
- (a) represents SEC-MALS experiments were conducted in 25 mM Ca^{2+} , - represents SEC-MALS experiments conducted in Ca^{2+} free conditions
- (b) SuperDex 200 chromatography column was used to filter and elute protein based on size
- (c) Stoichiometric ratio was calculated by dividing the calculated MALS value by the theoretical monomer mass